

TECHNOLOGIES TO IMPROVE IMPACT RELATED FIRE SAFETY

Kennerly H. Digges

Motor Vehicle Fire Research Institute (MVFRI)
United States

Paper Number 07-0480

ABSTRACT

The research reported in this paper is a follow-on to a five year research program conducted by General Motors in accordance with an administrative Settlement Agreement reached with the US Department of Transportation. In a subsequent Judicial Settlement, GM agreed fund more than \$4.1 million in fire-related research over the period 2001-2004. The purpose of this paper is to provide a public update report on the projects that have been funded under this latter research program, along with results to date. This paper is the sixth in a series of technical papers intended to disseminate the results of the ongoing research.

The projects and research results reported in this paper include statistical analyses of vehicle fires based on FARS and NASS and summaries of technologies to reduce crash induced fires

INTRODUCTION

The GM/DoT Settlement research program has been documented elsewhere [NHTSA 2001]. The research reported in this paper is a follow-on to that project.

The Fatality Analysis Reporting System (FARS) is a database maintained by the US Department of Transportation. It contains records of all fatal crashes that occur on public roads in the United States. The FARS database has been used to document the variations in fatal injuries annually since 1975.

The FARS database documents all fatalities that occurred as a result of the crash including those where a fire resulted. In this paper, the term “FARS Fatalities” designates the fatalities in which a fire occurred in the vehicle, regardless of whether or not the fire caused the fatality. Since 1979, FARS also coded the “most harmful event” (MHE). If the fire event has been coded as the most harmful event, burn or inhalation injuries are the most likely cause of the fatality. In many crashes, it may be difficult to discern the cause of the fatality (biomechanical trauma vs. fire trauma). This distinction was not investigated and the coding was taken directly from FARS. Previous studies have attempted to

investigate the uncertainty and difficulty in coding fire as the most harmful event [Davies 2002].

Earlier papers reported that between 1979 and 2000, when fire was coded as the most harmful event (MHE), the fatality rates for vehicles less than 5 years old had declined by 72.4% [Friedman 2003 and 2005; Digges 2003]. The MHE fire rates for pickups less than 5 years old had reduced by 82.4%, but their rates were still higher than the rate for passenger cars.

A follow-on analysis grouped years of FARS data to examine changes in the fatal crashes with fires [Bahouth, 2007]. The figures presented in the earlier papers showed that the fire rates of vehicles generally decreased during the decade of the 1980’s but have remained relatively constant since 1990. To examine these trends, the FARS years were aggregated into three groups – 1979-1989; 1990-1999; and 2000-2005. Figure 1 shows the FARS fire rate and FARS MHE fire rate using billions of annual vehicle miles traveled (VMT) as the denominator.

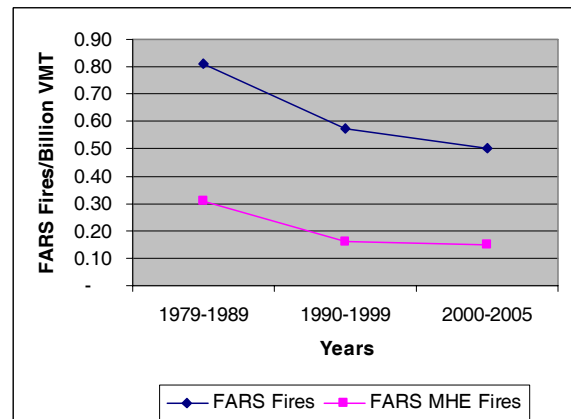


Figure 1. Fatalities in Vehicles with Fires and in Vehicles with Fire as the Most Harmful Event per Billion Vehicle Miles Traveled Annually - FARS

FARS does not record the direction of force in the crash. However, the location of principal damage is coded. In this coding, rollovers with damage from impacts with fixed objects or with other vehicles are coded according to the location of the damage. If the damage comes from ground contact, the crash is classified as a non-collision. Rollovers are classified according to the event during which it occurred (i.e. Non-rollover, rollover during 1st harmful event, or rollover during subsequent events). Most of the rollovers have damage to the front or sides of the vehicle. This damage may have been caused by impacts with fixed or non-fixed objects before or

during the rollover. In some cases, these impacts may have been the cause of the fatality. The FARS can be examined by damage area only and without identifying the rollovers. However, in the analysis to follow, all rollovers are grouped together, regardless of the area of damage. No crashes with rollover are included in the front, side or rear damage areas. When FARS is analyzed in this way, the average annual fatalities are shown in Figure 2.

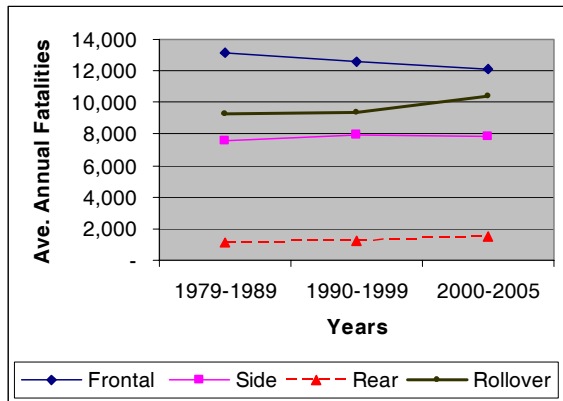


Figure 2. Average Annual Fatalities in Vehicles by Damage Area, with Rollover Separated - FARS

Using the same separation of rollovers as in Figure 2, the changes in fatalities when fire was the most harmful event can be examined. The results are plotted in Figure 3.

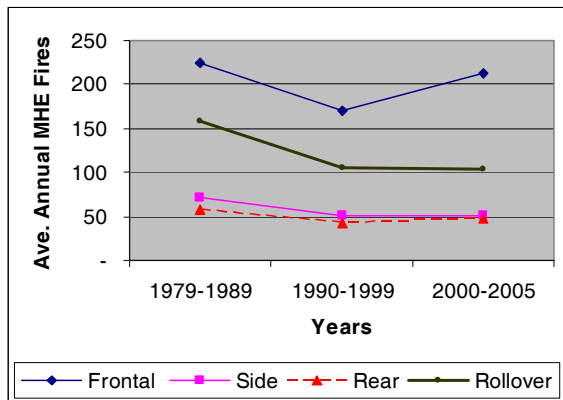


Figure 3. Average Annual Fatalities with Fire as the Most Harmful Event by Damage Area, with Rollovers Separated - FARS

Figure 4 shows the distribution of damage for the rollover fatalities in FARS years 2000 to 2005. The figure compares all rollover fatalities and rollover fatalities with fires. In the figure, non-collision and top damage were combined under “Roll”. Left and right side damage were combined. “UCarr” is an abbreviation for undercarriage damage.

FARS does not provide data on fire origin and the designation of crash direction is by damage area. NASS provides better information on these variables and can be used in conjunction with FARS to gain a better understanding of collision related fires.

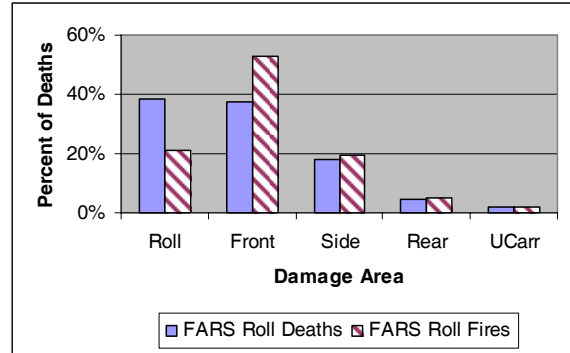


Figure 4. Damage Areas in Rollovers with Fatalities and Rollovers with Fires and Fatalities - FARS 2000-2005

NASS/CDS is a sample of tow away crashes that occur on US roads each year. The sample scheme stratifies cases by the severity of the crash. The sample rate for minor crashes is much lower than for severe crashes. In order to expand the stratified sample to the entire population it represents, an inflation factor is assigned to each case in the NASS/CDS sample. When the data is processed using the actual number of cases investigated, the data is referred to as “unweighted” or “raw.” When the data is processed using the total of the inflation factors, the results should represent the total population of vehicles involved in tow-away crashes and the data is referred to as “weighted.” In the analysis to follow weighted data estimates are reported. The figures to follow are based on a more detailed analysis of fires in NASS from George Washington University [Kildare, 2006]. This report contains both weighted and unweighted estimates.

One of the most significant variables in the analysis of fire occurrence is crash direction (mode). This variable specifies whether a crash is frontal, near side, far side, rear or rollover. Crash direction was defined using a combination of documented variables - principal direction of force (PDOF), general area of damage (GAD1) and rollover (ROLLOVER). The following criteria were used to establish crash direction.

Frontal - Frontal crashes were determined to be any crash where the PDOF was 1, 11, or 12 o'clock or was at either 10 or 2 o'clock with the highest deformation location coded as front (F).

Side - Side crashes were determined to be any crash where the PDOF was 3 or 4 o'clock or was at 2 o'clock with the highest deformation location not coded as front (F) or where the PDOF was 8 or 9 o'clock or was at 10 o'clock with the highest deformation location not coded as front (F).

Rear - Rear crashes were determined to be any crash where the PDOF was 5, 6 or 7 o'clock.

Rollover - Rollover crashes were determined to be any crash where a rollover was indicated by the variable ROLLOVER. It is important to note that crashes with any involvement of rollover were included as a rollover crash. Multiple impacts with any other planar impact occurring first would be included as a rollover crash.

Other - All Crashes not meeting the criteria of the other aforementioned crash directions was labeled as 'Other.' Some of the vehicles in NASS do not have a PDOF assigned. These vehicles with unknown PDOF were included in the 'Other' category.

NASS/CDS classifies fires as either Minor or Major. These fire severities are defined as the following:

A Minor Fire is a general term used to describe the degree of fire involvement and is used in the following situations:

- Engine compartment only fire
- Trunk compartment only fire
- Partial passenger compartment only fire
- Undercarriage only fire
- Tire(s) only fire.

A Major Fire is defined as those situations where the vehicle experienced a greater fire involvement than defined under "minor" above, and is used in the following situations:

- Total passenger compartment fire
- Combined engine and passenger compartment fire (either partial or total passenger compartment involvement)
- Combined trunk and passenger compartment fire (either partial or total passenger compartment involvement)
- Combined undercarriage and passenger compartment (either partial or total passenger compartment involvement)
- Combined tire(s) and passenger compartment (either partial or total passenger compartment involvement)

About 50% of the fires in NASS/CDS are classified as "Major". This is true for both weighted and unweighted data [Kildare 2006].

Figure 5 shows the distribution of all crashes (with and without fires) and crashes with major fires by crash direction. The distribution of minor fires is generally similar to major fire distribution [Kildare 2006].

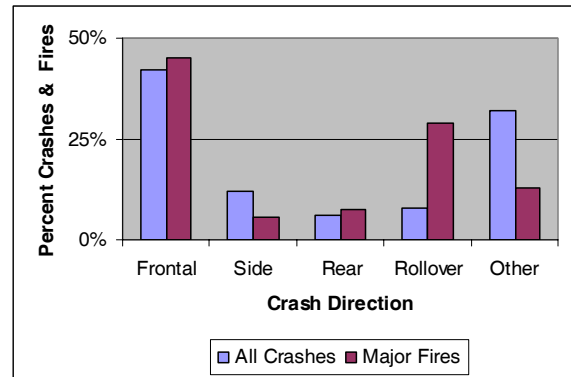


Figure 5. Distribution of Crashes and Crashes with Major Fires, by Crash Direction – NASS 1995-2004

Figure 6 shows the frequency of fires per 100 crashes for each crash mode. The denominator for the rate calculation is the total number of crashes in the crash mode under consideration.

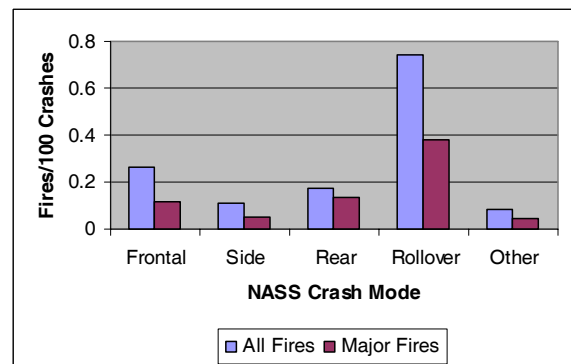


Figure 6. Rates of Crashes with Fires and Crashes with Major Fires, by Crash Direction – NASS 1995-2004

NASS also codes the fire origin. The distribution of the origins for major fires is shown in Figure 7. Over 60% of major fires originate in the engine compartment.

A further breakdown of major fire origins by frontal and rollover crash mode is shown in Figure 8. The engine compartment was the most frequent major fire origin for both the frontal and rollover crash modes. For the rollover crash mode, the fuel tank origin was a close second in major fire frequency.

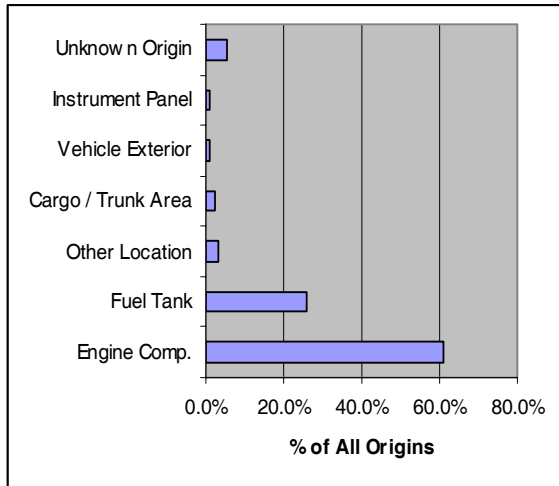


Figure 7. Distribution of Origins for Major Fires, All Crash Modes– NASS 1995-2004

Examination of individual cases of major fires in NASS 1997-2004 rollovers found that impacts prior to the rollover occurred in all cases with fuel tank fire origins for model year 1997 and later vehicles (Digges & Kildare, 2007). The study also found that seventy percent of the cases had engine compartment fire origins. About half of the cases with major engine compartment fires in rollovers did not involve significant impacts prior to the rollover.

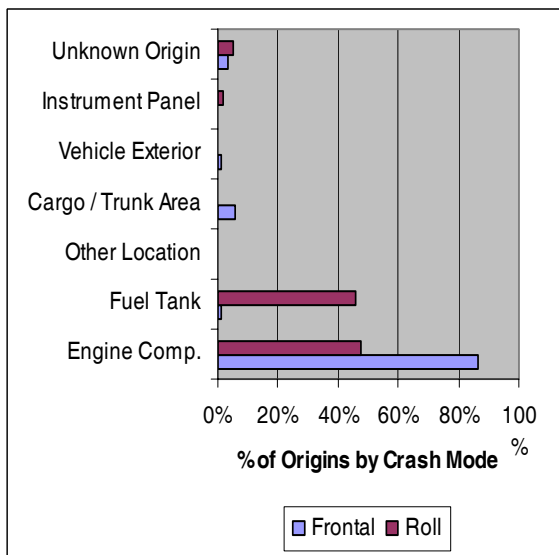


Figure 8. Distribution of Origins for Major Fires, Frontal and Rollover Crashes– NASS 1995-2004

The vehicle damage patterns exhibited by vehicles with fires in NASS have been analyzed and the results reported in a recent paper [Bahouth, 2006].

DISCUSSION OF FIRE DATA

As with other highway crash types, the rate of fires in fatal crashes per billion annual vehicle miles traveled has decreased significantly during the past twenty-five years. The decline is displayed in Figure 1.

During the same period, the annual average number of fatalities in vehicles with frontal damage has decreased, while fatalities in rollovers have increased. These trends are shown in Figure 2.

Except for frontal crashes, there is a downward trend in the annual number of fatalities where fire was the most harmful event (MHE). This trend is shown in Figure 3. However, for frontal damage crashes, the trend for fatalities with fire as the most harmful event has been upward during the past five years. During this same period, Figure 2 shows that the overall trend in fatalities in vehicles with frontal damage has been downward.

Figure 4 presents data on the location of vehicle damage in fatal rollover crashes. An examination of the vehicle damage areas in rollovers shows that the majority of FARS rollovers with fires also have frontal damage. These rollovers with frontal damage also have the highest fire rates. The lowest fire rates are in rollovers that have top damage or damage from the ground (non- collision). These latter two classes contribute about 20% of the rollovers with fires and fatalities.

The NASS data for major fires generally confirms the FARS data with regard to frequency of fires by crash direction or vehicle damage area. Figure 5 shows that nearly half of major fires are in frontal crashes. Rollovers contribute about 30% of the major fires and have the highest fire rate. The high fire rates for rollovers relative to the other crash modes are displayed in Figure 6.

Figures 7 and 8 provide information on the origins for major fires. Figure 7 shows that over 60% of major fires in NASS have their origins in the engine compartment. Figure 8 shows that for frontal crashes, over 80% of the major fires originate in the engine compartment. For rollovers, 47% originate in the engine compartment. This data indicates an opportunity to further improve fire safety by controlling engine compartment fires.

The lethality of engine compartment fires depends on the time available between the ignition of the fire and the time required for it to penetrate the occupant compartment. In the event occupants are trapped or

immobile due to injuries, the rescue time also becomes a critical factor. Data on rescue times has been published earlier [Digges 2005]. The 75% percentile rescue time for FARS rural cases was 24 minutes.

Data on the fire penetration time for selected tests conducted by General Motors has also been published [Tewarson, SAE 2005-01-1555]. In three tests of crashed vehicles with fires ignited in the engine compartment, the time to occupant compartment fire penetration varied from 10 to 23.5 minutes. The tests showed that once flames from the engine compartment penetrated the occupant compartment, the time to untenability was extremely short – a maximum of 3 minutes. This short tenability time of the occupant compartment when exposed to intense flames further amplifies the need to prevent or control engine compartment fires and delay their penetration of the occupant compartment.

The challenge of controlling engine compartment fires has increased with time due to the increasing amount of plastics used in motor vehicles. The amount of combustible materials has increased from 20 lbs per vehicle in 1960 [NAS 1979] to 200 lbs in 1996 [Tewarson, 1997, Abu, 1998,]. Combustible plastics now constitute the major fire load (twice the weight and heat content of the gasoline) in a typical vehicle and these combustible materials are often ignited and contribute to the intensity of an automobile fire [Aherns, 2005; Friedman, 2005].

SUMMARY OF ENGINE COMPARTMENT FIRE TESTS AND MATERIALS FIRE PROPERTIES

Under a contract with MVFRI, the GM/DOT Settlement research program in motor vehicle fire safety has been summarized by a team of fire experts led by FM Global [Tewarson, Vols I, II and III, 2005]. Of particular interest has been the analysis of eleven, highly instrumented burn tests using crashed vehicles. These tests included underhood ignition scenarios and spilled fuel fires of an intensity that could be possible after a crash. The test results were summarized in an earlier ESV paper [Digges 2005].

Three of the vehicles that had undergone frontal crashes were then subjected to underhood fires with ignition sources either at the battery location or by the ignition of sprays and pools of mixtures of hot engine compartment fluids from a propane flame located in and below the engine compartment.

For the three crashed vehicle burn tests with ignition in and under the engine compartment, flame penetration time into the passenger compartment varied between 10 to 23.5 minutes. Once the flame penetrated the passenger compartment, the environment rapidly became untenable. The time between flame penetration and untenability of the passenger compartment varied from 48 seconds to 3 minutes.

The windshield and the bulkhead were the principal ports of entry for the flame spread into the occupant compartment. If the hood remained relatively intact, the fire tended to enter through openings in the bulkhead. The windshield was the principal flame entry port when it was directly exposed to flame as a consequence of openings in the hood near the base of the windshield. Whether the windshield is intact or broken as a result of the crash will also influence the rate of flame spread into the passenger compartment.

Additional research summarized test procedures to determine fire behavior of materials [Tewarson Vol 2 2005] and thermophysical properties of automotive plastics and engine compartment fluids [Tewarson Vol 3, 2005 and SAE 2005-01-1560, 2005]. Data on the toxicity and thermophysical properties of automotive plastics was reported by Southwest Research under a related research project funded by NHTSA and MVFRI [Battipaglia, 2003; Griffith, 2005]. A comparison of the fire properties of plastics used in aircraft with those used in automotive applications was reported by Lyon and Walters [Lyon 2005].

ENGINE COMPARTMENT FIRE SAFETY FEATURES

Possible countermeasures for engine compartment fires fall into three categories: (1) fire prevention, (2) delay in fire penetration of the occupant compartment and (3) fire suppression. The three areas will be discussed separately.

Fire Prevention

Considerable fire prevention technology is present in vehicles on the road. To assess this technology, a database of 2003 model year vehicles was assembled and the technologies were documented in a database [Fournier 2001]. Lists of available fire prevention technologies were summarized in subsequent papers [Fournier, SAE 2005-01-1423 and Report R06-20, 2006]. The design considerations discussed included:

- Structural crashworthiness of the vehicle frame
- Tank placement
- Fuel line routing/compliance
- Tank materials selection
- Fuel filler connections
- Electrical grounding
- Battery placement

The technologies that were reviewed included:

- Check valves for the tank filler tube
- Roll-over valves
- Shut-off mechanisms for electronic fuel pumps
- Returnless fuel systems that reduce the exposure to damage
- Crash sensing battery disconnects or cut-offs
- Collapsible drive shafts

Research was initiated to explore possible ignition sources for engine compartment fires. Tests were conducted by Biokinetics to measure engine compartment and exhaust component surface temperatures of four different classes of vehicles during driving conditions and when the vehicle was stopped after driving [Fournier, R04-13, 2004 and R06-23, 2006]. While driving uphill, the maximum temperature measured on the surface of the exhaust manifold varied from a low of 241 °C for a minivan to a high of 550 °C for a passenger car. Tests of underhood fluids showed that the minimum temperature of a hot surface to cause ignition was in the order of 310 °C for lubricants and 518 °C for coolants [Tewarson, SAE 2005-01-1650].

The Friedman Research Corporation used state police reported accident data to examine the frequency of fires in pickup trucks of the same model but with different engines. The state data showed that the eight cylinder (V-8) engines had a higher fire rate than the inline six cylinder engines. An obvious difference is the increased exposure of the exhaust manifold in the V-8 [Friedman, 2006].

A considerable difference was noted in the maximum temperature of exhaust components for different vehicles under similar operating conditions. Control of the maximum underhood temperature, as exhibited by the vehicle with the lowest exhaust temperature, could provide an opportunity for improved fire safety, by reducing the intensity of a possible ignition source.

The prevention of fluid leakage offers another opportunity for improved fire safety. A research program by Biokinetics investigated and documented the technology in present day vehicles to prevent fuel

leakage when lines from the fuel tank are severed [Fournier, R0-6-20, 2006].

Biokinetics conducted leakage tests on 20 fuel tanks to study the fuel containment technologies employed and their performance. The tests simulated a vehicle rollover by rotating a tank, filled to capacity, about an axis that when installed in a vehicle would be parallel to the vehicle's longitudinal axis. The tanks were rotated to seven discreet positions during the rollover simulation. None of the tanks leaked when all hoses were intact. In each position, the fuel system hoses were disconnected one at a time to represent a damaged or severed line and the resulting leaks were observed. The results of the testing showed that six of the tanks leaked in every orientation and ten leaked in some orientations. However, four did not leak with each of the lines severed and when subjected to all orientations. The results of these tests are discussed in more detail in earlier papers [Fournier, R04-06c, 2004; Digges, 2005].

Another recent paper by Biokinetics has documented in detail the technology that prevents leakage when lines are severed [Fournier R06-20, 2006]. This report also evaluates the technology available to prevent siphoning of the fuel from the tank after a fuel line is severed.

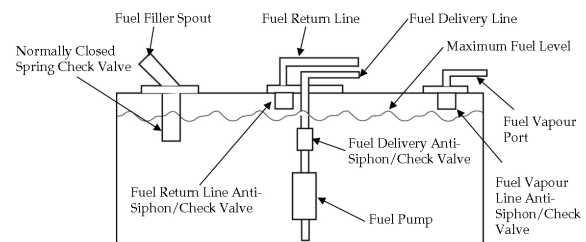


Figure 9 - Fuel Tank Leakage Prevention Components Found in Service (after Fournier, July 2006)

Some leakage prevention technologies currently incorporated in vehicles are illustrated in Figure 9. They include a check valve in the fuel filler spout, and check and anti-siphon valves in the fuel delivery line, the fuel vapor port and the fuel return line. Other leakage prevention technologies include inertia shut-off switches, logic built into engine computer controls and other monitoring devices that automatically shut down the fuel pump when a concern is detected. Some vehicles have eliminated the fuel return line, thereby reducing the opportunity for fuel to escape.

Delay of Fire Penetration

Test data and inspection of crashed vehicles with engine compartment fires indicates that there are two principal areas for fire entry into the occupant compartment – the firewall and the windshield. Once the flames breach the hood and impinge on the windshield, there is a large vulnerability to rapid occupant compartment penetration via a broken and collapsed windshield. If the flames are contained under the hood, the firewall becomes a vulnerable fire penetration area.

An opportunity for reducing the firewall vulnerability is by minimizing the area of openings through which the fire can penetrate. One approach to reduce openings studied during the GM/DoT research program was the use of intumescent materials that would expand with heat and close openings [Hamins, 2007]. The research was not successful with the intumescent materials that were used. Another suggested approach was to apply mechanical devices to close the largest openings. This approach was not investigated.

Even if technology is not applied to the firewall fire penetration problem, there are designs that may be beneficial. Competitive vehicles display large differences in the area of openings in the metal firewall. Typical examples are shown in Figures 10 and 11. Figure 10 shows a large opening on the left side for the heating and air conditioning system. The ducting for the system is flammable and could burn away in an engine compartment fire, providing an entry to the occupant compartment. The firewall in Figure 11 has a much smaller opening and, therefore, should be beneficial in resisting the penetration of flames into the occupant compartment.

Another path for flames to enter the occupant compartment is through the windshield. The fire shield offered by the firewall, hood and cowl can delay the spread of fire in the direction of the windshield. However, in recent vehicles, the metal in the cowl area has been replaced with combustible plastics. As a consequence, the opportunity for fire to burn through the cowl area and impinge on the windshield is increased.

Figure 12 illustrates that the plastic cowl between the hood and firewall burns away during an engine compartment fire. For crashes in which the hood remains intact, cowl designs to resist fire penetration could extend the time until flames impinge on the windshield and expose the occupant compartment to the fire.



Figure 10 – Vehicle Firewall with Large Openings



Figure 11 – Vehicle Firewall with Small Openings



Figure 12 – Vehicle with Plastic Cowl Consumed

During the MVFRI survey of fire safety technologies in new vehicles, several car sales personnel indicated that the underhood liners on their vehicles could serve as fire blankets and act to smother engine compartment fires. These claims prompted a research project to evaluate the fire resistant properties on underhood insulation materials. During

this project, Biokinetics measured the heat release rate of twenty different underhood liners to examine the extent that these materials might mitigate or aggravate the containment of an underhood fire [Fournier R06-23, 2005; Digges, 2006]. The results showed that the differences in heat release rate ranged over two orders of magnitude. The materials with the lowest heat release rate resisted combustion and could have aided in reducing the fire intensity. Those with the highest heat release rate contributed fuel to the engine compartment fire. There appeared to be no correlation between the cost of the vehicle and the heat release rate of the underhood liner. Additional specifications to improve the fire resistance of underhood liners could reduce the fuel load in the engine compartment and might contribute to reducing the fire growth rate.

Fire Suppression

Fire suppression of underhood fires is in the early stages and offers considerable promise. Several technologies have been researched and there are fire suppression products for a variety of applications on the market [Hamins, 2007]. In an earlier research project, University of Maryland demonstrated a foam based underhood fire suppression system [Gunderson 2005]. The system demonstrated the ability to extinguish an 80kW fire fed by a pool of fuel located near the battery.

One of the impediments to the deployment of an underhood fire suppression system is the lack of specifications to determine its efficacy. To assist in understanding the requirements for suppression systems specifications, a research project was undertaken by NIST. A summary report outlined the requirements and considerations for motor vehicle fire suppression, including suppression of underhood fires [Hamins, 2007]. Some of the considerations are as follows:

- Post-crash vehicle fires differ from fires in intact vehicles, as the geometric configuration may be modified by the collision in ways that cannot be precisely defined beforehand.
- The final orientation of the crashed vehicle may influence the fire ignition and growth rate, and the suppression system requirements.
- Underhood fires occur in a compartment that is partially open to the environment, which can lead to suppressant loss.
- The time of initiation of a fire after a collision can vary.
- Re-ignition of the fire may occur if the fire sources remain after the suppressant has been expended.

- Ambient factors such as temperature, wind, and incline of the road may influence suppression system performance.

CONCLUSIONS

Frontal and rollover crashes account for most major fires in NASS. The engine compartment is the most frequent origin of major fires in frontal and rollover crashes. The fuel tank is also a frequent origin of major fires in rollovers, but impacts prior to the rollover may be a major cause of fuel tank spillage in these events.

When examining 2000-2005 FARS fatalities with fire as the most harmful event, frontal damage crashes account for more than half of the population. Rollovers account for another twenty-five percent.

Controlling fires in frontal and rollover crashes offers the largest opportunity for fire safety improvements. A number of present-day vehicles incorporate technologies to prevent fuel leakage in rollovers. There are other technologies to delay the fire penetration into the occupant compartment. However, these technologies are not universally employed. Additional attention to the fire safety in frontal and rollover crashes is needed to offset the increased fuel load from combustible plastics that is present in today's motor vehicles.

ACKNOWLEDGMENTS

The author would like to recognize that funding for this research was provided by General Motors in accordance with the White, Monson and Cashiola vs. General Motors Settlement Agreement. The author also recognizes the valuable contributions of Dr. R. R. Stephenson in reviewing this paper in monitoring some of the research contracts on which the paper was based.

Further details of research and progress associated with this work may be obtained at: www.mvfri.org

REFERENCES

Abu-Isa, I., Cummings, D., LaDue, D., and Tewarson, A., "Thermal Properties and Flammability Behavior of Automotive Polymers," Paper No. 98-54-P-17, *16th International Technical Conference on Enhanced Safety of Vehicles*, Windsor, Canada, June, 1-4, 1998.

Ahrens, M., "U.S. Vehicle Fire Trends and Patterns," National Fire Protection Association, Quincy, MA, August, 2005.

Bahouth, G., "Analysis of Fire Related Crash Fatalities and Crashed Vehicle Rescue Times", MVFRI Report, March, 2007, www.mvfri.org

Bahouth, G., "Post Crash Exterior Crush Patterns and Motor Vehicle Fire Occurrence" SAE 2006-01-0789, 2006

Bahouth, J., and Kuznetsov, A., "Automotive and Fire Safety Research", The George Washington University, January, 2005. www.mvfri.org

Battaglia, K., Griffith, L., Huczek, J., Janssens, M., Miler, M. and Wilson, K., "Comparison of Fire Properties of Automotive Materials and Evaluation of Performance Levels", SwRI Project No. 01.05804, October 2003. www.mvfri.org

Committee on Fire Safety Aspects of Polymeric Materials, "Fire Safety Aspects of Polymeric Materials, Volume 8, Land Transportation Vehicles," National Materials Advisory Board, National Academy of Sciences, Publication NMAB 318-8, Washington, D.C., pp. 158, 1979.

Digges, K., and Kildare, S., "Fire Occurrence in Rollover Crashes Based on NASS/CDS", SAE 2007-01-0875, April, 2007.

Digges K., and Stephenson, R., "Summary of Recent Research in Crash-Induced Vehicle Fire Safety," SAE 2006-01-0551, April, 2006.

Digges, K. and Stephenson, R. "A Research Program to Study Impact Related Fire Safety" *19th International Technical Conference on the Enhanced Safety of Vehicles*, Washington DC., May, 2005.

Digges, K, Stephenson, R., and Bedewi, P., "Research Programs in Crash-Induced Fire Safety," SAE 2005-01-1425, April, 2005

Digges, K., Stephenson, R., and Bedewi, P., "A Research Program in Crash-Induced Fire Safety," SAE 2004-01-0475, March, 2004.

Digges, K., Stephenson, R., and Bedewi, P., "Fire Safety Performance of Motor Vehicles In Crashes," *18th International Technical Conference on the Enhanced Safety of Vehicles*, May, 2003.

Fell, J., "Interim Report to MVFRI on FARS Missing Data", Pacific Institute for Research and Evaluation, prepared for MVFRI, November 2004. www.mvfri.org

Fournier, E., and Bayne, T., "Anti-siphoning and Leak Prevention Technology Review," Prepared for Motor Vehicle Fire Research Institute by Biokinetics and Associates, Ltd., Report R06-20, September, 2006. www.mvfri.org

Fournier, E., and Bayne, T., "Assessment of Thermocouple Attachment Techniques for Measuring Exhaust Manifold Temperature" Prepared for Motor Vehicle Fire Research Institute by Biokinetics and Associates, Ltd., Report R06-23, September 2006. www.mvfri.org

Fournier, E. and Bain, T., "Cone Calorimeter Testing of Under Hood Insulation", Prepared for Motor Vehicle Fire Research Institute by Biokinetics and Associates, Ltd., Report R05-13b, August, 2005. www.mvfri.org

Fournier, E., Kot, J., and Sullivan, D., "Assessment of Fuel System Technology Use in 2003 Model Year Vehicles", SAE 2005-01-1423, April, 2005

Fournier, E. and Bain, T., "Underhood Temperature Measurements of Four Vehicles", Prepared for Motor Vehicle Fire Research Institute, by Biokinetics and Associated Ltd., Report R04-13, September, 2004. www.mvfri.org

Fournier, E., and Kot, J., "Comparison of Internal Tank Components – 20 Fuel Systems," Prepared for Motor Vehicle Fire Research Institute by Biokinetics and Associates, Ltd., Report R04-06c, July, 2004. www.mvfri.org.

Fournier, E., Bayne, T., and Kot, J., "Survey of the State-Of-The-Art in Fuel System Fire Safety – Phase II," Prepared for Motor Vehicle Fire Research Institute by Biokinetics and Associates, Ltd., R03-01, May, 2003. www.mvfri.org.

Fournier, E., and Keown, M. "Survey of the State-Of-The-Art in Fuel System Fire Safety – Phase I," Prepared for Motor Vehicle Fire Research Institute by Biokinetics and Associates, Ltd., R02-04 April, 2002. www.mvfri.org.

Friedman, K., Holloway, E., and Kenny, T., "Impact Induced Fires: Pickup Feature Design Analysis", SAE 2006-01-0550, April, 2006.

Friedman, K., Holloway, E., and Kenny, T., "Impact Induced Fires: Statistical Analysis of FARS and State Data Files (1978-2001)", SAE 2005-01-1421, April, 2005

Friedman, K., Holloway, E., and Kenny, T., "Final Report, Impact Induced Fires & Fuel Leakage: Statistical Analysis of FARS and State Data Files (1978-2001)", prepared for MVFRI by Friedman Research Corporation, July, 2003. www.mvfri.org

Griffith, L., Janssens, M., and Wilson, K., "Evaluation of Smoke Toxicity of Automotive Materials According to Standard Small-Scale Test Procedures", SAE paper 2005-01-1558, April, 2005.

Gunderson, J., and di Marzo, M., "Feasibility Study for a Vehicle Under Hood Nitrogen Foam Fire Suppression System," SAE paper 2005-01-1789, April, 2005.

Hamins, A., "Vehicle Fire Suppression Research Needs", NIST Report for MVFRI, February 23, 2007. www.mvfri.org

Judicial District Court "Agreement of Settlement, White, Monson and Cashiola vs. General Motors", Number 42,865, DIV."D", 18th Judicial District Court, Parish of Iberville, Louisiana, June 27, 1996.

Kildare, S, and Digges, K., "Analysis of Fire Occurrence in Automotive crashes Using NASS CDS Data (1994-2004), GWU Report, November, 2006. www.mvfri.org,

Lyon, R., and Walters, R., "Flammability of Automotive Plastics", Report prepared for MVFRI, August, 2005. www.mvfri.org

National Highway Traffic Safety Administration, "U.S. DOT/General Motors Settlement Agreement Status Report, Year 4", NHTSA 2001.

Tewarson, A., Quintiere, J., and Purser, J., "Post Collision Motor Vehicle Fires." Report prepared for MVFRI by FM Global Technical Report #0003018009, Volume I, October 2005. www.mvfri.org

Tewarson, A., Quintiere, J., and Purser, J., "Theory and Testing for the Fire Behavior of Materials for the Transportation Industry" Report prepared for MVFRI by FM Global Technical Report #0003018009, Volume II, October 2005. www.mvfri.org

Tewarson, A., Quintiere, J., and Purser, J., "Thermophysical and Fire Properties of Automobile Plastic Parts and Engine Compartment Fluids" Report prepared for MVFRI by FM Global Technical Report #0003018009, Volume III, October, 2005. www.mvfri.org

Tewarson, A., Quintiere, J., and Purser, D., "Fire Behavior of Materials in Vehicle Crash Fires and Survivability of the Passengers", SAE paper 2005-01-1555, April, 2005.

Tewarson, A., "Thermophysical and Fire Properties of Engine Compartment Fluids", SAE paper 2005-01-1560, April, 2005.

A. Tewarson, "A Study of the Flammability of Plastics in Vehicle Components and Parts, Technical Report FMRC J.I. 0B1R7.RC, Factory Mutual Research Corporation, Norwood, MA, October, 1997.

A FINITE ELEMENT MODELLING INVESTIGATION OF LOWER LEG INJURIES

**Michael Neale
Regis Thomas
Helen Bateman
David Hynd**

TRL Limited
United Kingdom

Paper Number 07-0077

ABSTRACT

A detailed finite element (FE) model has been developed of the human lower leg in order to investigate the mechanisms that cause severe ankle injuries in frontal impacts.

Predictions from the model have been validated against the results from two separate sets of sub-injurious and injurious PMHS tests. The model correlated well against the test results and it was estimated that a predicted von Mises stress of 120 MPa correlates to a predicted risk of injury to the calcaneus and talus bones in the model.

A series of predictive model runs were also carried out to investigate the influence that environmental and subject variations have on the predicted injury risk of the ankle. The set-up of all these model runs were based on sled impact tests in which PMHS legs were mounted on a sled rig with the feet resting on a heel and mid-foot pad. The environmental investigations included model runs with and without the heel pad and loading the foot in eversion and a neutral position. Subject variations investigated the influence that the stiffness of the ligaments joining the mid-foot to the hind-foot have on the predicted injury risk.

Without the heel pad there was considerable dorsiflexion of the foot and a predicted increased injury risk to the neck of the talus and a reduced injury risk to the calcaneus. Loading the foot in eversion it was predicted that the greatest injury risk was to the lateral aspect of the talus where the lateral malleolus of the fibula articulates with the talus. Increasing the ligament stiffness reduced the shearing motion in the joints between the mid-foot and the hind-foot and there was an increased injury risk to the neck of the talus.

INTRODUCTION

Injuries to the foot and ankle, as a result of automotive accidents, are typically not life threatening, but are relatively common and can

result in long-term medical complications and permanent disability (Owen *et al.*, 2001, Wheeler *et al.*, 2000). These complications can have dramatic consequences on the individual's quality of life and also amount to a sizeable societal cost (McMaster *et al.*, 2000).

Despite the known complications of ankle injuries the mechanisms conspiring to cause them are not fully understood. This presents difficulties in developing comprehensive and robust assessment techniques and/or injury criteria that could promote the design of effective countermeasures that will reduce the likelihood of debilitating ankle injuries.

Biomechanical testing can be used to develop the necessary understanding on ankle injuries, but biomechanical tests are often complicated by difficulties in obtaining quality test specimens in sufficient numbers and recreating realistic impact conditions. There are also ethical and physical restrictions that may limit the types of tests that can be carried out and the physical measures that can be made in order to appreciate fully the mechanisms contributing to the most debilitating ankle injuries.

As an alternative and complimentary means of developing an understanding of ankle injuries a finite element (FE) model of the human lower leg and ankle could be used. The expected benefits in using a leg model include:

- Carrying out virtual loading tests that would be difficult or impossible to achieve with physical tests;
- An ability to measure parameters that would be difficult or impossible to assess in Post Mortem Human Subject (PMHS) tests;
- A cost-effective means of completing large parameter sweeps investigating the influence that impact conditions and leg posture have on the injury risk to the ankle;
- Accurate and consistent control over the physical structure and material properties of the leg;

- The potential to alter and scale material properties and physical features of the leg model to match specific groups or individuals of the population;
- An ability to look at the sensitivity of the injury risk assessment criteria under different loading situations and severities.

As part of a three year lower leg injury research project funded by the UK Department for Transport (DfT) TRL Limited has developed a FE human lower leg model. This paper details the work carried out in developing the model and the validation of the model against two separate sets of PMHS test data (Wheeler *et al.*, 2000 and Hynd *et al.*, 2003). The paper also details the results from a series of predictive model runs carried out to investigate the influence that environmental and subject variations have on the predicted injury risk of the ankle.

THE FINITE ELEMENT MODEL OF THE LOWER LEG

The leg model was developed in the LS-DYNA FE software package. In total the model was structured from 59515 finite elements and 33444 nodes.

The Modelled Bones of the Leg, Ankle and Foot

The geometrical information used to create the separate bones of the model was purchased from a commercial library of 3D digital data (Viewpoint.com).

To simplify the structure of the model and reduce model run times the less important bones of the foot, with respect to injury risk, were modelled as a single non-deformable rigid body; this included the phalanges, metatarsals, cuneiforms, cuboid and navicular bones. The femur was also modelled as a single rigid body, in addition to the upper part of the tibia, fibula and patella (see Figure 1). These latter structures were modelled as a single rigid body in order that a rigid kinematic revolute (hinge) joint could be used to approximate the articulation of the knee joint.

All remaining bones of the leg model were represented as deformable bodies with elastic-plastic material properties. Each of these bones was modelled with an inner cancellous and outer cortical bone structure. The cancellous bone was modelled with solid elements and the cortical layer modelled with shell elements. Details of the structure and material properties of the bones in the model are provided in Table 1. With the exception of the tibia and fibula the material properties and thicknesses of the bone layers were based on values

presented in the published literature (Yamada, 1970 and Beillas *et al.*, 2001).

The cortical bone layer thicknesses and material properties for the tibia and fibula were obtained through reverse engineering in which the properties of the bones were altered in a series of model runs until the model's predictions adequately matched the results from PMHS three-point bending tests on tibia and fibula bones carried out by Takahashi *et al.*, (2000 and 2003). As shown in Figure 2, the thickness of the cortical bone layer for the tibia was varied along its length to provide a better representation of the variation in cortical bone thickness for the tibia and the best approximation of the three-point bending test results.

Joints explicitly represented in the foot and ankle were defined by sliding contact interfaces between the surfaces of the modelled bones. This approach provided an accurate representation of the joints, as it relied on the geometrical shape of the bones and the ligament properties to control the range and limits of joint movement. The coefficient of friction for the joints was set at 0.01.

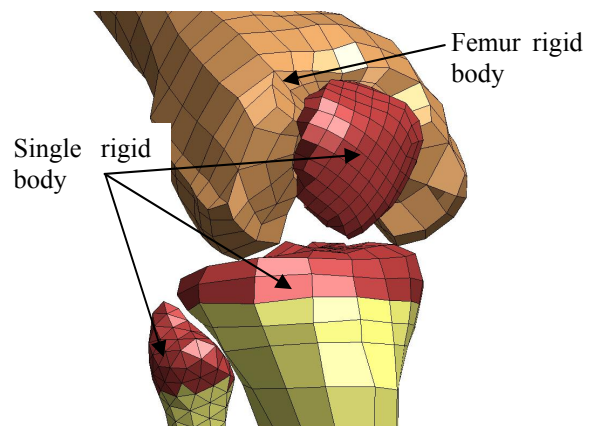


Figure 1. Parts of the tibia, fibula and patella modelled as a single rigid body.

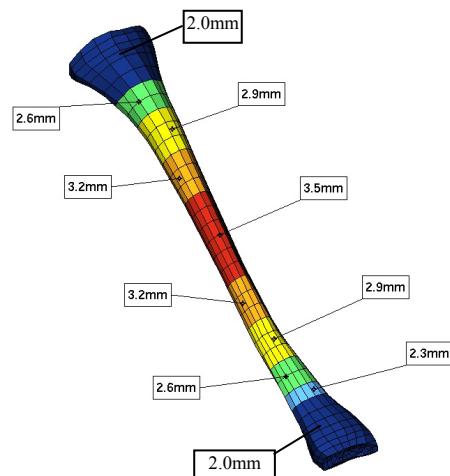


Figure 2. The distribution in the thickness of the cortical bone layer in the modelled tibia.

Table 1. Structure and material properties of the leg model's bones.

| Bone | Bone Type | Element Type | Material Type | Thickness | Density (kg/m ³) | Young's Modulus (MPa) | Poisson's Ratio | Yield Stress (MPa) | Plastic Modulus (MPa) |
|---|------------|--------------|---------------------|-----------|------------------------------|-----------------------|-----------------|--------------------|-----------------------|
| Femur | N/A | Shell | Rigid | N/A | 2000 | 16000 | 0.3 | N/A | N/A |
| Tibia | Cortical | Shell | Elastic/ Plastic | Figure.2 | 2000 | 16000 | 0.3 | 120 | 1000 |
| | Cancellous | Solid | Elastic/ Plastic | N/A | 1600 | 300 | 0.3 | 10 | 56 |
| Fibula | Cortical | Shell | Elastic/ Plastic | 3.0 | 2000 | 17050 | 0.3 | 120 | 2250 |
| | Cancellous | Solid | Elastic/ Plastic | N/A | 1600 | 300 | 0.3 | 10 | 56 |
| Patella | N/A | Shell | Rigid | N/A | 2000 | 13500 | 0.3 | N/A | N/A |
| Talus | Cortical | Shell | Elastic/ Plastic | 1.0 | 2000 | 13500 | 0.3 | 90 | 2250 |
| | Cancellous | Solid | Elastic/ Plastic | N/A | 1600 | 300 | 0.3 | 10 | 56 |
| Calcaneus | Cortical | Shell | Elastic/ Plastic | 1.0 | 2000 | 13500 | 0.3 | 90 | 2250 |
| | Cancellous | Solid | Elastic/ Plastic | N/A | 1600 | 300 | 0.3 | 10 | 56 |
| Navicular, Cuboid, Cuniforms, Metatarsals, Phalanges | N/A | Shell | Rigid | N/A | 7200* | 13500 | 0.3 | N/A | N/A |

*Density artificially increased to allow for the missing flesh surrounding the foot, as detailed later in the paper section covering "The Modelled Flesh".

The Modelled Ligaments and Tendons

Altogether 26 ligaments were represented in the model, choosing those that would have the greatest influence on the impact response of the lower leg and ankle. At the knee the cruciate, collateral, anterior ligament of the head of the fibula and the inter-osseous ligament between the tibia and fibula were modelled. The modelled ligaments surrounding the foot and ankle joints are detailed in Figure 3.

The location and geometrical size of the ligaments in the model were based on subjective examinations of images in published sources such as Gray's Anatomy and information available on the internet (e.g. www.bartleby.com). Advice on the anatomical structure of the model was also obtained from orthopaedic surgeons based at the Queen's Medical Centre Hospital in Nottingham in the UK.

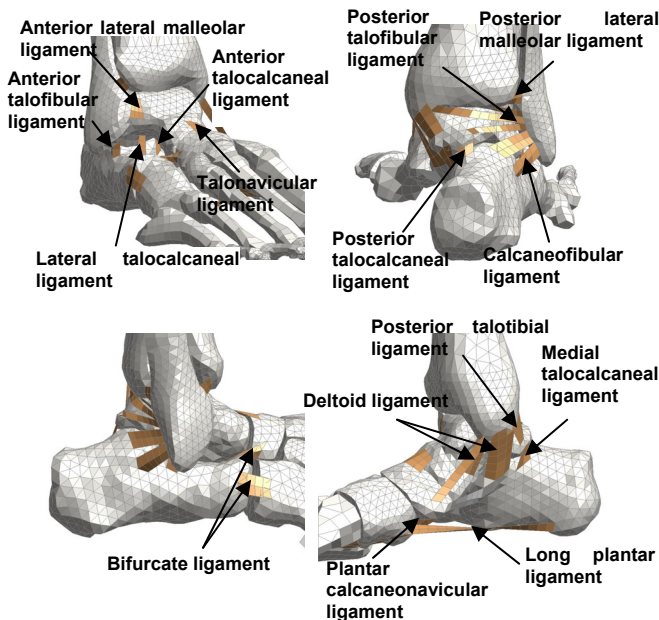


Figure 3. The modelled ligaments surrounding the foot and ankle joints in the leg model.

The stretching behaviour of ligaments is characterised by a 'J' shaped response, as shown in Figure 4. To represent this response in the model the ligaments were modelled with low stiffness shell elements with parallel sets of springs and damper elements attached to the nodal points of the shell elements, as shown in Figure 5. The shell elements were used to define contact between the ligaments and the bones, while the spring elements were used to create the characteristic 'J' shaped stretch response of ligaments. The dampers were used to remove erratic and unrealistic oscillations observed in the ligaments when stretched.

Material properties for the ligaments were initially based on preliminary results from PMHS ligament stretch tests carried out by Lowne *et al.*, (2001) and information on ligament behaviour presented in Yamada (1970). Reverse engineering was then used to fine tune and balance the material properties of the ligaments using the results from a 'basic' series of ankle articulation tests carried out by McMaster *et al.*, (2000) on 21 fresh frozen PMHS lower legs. The articulation tests investigated the torque rotation characteristics of the ankle in inversion, eversion, dorsi-flexion and plantar-flexion. The leg model was set up to match the test configuration of McMaster and the modelled ligament properties were altered between repeated model runs until a good correlation was obtained between the model's predictions and the PMHS test results.

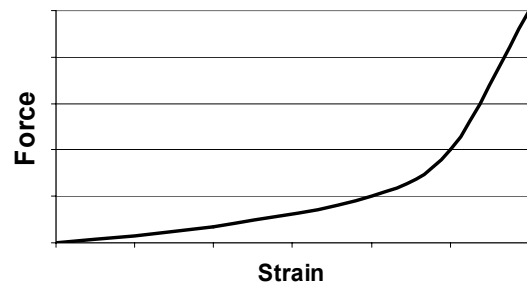


Figure 4. The characteristic 'J' shape stretch response of ligaments.

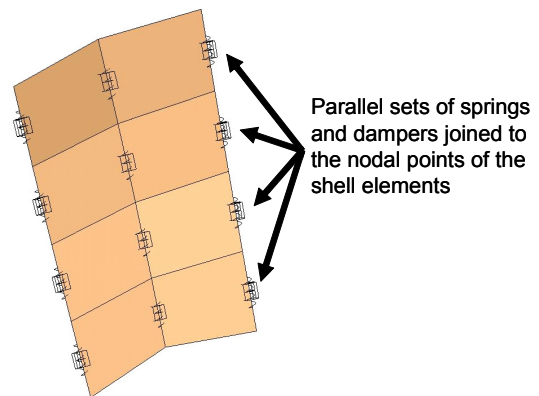


Figure 5. Structure of the ligaments in the leg model.

It is understood that ligaments are in an initial state of tension even when joints are in a neutral position. It was considered important to represent this initial state of ligament tension in the model. This was achieved by defining initial extended offsets in the ligament springs (Figure 5) and the model was run for an effectively infinite length of time in order to achieve an initial balanced and steady-state set-up for the leg model and the ligament offsets. It was rationalised that in a neutral position, when the leg is not supporting the body

weight, that the load through the articular surfaces of the ankle joints due to initial tensions in the ligaments and hydrostatic pressure would be approximately 30-40 N. This value was used as a basis to set the initial offsets in the springs of the modelled ligaments.

In order to simulate the loading conditions under which the model was validated, as detailed later in the paper, it was necessary to represent the Achilles tendon in the model. This tendon was modelled using inelastic seat-belt elements attached to the calcaneus at one end and to an Achilles spring at the other (see Figure 6). The seat-belt elements passed through a seat-belt slip-ring positioned close to the distal end of the tibia in order to tether the tendon closer to the tibia and make the line of action of the tendon more representative of the *in-vivo* situation.

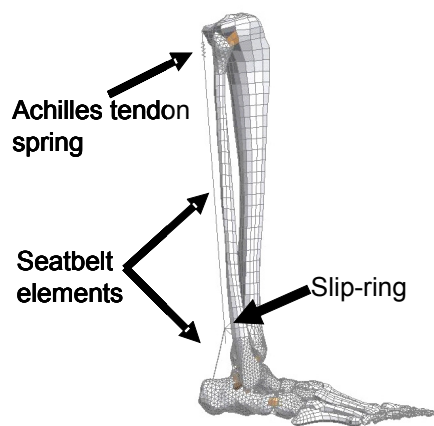


Figure 6. Set-up of the Achilles tendon in the human leg model.

The Achilles spring was connected between the seat-belt elements and the rigid part of the tibia as detailed in Figure 1 above. The spring was introduced so that initial offsets could be set in the spring in order to represent initial active loads in the tendon due to active muscle responses.

Two further 'hypothetical' ligaments were also introduced into the model to represent the soft anatomical features, such as ligaments, tendons and flesh not explicitly represented in the model. The decision to introduce these 'hypothetical' ligaments was based on the results of preliminary model runs where it was found during dorsiflexion of the modelled foot that the talus came away from the tibia creating a large gap between the articular surfaces of these bones, as shown in Figure 7. It was apparent from observations of the model animations that the talus pivoted against the tibia rather than the bones rotating or sliding against each other as expected.

It was believed that the pivoting motion of the talus was due to an imbalance of the ligament forces surrounding the talocrural joints. To compensate for the imbalance and resolve the problem of the pivoting talus it was decided to introduce two additional ligament springs in the model to act as 'hypothetical' ligaments to help correctly control the motion of the talus. A ligament spring was added between the fibula and the front of the calcaneus and a further ligament spring was introduced between the rear of the tibia and the calcaneus, as shown in Figure 8. Properties for these springs were consistent with the properties that were used for the other ligaments in the model. As shown in Figure 7 the introduction of the two 'hypothetical' ligaments improved the motion of the talus during dorsiflexion.

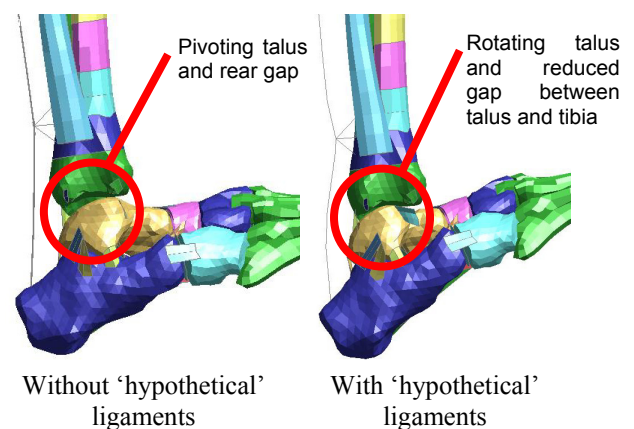


Figure 7. Change in the rotation of the talus with the introduction of two 'hypothetical' ligaments.

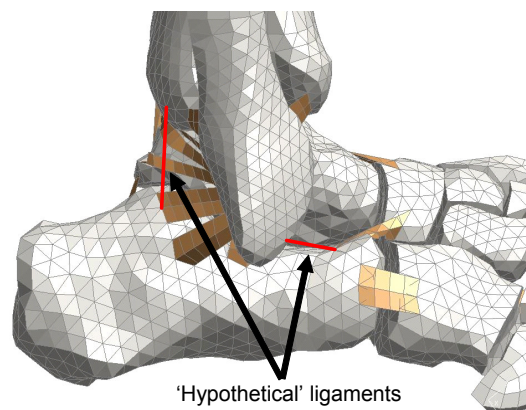


Figure 8. The two 'hypothetical' ligaments added to the leg model.

The Modelled Flesh

The geometrical data for the leg flesh was purchased from 'Viewpoint.com'. The flesh geometrical data provided an external boundary for creating the FE mesh of the flesh (see Figure 9) and the modelled bones provided an internal boundary. A tied surface contact was used to fix the modelled

flesh to the external surfaces of the bones. This avoided the problem of matching and merging the mesh of the flesh with that of the bones.

Flesh was not modelled around the foot because of the relatively greater geometrical complexity of the model in this region. In order to allow for the absence of flesh in this region weight was added to the bones of the modelled foot by scaling the density of the modelled bones, as detailed in Table 1 above.

Material properties for the flesh were derived using data from compression and indentation tests carried out on PMHS leg flesh samples (Untaroiu *et al.*, 2005). Based on this data the viscoelastic material model in LS-DYNA was found to provide the most efficient model for characterising the dynamic behaviour of the flesh.

MODEL VALIDATION

Results from two sets of sub-injurious and injurious PMHS tests were used to validate the predictions of the leg model:

- Pendulum impact tests;
- Sled impact tests.

The Pendulum Impact Tests

Wheeler *et al.* (2000) reported on sub-injurious pendulum impact tests carried out on eight PMHS leg specimens in order to develop biofidelity target corridors. A rigid pendulum impactor instrumented with a single axis accelerometer was used to impact the PMHS feet. The impact occurred on the plantar surface of the PMHS feet, centred at the level of the ball of the foot (Figure 9).

The pendulum weighed 1.5 kg and had an initial impact velocity of 6 m.s⁻¹. In the tests a constant load of 960 N was developed in the Achilles tendon. Pre-impact, a stirrup was placed around the foot to prevent plantar flexion of the foot due to the Achilles load. An equivalent Achilles load was generated in the model by modifying the characteristics and offset in the modelled Achilles tendon spring. Pre-impact plantar flexion of the modelled foot was prevented by initially resting the plantar surface of the modelled foot against a rigid contact plane. This contact plane was removed immediately after the pendulum struck the modelled foot.

In the model the pendulum impacted a 10 mm thick soft pad that was introduced to represent the flesh on the sole of the foot (Figure 9). This pad was rigidly fixed to the rigid forefoot of the model. The upper rigid part of the tibia, as shown in Figure 1 above, was also rigidly fixed in inertial space in order to represent the potting of the PMHS specimens in the Wheeler *et al.* tests.

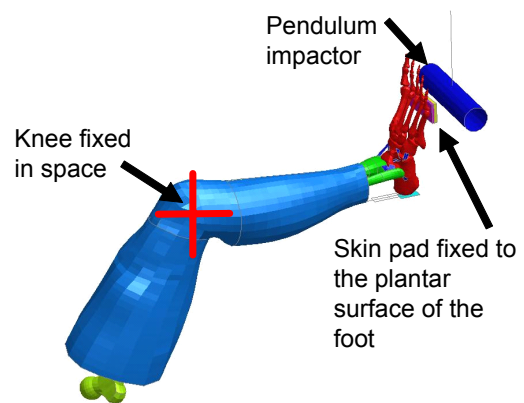


Figure 9. The set-up of the model for the pendulum impact tests.

The Sled Impact Tests

Figure 10 details the set-up of the sub-injurious and injurious PMHS sled impact tests reported by Hynd *et al.*, (2003). The design of the sled tests was intended to create the dual loading of the leg during automotive accidents caused firstly by the deceleration of the vehicle and pelvis, and secondly by the intrusion of the footwell. In the tests the deceleration of the vehicle and pelvis was characterised by the deceleration of the sled by a honeycomb energy absorber (A in Figure 10) and the footwell intrusion was represented by a foot plate on the rig impacting a separate honeycomb energy absorber (C in Figure 10). The design of the sled impact resulted in the footplate moving in the aft direction relative to the sled rig 30 ms into the impact. In all the PMHS tests the deceleration of the sled rig was relatively constant. In contrast, the deceleration of the footplate was varied by impacting honeycomb of the same stiffness, but with widths of 40, 100 and 200 mm, respectively representing low, medium and high severity impacts.

In the tests the PMHS legs were above knee amputations and were secured to a purpose designed metal femur that allowed free biofidelic movement of the knee joint. The mid-part of the PMHS foot rested on a curved pad representing a brake pedal and an additional pad was used to support the heel of the PMHS foot. Both mid-foot and heel pads were mounted on the footplate of the sled rig. Each pad was covered with 'Velbex'(PVC) to represent the stiffness characteristics of a shoe.

The PMHS legs were secured in position using a knee restraint, as shown Figure 10. The restraint looped over the top of the metal femur and represented the active extension response of the knee in pre-crash emergency braking. In addition a constant Achilles tension force of 500 N was

generated in the tests using a pressurised pneumatic cylinder (D in Figure 10).

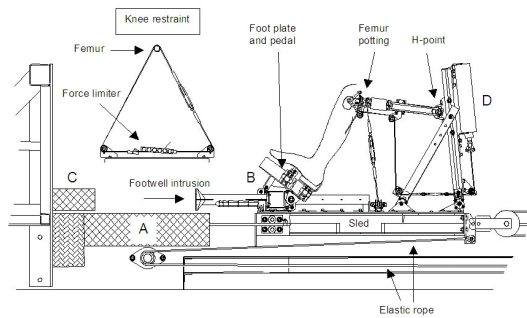


Figure 10. Schematic of the sled impact tests of Hynd *et al.* (2003).

Figure 11 shows the set-up of the model for simulating the sled impact tests. In this figure the leg flesh has been removed, but the flesh was present for the simulations.

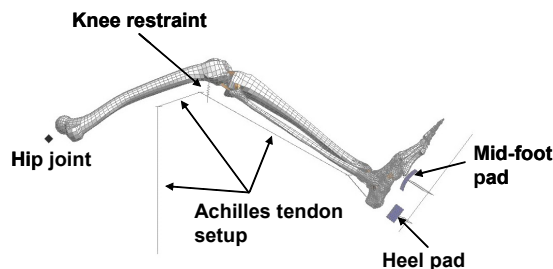


Figure 11. The leg model set-up for the sled impact tests.

The head of the modelled femur was fixed in inertial space using a rigid kinematic revolute (hinge) joint. This set-up represented the connection used to fix the metal femur to the sled rig in the sled tests. A spring, with a constant spring force characteristic of 760 N, was used to represent the knee restraint and a series of very stiff seat belt elements and slip-rings were used to represent the set-up of the Achilles tendon attachment. The seat-belt elements were attached to a single spring, fixed to inertial space, which had a constant spring force characteristic of 500 N to represent the pneumatic cylinder used in the tests.

Comparable to the tests the modelled foot rested on a mid-foot and heel pad. Two layers of material were simulated on the pads; the first represented the Velbex fixed to the pads in the tests, the second layer represented the skin on the sole of the foot. The model was loaded by applying the sled deceleration to the whole leg model. In addition to this a separate acceleration was applied to the modelled mid-foot and heel pads to represent the relative acceleration between the footplate and the sled rig.

Validation Results - Pendulum Impact Tests

The predicted pendulum acceleration was compared against a corridor of results obtained from the eight PMHS pendulum impact tests (see Figure 12). The model over-predicts the peak upper corridor response by approximately 20 g (13%). The model predicted a second smaller peak acceleration of 80 g at 10 ms that closely matched the magnitude, but not the timing, of the second peak observed in the PMHS test corridor.

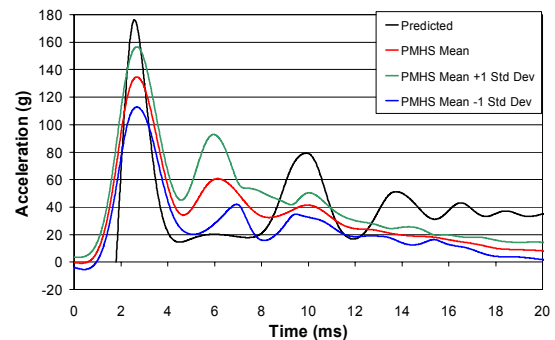


Figure 12. Comparison of the predicted and measured PMHS pendulum accelerations reported by Wheeler *et al.* (2000).

Validation Results – Sled Impact Tests

Predicted heel and mid-foot pad impact forces were compared against comparable measures made in the low, medium and high severity sled impact tests. In order to assess the capability of the model to predict ankle injuries, predicted von Mises stresses in the model were compared against the injury patterns found in the PMHS test specimens post impact.

Heel and Mid-foot Pad Forces – In Figure 13 predicted heel and mid-foot pad forces for the low, medium and high severity impacts are compared against comparable results from three PMHS tests carried out at each impact severity. It is noticeable that there are considerable differences in the predicted and measured forces in the early stages of the impact. Between 10 and 30 ms predicted heel and mid-foot pad forces rise to approximately 2 kN, while measured heel and mid-foot pad forces are relatively steady over this period at 1 kN and 2 kN respectively. These differences are attributed to the fact that in the tests the PMHS feet were balanced on the heel and mid-foot pads pre-impact. In contrast the modelled foot was not balanced on the heel and mid-foot pad pre-impact because of time limitations in carrying out the validation work. Consequently this resulted in the modelled foot impacting the heel and mid-foot pad during the initial sled rig deceleration, while the PMHS feet pressed against the heel and mid-foot pads in the early stages of the impact (<30 ms).

Following the initial deceleration of the sled rig and the onset of the secondary footplate pulse at 30 ms, there is better correlation between the measured and predicted heel pad forces. In comparison greater differences are observed between the measured and predicted mid-foot pad forces after 30 ms. For instance, under the medium severity impact conditions the peak measured mid-foot forces are approximately twice as large as the predicted results. It is anticipated that this difference is a result of the ligaments joining the hind-foot to the mid-foot being weaker in the model compared to those in the PMHS feet. This was suggested in the animations for the model runs where it was noticed that there appeared to be excessive motion and shearing in the joints between the mid and hind-foot. This was later investigated in a series of predictive model runs that are detailed later in the paper.

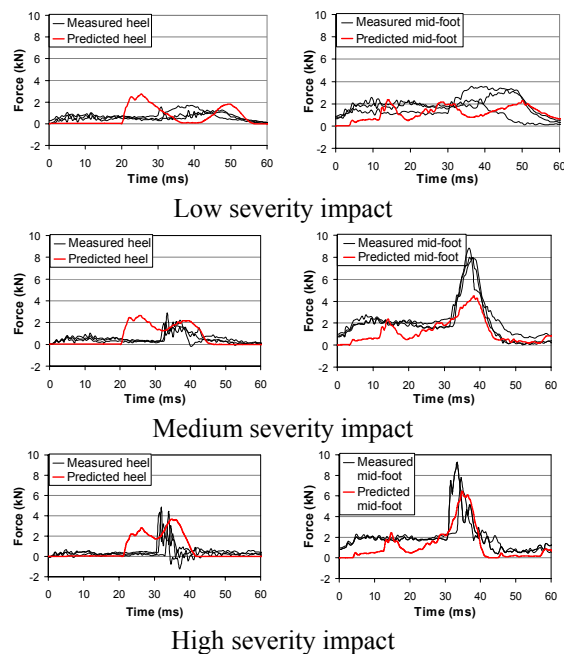


Figure 13. Comparison of the predicted and measured heel and mid-foot pad forces from the PMHS sled tests reported by Hynd *et al.* (2003).

Injury Prediction - Hynd *et al.* (2003) reported that in general the low severity impacts into the 40 mm honeycomb did not initiate injuries in the PMHS legs. This test was therefore used to set a threshold injury limit for the model's predicted von Mises stresses. The maximum predicted von Mises stress in the calcaneus and talus for the low severity impact peaked at approximately 120 MPa. Consequently, this threshold was used as the criteria for predicting injury with the model.

Calcaneus fractures were consistently found in the in the PMHS sled tests in which injuries occurred, although some fractures to the talus and tibia were

also noted. In line with the injury results the model predictions also indicated a predominance of calcaneus injuries and a reduced likelihood of talus injuries. As shown in Figure 14, for the low severity impact the predicted von Mises stress threshold of 120 MPa is reached in a small region on the calcaneus, but the stress threshold is reached over a greater area of the calcaneus for the medium and high severity impacts. This predicted stress pattern approximates the location of the intra-articular calcaneus fractures observed in the PMHS legs, as shown in the X-ray image in Figure 14. In contrast peak predicted von Mises stresses in the talus did not rise above 120 MPa to the same extent that they did in the calcaneus.

Resultant predicted loads in the intra-articular surfaces between the calcaneus and talus peaked at approximately 2 kN for the low severity impact, up to 2.6 and 3.8 kN for the medium and high severity impacts respectively. Comparable loads against which the model's predictions could be compared were not measured in the tests.

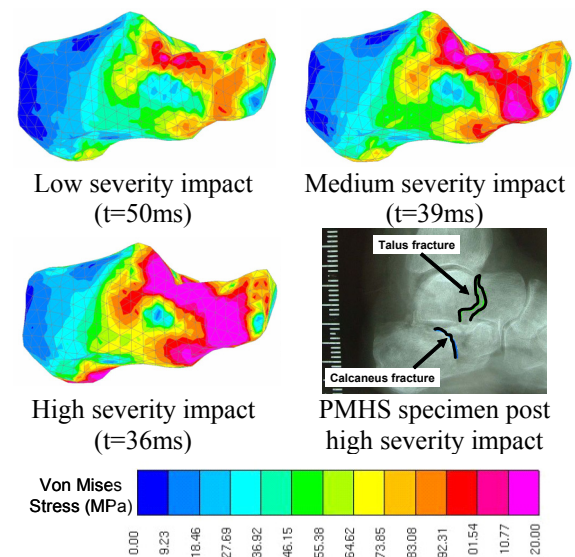


Figure 14. Predicted peak von Mises stresses in the calcaneus compared against observed injuries in a PMHS leg.

Predictive model runs

Two sets of predictive model runs were carried out to investigate the influence that environmental variations have on the predicted injury risk. A further set of model runs were carried out to investigate the influence that subject (ligament stiffness) variations have on the predicted injury risk from the model. The set-ups of all these model runs were based on the PMHS sled impact test conditions under which the model was previously validated.

Environmental Variation – Heel Pad Influence on Predicted Injury Risk

An additional model run was carried out to investigate the influence of removing the heel pad (Figure 11 above) from the medium severity sled impact conditions. The predictions from the medium severity simulated sled impact conditions, obtained in the leg model's validation, provided a baseline against which the predictions from this additional model run were compared.

Environmental Variation – Effect of Eversion on Predicted Injury Risk

Further to the medium severity sled impact model run a further model run was carried out in which the foot, heel pad and mid-foot pad were set at 21° of eversion. The alteration in the set-up of the model for this additional model run is shown in Figure 15. The predictions from the medium severity sled impact conditions, obtained in the validation of the leg model, provided a baseline or neutral response against which the predictions from the additional model run were compared.

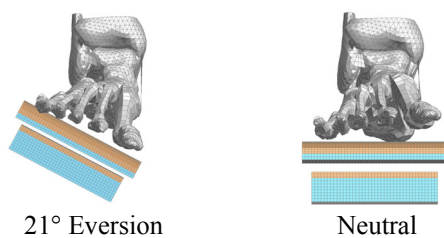


Figure 15. Variation in the eversion of the leg model for the predictive model runs.

Subject Variation - The Effect of Ligament Stiffness on Predicted Injury Risk

One of the main issues arising from the validation of the model against the sled impact test results concerned the predicted mid-foot pad forces which were lower than those measured in the PMHS tests. Furthermore excessive motion and shearing was predicted in the joints in the mid-foot region. There were concerns that the differences in the measured and predicted pad loads and the excessive motion in the mid-foot joints could be because of weak properties defined for the ligaments connecting the mid and hind-foot. In response to these concerns, two model runs were carried out to investigate the influence that the stiffness of the ligaments joining the mid-foot to the hind-foot would have on the model's predictions.

Both model runs were carried out under the high severity sled impact conditions, but in comparison to the validation model runs the heel pad was positioned 23.5 mm closer to the modelled heel. It

was felt that moving the heel pad would increase the loading across the foot and assess better the influence that ligament stiffness has on the predicted injury risk of the leg.

For one of the model runs, termed the baseline model run, the set-up of the ligaments matched that used in the validation of the model. For the second model run the Young's modulus of the shell elements for the ligaments joining the hind-foot to the mid-foot, which included the Calcaneocuboid, Bifurcate (calcaneonavicular), Talonavicular and Plantar calcaneocuboid ligaments, were increased from 2 MPa to 1000 MPa, equating to a potential 500-fold increase in the ligament stiffness. The true increase in the stiffness of the ligaments would also be influenced by the parallel sets of springs knitted between the nodes of the ligament shell elements (as shown in Figure 5). It was expected that the chosen increase in the ligament stiffness would be adequate to reduce the movement and shearing in the joints of the mid-foot.

Results - Heel Pad Influence on Predicted Injury Risk

Figure 16 shows the predicted difference in the sled impact response of the ankle with and without the heel pad. With a heel pad the foot remains in a relatively neutral position during the impact. Without a heel pad there is extreme dorsiflexion of the foot.

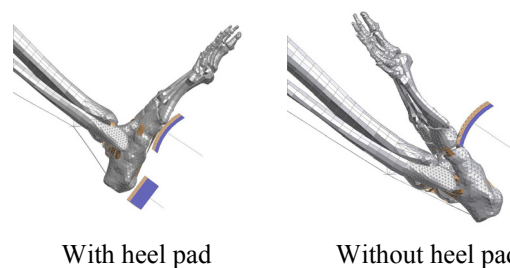


Figure 16. Predicted difference in the ankle response with and without a heel pad.

As in the validations of the model a von Mises stress threshold of 120 MPa was used to indicate an injury risk to the talus and calcaneus in the model. Differences in the peak von Mises stress predicted for the talus and calcaneus with and without a heel pad are shown in Figure 17. It is noticeable that without a heel pad there are large stresses surrounding the neck of the talus indicating an increased potential for this region of the talus to fracture under these loading conditions. These high stresses are initiated by the neck of the talus contacting the tibia due to the extreme dorsiflexion. In comparison peak talus von Mises stresses for the model run with a heel pad are concentrated on the articular surfaces of the talus.

Looking at the predicted stresses in the calcaneus these are generally greater and more widespread for the sled impact condition with a heel pad. The suggestion from these results is that without a heel pad (i.e. with large dorsiflexion) the talus is at a greater predicted risk of injury, and with a heel pad (i.e. a more neutral ankle position) the calcaneus is at a greater predicted risk of injury.

Despite the predicted differences in the injury patterns for the ankle with and without a heel pad the predicted peak loads in the joints of the ankle were similar for both model runs (Figure 18). However, the peak loading response was later in the run without a heel pad, than when the pad was present.

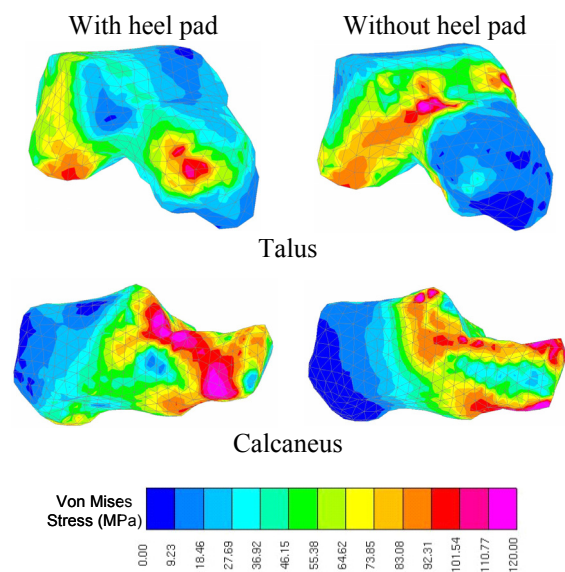


Figure 17. Differences in the peak predicted von Mises stress in the talus and calcaneus for the sled impacts with and without a heel pad.

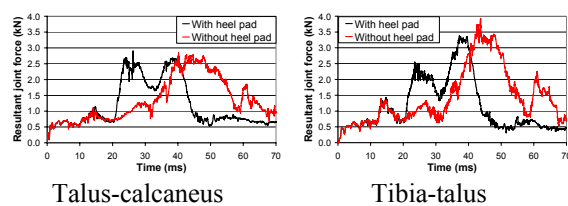


Figure 18. Resultant predicted loads in the joints of the ankle for sled impacts with and without a heel pad.

Results - Effect of Eversion on Predicted Injury Risk

With eversion there were greater predicted von Mises stresses on the lateral aspect of the talus, at the location where the lateral malleolus of the fibula articulates with the talus (Figure 19). These high stresses did not result from direct contact between the fibula and the talus as the fibula was

levered away from the talus by the calcaneus. It was therefore considered that the high stresses in the talus were due to direct loads between the calcaneus, talus and tibia. In contrast the maximum predicted von Mises stresses in the calcaneus were greatest for the neutral model run. It is implied from these results that with eversion the lateral aspect of the talus is at greatest risk of injury. The calcaneus is at greatest risk of injury under the neutral loading sled impact conditions.

The predicted ankle joint loads peaked at approximately 3.5 kN in both the neutral and eversion loading conditions (Figure 20). However, the greatest loads were predicted in the tibia-talus articular surface for the neutral impact conditions and the talus-calcaneus articular surface had the greatest predicted loads for the eversion impact conditions.

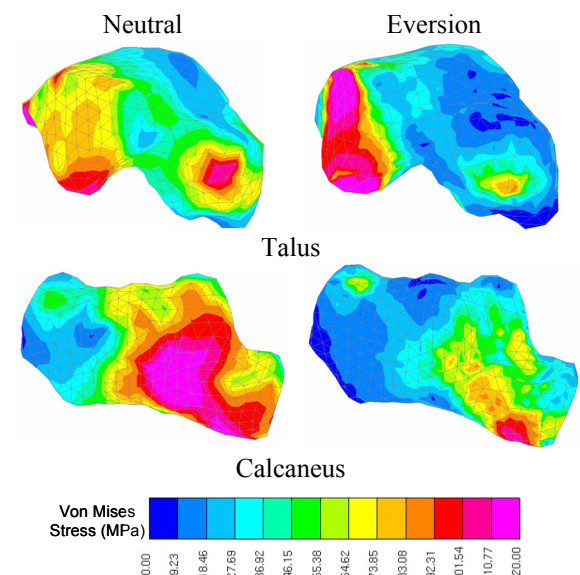


Figure 19. Difference in the peak predicted von Mises stress in the talus and calcaneus for the sled impacts with eversion and the ankle in a neutral posture.

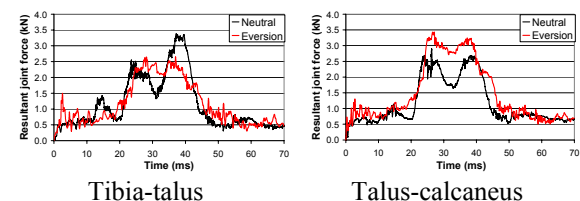


Figure 20. Resultant predicted loads in the joints of the ankle when loaded in eversion and a neutral posture.

Results – The Effect of Ligament Stiffness on Predicted Injury Risk

Stiffening the ligaments joining the hind-foot to the mid-foot reduced the amount of motion and

shearing in the joints in the mid-foot region (Figure 21). Weaker ligaments between the hind-foot and mid-foot reduced the amount of load going through the ankle joints (Figure 22). On the whole predicted forces in the ankle joints of the model with the stiffer ligaments were approximately 1.5-2 kN (37-78%) greater than those predicted for the baseline model run.

Stiffening the ligaments between the mid-foot and hind-foot increased the loading in the mid-foot and heel pads (Figure 23). In the validation of the leg model the predicted mid-foot pad forces were lower than those measured in the comparable PMHS tests, as shown in Figure 13 above. It is therefore possible that these differences could be caused by differences in the stiffness of the ligaments in the model compared with those in the PMHS specimens tested.

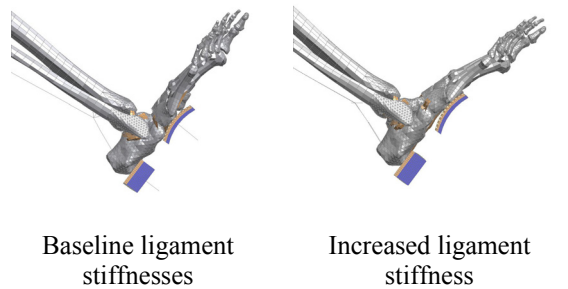


Figure 21. Change in the impact response of the foot with an increase in the stiffness of the ligaments joining the mid and hind-foot.

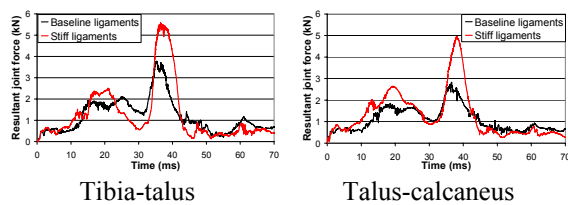


Figure 22. Resultant predicted loads in the ankle joints for sled impacts with baseline and stiffer ligaments joining the hind-foot to the mid-foot.

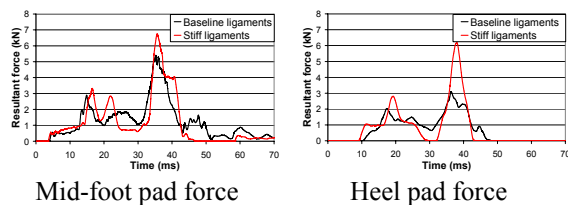


Figure 23. Resultant predicted loads in the mid-foot and heel pads for sled impacts with baseline and stiffer ligaments joining the hind-foot to the mid-foot.

Predicted von Mises stresses (Figure 24) exceeding the threshold injury limit of 120 MPa were more widespread in the model with the stiffer ligaments. Furthermore, it is also noticeable in the model with

the stiffer ligaments that there was a concentration of peak predicted von Mises stresses surrounding the neck of the talus, which was not predicted in the baseline model run.

DISCUSSION

Discussion - Model Development

A number of assumptions have been made in the development of the leg model that may have a considerable influence on the biofidelity of its behaviour. For instance, the fore-foot was modelled as a single rigid body and the flesh was not modelled. It is understood that these assumptions may limit the types of loading conditions that the model can be used to investigate.

In terms of the present study the injurious sled impact loads have centred on the mid-foot and heel regions with foot flesh added to the impacting surfaces. It is believed that the model is adequately developed to simulate these impact conditions, but further development of the model may be needed to consider a broader range and type of lower leg loading conditions. A benefit of the assumptions made in the development of the model is that they reduce the size, complexity and run times of the model. This will be an advantage when carrying out parametric investigations that involve considerable numbers of model runs.

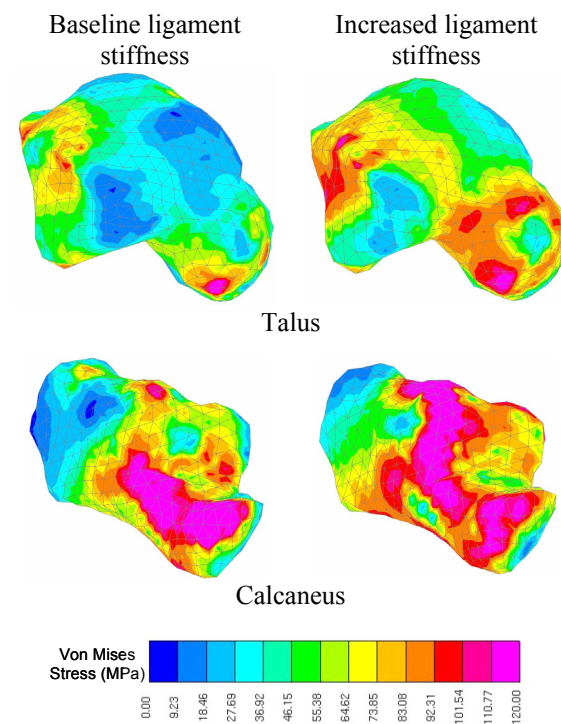


Figure 24. Differences in the peak predicted von Mises stress in the talus and calcaneus for the sled impacts with baseline and stiffer ligaments joining the hind-foot to the mid-foot.

Failure properties have not been defined for the ligaments and bones in the model. This is an important omission in the set-up of the model as the principal intention for developing the model was to investigate ankle and lower leg injuries. A lack of reliable biomechanical data was the principal reason for not defining failure properties in the model. Furthermore, in preliminary model runs in which failure properties were defined for the bones of the foot and ankle, unreliable failure of the bones occurred, especially at localised stress concentrations, e.g. where the ligaments insert into the bones. Consequently, thresholds of predicted stress, rather than failure properties were used to provide a more reliable and trustworthy method of predicting injury risk. This approach neglects changes in the load distribution in the ankle as yielding and failure of anatomical features occurs and limits the potential of the model to predict the global pattern of ankle injury following impact. Additional work is therefore needed to develop a comprehensive failure response for the model, but the current model can be used to identify the primary anatomical features at risk of injury in an impact.

With the exception of the Achilles tendon the leg model does not currently consider the bracing response in the leg caused by active muscle responses and the influence that this has on injury risk. Further work is needed to develop the principal tendons that control the response of the foot and ankle. This may supersede the need for the 'hypothetical' ligaments implemented in the model and this should improve the confidence in the biofidelic response of the model under a more diverse range of loading conditions.

Discussion - Pendulum Impact Validation

In comparison to the PMHS test results the model over-predicted the initial peak acceleration of the pendulum impactor by 20 g (13%). In this early stage of the impact it is anticipated that the response of the pendulum will be influenced by the mass of the foot and the stiffness and thickness of the impacting surfaces. The mass of the tested PMHS feet was not known and so it was not possible to match the modelled foot mass with the average mass of the tested feet. Estimates were also made for the thickness of the flesh pad struck by the pendulum in the model and the material properties for the pad matched the characteristics used for the flesh in the model. These uncertainties in the set-up of the model could contribute to the observed differences in the measured and predicted responses for the pendulum impact studies. Furthermore, the model has a rigid forefoot that could result in a greater effective impact mass and consequently greater peak acceleration of the

pendulum in the initial phase of the impact. It is considered that a parametric study of these variables in the model would be useful to identify the principal variable(s) that could contribute to the observed difference in the measured and predicted responses.

Discussion - Sled Impact Test validation

Limitations of time remaining on the project prevented the modelled foot from being correctly balanced on the heel and mid-foot pads for the simulated impacts. This contributed to considerable differences between the model's predictions and the PMHS results, especially in the early phases of the impact (<30 ms). It is expected that addressing this limitation in the set-up of the model would lead to a better correlation between the predicted and measured results for the sled impacts.

Despite the obvious limitation in the set-up of the model peak predicted von Mises stresses in the model correlated well against the consistent recorded injury of fractures to the calcaneus observed in the PMHS tests. Further to this injury, smaller numbers of injuries were recorded in the talus and tibia of the PMHS, although no equivalent indications were predicted by the model that these injuries would occur. It is most likely that the variations in the injury patterns observed in the test specimens could be due to uncontrollable factors in the tests such as the quality and size of the test specimens, the installation of the test specimens on the sled rigs and subtle variations in the impact conditions. In comparison the model is not influenced by these variables. However, a parametric study could be carried out with the model to assess the influence that these variables have on the predicted injury risk of the model. This would contribute to developing an understanding on the principal factors that contribute to debilitating ankle injuries.

Dubbeldam *et al.* (1999) completed parametric investigations with their MADYMO multibody model of the foot and ankle. For localised impacts to the sole of the foot they investigated how the impact conditions, foot dorsiflexion, Achilles tension, foot mass, and the position of joints in the foot influenced their model's predictions. They found that the mass of the foot had a limited influence on the model's predictions, while all the remaining investigated variables had a considerable influence on the predicted loads in the model. However, being a multibody model it was not possible to determine the injury risks to specific anatomical features, which would be possible with a FE model of the foot and ankle.

By comparing the model's von Mises stress predictions against PMHS test results in which ankle injuries did not occur, a predicted von Mises stress of 120 MPa has been determined as a preliminary threshold of injury risk to the talus and calcaneus in the model. Loads in the articular surfaces between these two bones reached values of 2.0 kN and in model runs in which injuries to the calcaneus were estimated to occur the loading between the articular surfaces of the two bones ranged between 2.6 and 3.8 kN. It is not certain how representative these values are of the threshold injury response of the ankle. It is anticipated that these values may well be model-specific and dependent on the type and pattern of loading applied through the bones. Further testing and modelling work is needed to establish the exact injury response of the ankle. However, the current results provide a positive basis on which to develop improved injury assessment techniques and/or injury criteria for severely debilitating ankle injuries.

Discussion – Heel Pad Influence on Predicted Injury Risk

Removal of the heel pad resulted in extreme dorsiflexion of the foot and a predicted injury risk at the neck of the talus. This result was very different from the situation when the heel pad was present when the principal injury risk was predicted to be at the calcaneus. Talar neck fracture has been previously linked to large dorsiflexion angles. The result therefore adds additional confidence in the biofidelic response and accuracy of the model to predict injury risks to the ankle under different loading conditions. It also suggests that the types of ankle injuries are sensitive to the loading conditions.

Discussion – Effect of Eversion on Predicted Injury Risk

Despite the identified limitations in the set-up of the model, it was suggested by the predictions that eversion would increase the injury risk to the lateral aspect of the talus. This is an important result as it suggests that the risks of ankle injuries are sensitive to the posture of the foot in the impact. Current injury criteria and test protocols fail to consider the influence that foot posture has on ankle injury risk. Further work is needed to determine the full implications that foot posture has on ankle injury risk.

Discussion – The Effect of Ligament Stiffness on Predicted Injury Risk

In the validation of the model against the sled impact results it was anticipated that differences in

the model's predicted mid-foot forces and those measured were because of poorly defined properties for the ligaments joining the mid-foot to the hind-foot. The predictions from the model runs investigating ligament stiffness effects confirmed that stiffening the ligaments between the hind-foot and mid-foot can increase the loading on the mid-foot pad for the sled impact conditions. It was further found that this had a considerable influence on reducing the shearing and motion in the joints between the hind-foot and mid-foot, which was a further problem identified in the model validation against the sled impact PMHS test results.

The stiffer ligaments also resulted in different injury risk patterns with high stresses concentrated around the neck of the talus. In contrast the model did not predict an injury risk to the talus in the sled impact test validation model runs with the baseline ligament stiffnesses. Consequently, based on predictions from the model runs investigating ligament stiffness effects, differences in the predicted and recorded injuries could be attributed to inherent variations in the biomechanical tolerance of the test specimens. The results from this set of predictive model runs highlight the importance of correctly defining the ligament properties in the model in order to predict accurately the injury risk to the foot and ankle. There is obviously a need for further biomechanical testing to develop this knowledge and understanding.

Similar to the present study Beillas *et al.* (1999) experienced problems in defining ligament properties in their foot and ankle model. To address these uncertainties they carried out a parametric study investigating the influence that ligament properties had on the predictions from their model. Ligament stiffnesses in their model were scaled by factors of 0.2, 1 and 5. In contrast to the results of this present study they found that these changes had only a limited influence on the predictions from the model under dynamic impacts, but considerable variations in the model's predictions occurred under static loading conditions. It is implied from these investigations that the stiffness of the ligaments may not be so important to the dynamic behaviour of the foot under certain loading conditions. The dynamic loading investigated by Beillas *et al.*, (1999) involved axial loading of the foot with a rigid flat plate. It is anticipated that this loading would initiate very little rotation of the joints in the ankle and may explain the limited influence that changes in ligament stiffness had on the predictions from their model. Parametric investigations under more diverse impact conditions are therefore needed to assess the full extent that ligament properties have on the impact response of the foot and ankle.

Discussion - Influence of the Foot Loading Conditions on Ankle Injury Risk and Ankle Injury Criteria

It is suggested from the model's predictions that variations in the environmental and subject conditions can have a considerable influence on the severity and pattern of ankle injuries and on the magnitude of the loads that initiate ankle injuries. This latter point has important implications on ankle injury criteria that are typically based on the axial load in the tibia such as the injury risk curve developed by Hynd *et al.* (2003) for the Thor-Lx dummy leg. In this work the injury risk curve was based on repeated sled impacts of PMHS legs and the Thor-Lx dummy leg with the ankle in a neutral position. The injury risk curve may therefore not provide a conservative estimate of the true injury risks to the ankle in automotive impacts where the loading conditions and the magnitude of the loads initiating ankle injuries could be very different from the neutral conditions investigated in the tests.

These expectations are supported by the predictions from the model. For instance, in the eversion and neutral model runs differences in the predicted injury initiating loads in the ankle joints were as high as 1.0 kN and differences in predicted peak loads in the heel and mid-foot pads for these two model runs were as high as 2 kN.

It is evident from the model's predictions that additional work is needed to determine how alterations in the loading conditions alter the loading limits that initiate ankle injuries. This will contribute to the development of more comprehensive ankle injury criteria focused on mitigating the most serious and debilitating ankle injuries. It is proposed that this knowledge could be developed with the FE model developed in this study, where the model could be used to carry out a large scale parametric investigation of the influence that loading conditions have on the injury risk to the ankle. This would need to be supported by biomechanical tests to validate the behaviour of the model and to provide supporting evidence on the conclusions and proposals of the modelling work. The expected outcomes from the work would be improvements in existing ankle injury risk curves and the possible development of new injury criteria that may for instance be based on the coupled rotation and axial loading of the ankle in an impact. The benefits of these developments would be reductions in severely debilitating ankle injuries in automotive impacts and the societal cost associated with ankle injuries.

CONCLUSIONS

A FE computer model of the human lower leg has been developed which accurately defines the geometrical shape of the bones, the principal ligaments in the lower leg and foot and the articular surfaces of the joints in the ankle. Predictions from the model have been validated against the results from two separate sets of PMHS legs tests that involved sub-injurious pendulum impacts to the sole of the foot and sub-injurious and injurious sled impacts to above knee PMHS specimens. A series of predictive model runs have also been carried out with the model to assess the influence that environmental and subject variations have on the predicted ankle injury risk. All these model runs were based on PMHS leg sled impact conditions in which the PMHS foot rested on a heel and mid-foot pad. The environmental variations included model runs with and without the heel pad and loading the foot in eversion and a neutral position. Model runs were also carried out in which the stiffness of the ligaments joining the mid-foot to the hind-foot were increased in order to consider subject variations. The principal conclusions of the work are as follows:

- The locations of peak predicted von Mises stresses in the modelled ankle correlated well against recorded injuries in PMHS test specimens. Based on these correlations a predicted von Mises stress of 120 MPa has been proposed as the threshold of injury to the talus and calcaneus in the model.
- Predicted loads in the ankle joints ranged between 2 kN for sub-injurious sled impact conditions up to 2.6-3.8 kN for injurious sled impact loading conditions.
- It was predicted that loading the foot in dorsi-flexion increases the risk of injury to the neck of the talus and reduces the injury risk to the calcaneus.
- Loading the foot in a neutral position it is predicted that the calcaneus is at a greater risk of injury compared with the talus.
- With the foot loaded in eversion it is predicted that the lateral aspect of the talus would be at greatest risk of injury. Under equivalent loading conditions and loaded in a neutral position, the calcaneus is at a greater predicted risk of injury.
- Loading the foot in a neutral posture and with 21° of eversion the difference in the predicted injury initiating loads in the ankle joints were as high as 1.0 kN and differences in the predicted peak loads in heel and mid-foot pads were as high as 2 kN.
- A potential 500-fold increase in the stiffness of the ligaments joining the mid-foot to the

hind foot resulted in a 1.5-2 kN (37-78%) increase in the predicted ankle joint loads and a considerable reduction in the relative shearing and motion between the mid-foot and hind-foot.

- A potential 500-fold increase in the stiffness of the ligaments joining the mid-foot to the hind-foot resulted in a greater predicted injury risk to the neck of the talus.

ACKNOWLEDGEMENTS

The work described in this report was carried out in the Vehicle Engineering Department of TRL Limited. The authors are grateful to the UK Department for Transport, Transport Technology and Standards Division for funding the work and to the orthopaedic surgeons based at the Queen's Medical Centre Hospital in Nottingham who provided valuable medical input in the development of the model.

REFERENCES

- Beillas P, Begeman PC, Yang KH, King AI, Arnoux P, Kang H, Kayvantash K, Brunet C, Cavallero C, and Prasad P (2001).** *Lower Limb: Advanced FE model and new experimental data.* STAPP Car Crash Journal, Vol. 45, November 2001. Paper no. 2001-22-0022, pp. 469-494.
- Beillas, P, Lavaste F, Nicolopoulos D, Kayventash K, Yang K and Robin S (1999).** Foot and ankle finite element modelling using CT-scan data. Proceedings of the 43rd STAPP Car Crash Conference, 25-27 October, San Diego, California.
- Dubbeldam R, Nilson G, Pal B, Eriksson N, Owen C, Roberts A, Crandall J, Hall G, Manning P and Wallace A (1999).** *A MADYMO model of the foot and leg for local impacts.* Proceedings of the 43rd STAPP Car Crash Conference, 25-27 October, San Diego, California.
- Hynd D, Willis C, Roberts A, Lowne R, Hopcroft R, Manning P and Wallace W A (2003).** *The development of an injury criteria for axial loading to the THOR-LX based on PMHS testing.* 18th International Technical Conference on the Enhanced Safety of Vehicles, May 19-22, Nagoya, Japan.
- Lowne R W, Owen C, Wallace W A, Ellis J, Taylor A, Manning P and McMaster J (2001).** *Research Project on Lower Limb Injury – Final Report.* TRL Project Report.
- McMaster J, Parry M, Wallace, A, Wheeler L, Owen C, Lowne R, Oakley C, Roberts A (2000).** *Biomechanics of ankle and hindfoot injuries in dynamic axial loading.* 44th STAPP Car Crash Journal, pp357-377.
- Owen C, Lowne R and McMaster J (2001).** *Requirements for the evaluation of the risk of injury to the ankle in car impact tests.* 17th International Technical Conference on the Enhanced Safety of Vehicles, June 4-7, Amsterdam, Netherlands.
- Takahashi Y, Kikuchi Y, Mori F and Konosu A (2003).** *Advanced FE lower limb model for pedestrians.* 18th International Technical Conference on the Enhanced Safety of Vehicles, Nagoya, Japan, May 2003. Paper no. 218.
- Takahashi Y, Kikuchi, Y, Konosu A, Ishikawa H (2000).** *Development and Validation of the Finite Element Model for the Human Lower Limb of Pedestrians,* STAPP Car Crash Journal, Vol. 44, 2000.
- Untaroiu C, Darvish K, Crandall J, Deng B, and Wang J.T (2005).** *Characterisation of the Lower Limb Soft Tissues in Pedestrians Finite Element Models.* 19th International Technical Conference on the Enhanced Safety of Vehicles, Nagoya, Japan, May 2003, paper number 05-0250.
- Wheeler L, Manning P, Owen C et al (2000).** *Biofidelity of dummy legs for use in legislative crash testing.* IMechE Safety 2000 Conference Transactions 2000, pp 183-198.
- Yamada H (1970).** *Strength of Biological Materials.* The Williams & Wilkins Company Baltimore, edited by Evans G.

AN APPROACH TOWARDS DEVELOPING A THEORETICALLY BASED, STATISTICALLY JUSTIFIED, THORACIC INJURY CRITERION

J. Quinn Campbell

Rabih E. Tannous

AASA, Inc.

Erik G. Takhounts

Peter Martin

Rolf Eppinger

Stephen Ridella

National Highway Traffic Safety Administration

Thuvan Nguyen

CSMI Inc.

United States

Paper Number 07-0229

ABSTRACT

As measurement capabilities in crash test dummies improve, new injury criteria should be considered to take advantage of these improvements. The THOR-NT dummy thorax has been designed with three-dimensional displacement measurement capability at four points in the chest. To correlate those measurements with injury, chestband displacements from Post Mortem Human Subjects (PMHS) tests corresponding to the THOR-NT chest displacement points were used to simulate thorax loading in a 2-D finite element model of the human thorax. The model, method and model validation were described in Campbell et al. (2005). In the current study, data from both upper and lower chestbands were used to predict rib fractures in the PMHS crash tests. Due to the close proximity of the two upper THOR-NT chest displacement points, some of the simulations did not adequately represent the PMHS loading. To improve the simulations, a new set of runs were created using wider chest displacement points to determine if they would be more successful in simulating injury. Rib stress and strain from the 2-D finite element model of the PMHS thorax were used to predict injury or non-injury in the PMHS tests. Statistical analysis using logistic regression was used to investigate a new thoracic injury criterion based on the finite element model simulations.

INTRODUCTION

Thoracic injuries are among the most prevalent and serious in automobile collisions. Head injuries were the only category ranked ahead of thorax injuries in area most often injured (Ruan et al., 2003), overall number of fatalities and serious injuries (Cavanaugh, 1993), and overall societal harm (Malliaris, 1985). Improving the understanding of

thoracic injury mechanisms will lead to better restraint systems that can reduce injuries and save lives.

Factors such as crash speed and intrusion contribute to thoracic injuries, as well as the presence of restraint systems, including airbags, seatbelts, load limiters, and seatbelt pretensioners. Currently experimental research using cadavers and crash test dummies is used to understand thoracic injury mechanisms. While this is an important step, computer models offer more flexibility at a lower cost. Computer models also have the ability to produce more detailed observations of stress and strain than are possible with the instrumentation used with cadavers and test dummies. The information from chest deflection and spine acceleration can be used to calculate many thoracic injury criteria, but these measures do not provide much guidance in how to improve an automobile design. The flexibility and increased measurement possibilities of computer models allow researchers to pinpoint what dummies need to measure, which will improve the ability to regulate effectively.

To design more effective restraint systems and improve regulations, researchers need to be able to investigate hypothetical scenarios, not just focus on passing a specific metric. In fact, focusing on a single value could lead a researcher in the wrong direction. Computer models provide information on a variety of factors which are all related to injury risk. This paper presents a 2-D finite element model of the human thorax designed to study injury mechanisms and restraint conditions in an automotive crash environment.

METHODS

The purpose of this study was to research a new thoracic injury criterion based on finite element model simulations of the human thorax. The method

was developed to predict injury based on the thoracic measurements obtained from THOR-NT, the advanced frontal impact dummy developed by the NHTSA. The THOR-NT dummy measures chest deflection relative to the spine at 4 crux points on the chest, two upper and two lower (Figure 1). Time histories for displacement of the crux points in the x, y, and z directions are recorded. To predict injury, two finite element simulations are completed, the first using the upper crux points and the second using the lower crux points. Crux point displacements are applied directly to the model and injury is predicted based on stresses and strains measured in the model.

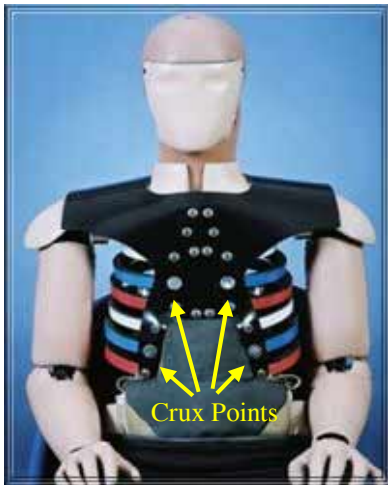


Figure 1. THOR Crux Points.

To correlate the model with injury, a set of 62 Post Mortem Human Subjects (PMHS) frontal crash tests were used. Upper and lower chestband data was recorded in each of the tests. The chestband data was processed to develop displacement time histories of points on the PMHS chest, normalized to a 50th percentile male and corresponding to the 4 crux points on the THOR-NT dummy. The displacement time histories were used to run an upper and lower thorax simulation for each PMHS test. Logistic regression was used to correlate stresses and strains in the model to the injury found during the PMHS tests.

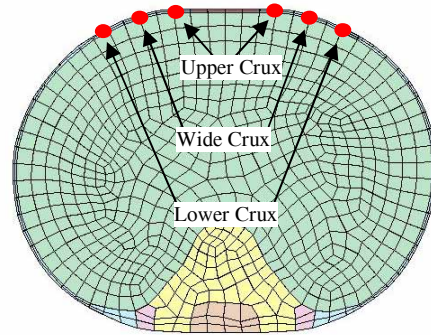


Figure 2. Crux Point Locations on 2-D Thorax Model.

A second set of PMHS simulations were also completed to test the crux point locations. The THOR-NT upper crux points are relatively close together which may affect the loading of the model. When loading occurs far away from the crux points, that loading is not simulated as well. Having the upper crux points so close together reduces the model's ability to simulate lateral loading. The second set of simulations used wider spacing for the upper crux points (Figure 2). The lower, upper, and wider crux points are spaced at 16.1cm, 11.8cm, and 7.2cm respectively. Using the wider crux points may result in more accurate simulations. To test this hypothesis these simulations were compared to the first set to determine if either set of simulations correlated more closely with injury.

In addition to peak stresses and strains, a cumulative strain damage measure (CSDM) was developed and correlated with injury. CSDM records the percent volume in the rib that has exceeded a particular strain threshold. This metric may be better suited to predicting multiple rib fractures than peak stress or strain because it takes into account the whole rib volume rather than just a localized peak stress or strain.

The finite element model of the thorax and its validation was presented in Campbell (2005). The model was designed using the LS-Dyna software package. The model represents a 50th percentile male thorax. It was created in two dimensions to allow simulation of the overall thorax response while dramatically reducing the solution time. The thorax model (Figure 3) contains six parts: rib, sternum, viscera, elastic spine, rigid spine, and spine/rib joint. The material properties for the model were determined through a review of the literature. The model was validated using fourteen experimental tests from Kroell et al. (1971 and 1974).

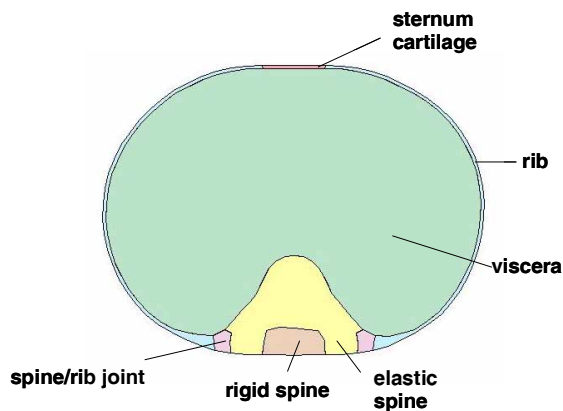


Figure 3. 2-D Human Thorax Finite Element Model.

RESULTS

Two sets of PMHS simulations were completed. Set 1 used crux points corresponding to the THOR-NT and Set 2 used wider upper crux points. A variety of logistic regressions were performed for each data set using different outputs from the simulations and different injury thresholds from 2-6 rib fractures. Simulations for the upper and lower ribs were considered both separately and together. Confounding variables were tested in the regressions as well, including PMHS age, weight, and sex. The regression with the most significance (p-value 0.0001) and highest Chi^2 (20.2) used CSDM (strain threshold of 0.01) from the lower crux simulations with cadaver age to predict injury defined as greater than four rib fractures in the entire thorax. 77% of the tests used in the regression had correct prediction of injury using the model. Figure 4 shows the probability of injury for this model at different ages using the following equation:

$$P = 1 / (1 + \text{EXP}(-(-3.01 + 27.5 * \text{CSDM}0.01 + 0.0365 * \text{OCCAGE})))$$

The receiver operator characteristic (ROC) curve in Figure 5 shows the fraction of true positives to the fraction of false positives over all possible CSDM volume thresholds. A volume of 4.6% of the rib exceeding a strain of 0.01 results in a 50% probability of injury (greater than four rib fractures).

Using both lower and upper crux simulations together did not improve the model. The best model using this scenario had a p-value=0.0007 with $\text{Chi}^2=17.1$ and 69% predicted correctly. Using wider crux points for the upper rib simulations resulted in little change in the results. The best

model using the THOR upper crux points had a p-value=0.0007 with $\text{Chi}^2=17.1$ and 70% predicted correctly. The best model using the wider crux points had a p-value=0.003 with $\text{Chi}^2=14.2$ and 73% predicted correctly.

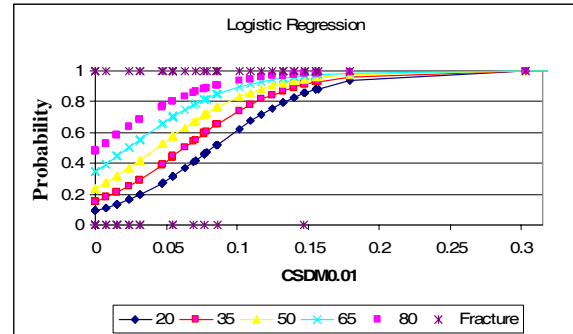


Figure 4. Logistic Regression, separated by age, with injury defined as greater than four rib fractures.

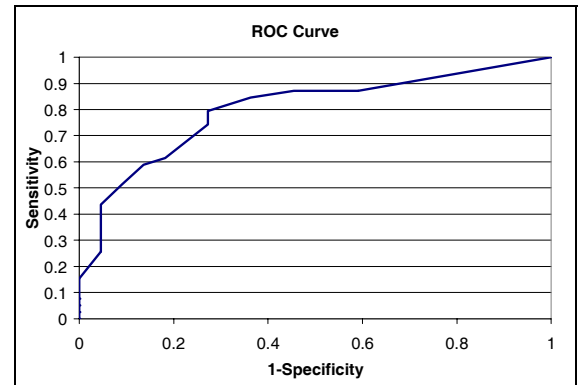


Figure 5. ROC Curve for regression model using lower rib CSDM with strain threshold of 0.01.

DISCUSSION

The results from the simulations of the PMHS tests showed that the best model for predicting injury used lower rib simulation CSDM with a strain threshold of 0.01 with PMHS age as a confounder. This result shows that CSDM is a promising method for predicting rib fractures. Since strain is linked to fracture, calculating the volume of rib that exceeds a strain threshold is a logical way to predict multiple fractures.

Figure 4 shows the regression curves for the chosen model. One may note that there is a non-zero probability when the CSDM volume equals zero. While this is a function of logistic regression, we acknowledge that it implies an unrealistic result.

A variety of other factors were tested using logistic regression including: maximum principal strain, strain rate, the product of strain and strain rate,

and maximum principal stress. These factors resulted in less significant models than CSDM.

A surprising result is that the lower rib simulations had far more significance in predicting rib fractures than either of the upper rib simulations. The two different upper crux widths were tested and only a small difference was found in the results. Therefore the wider crux points do not seem to improve the loading of the model. This also suggests that the crux position is not the cause of the upper versus lower rib discrepancy. Also, based on the success of the lower rib simulations, the basic method of applying two displacement points does not seem to account for the problem with the upper ribs. It is possible that for the current dataset more information is provided in the lower chestbands.

The method of simulating thoracic loading with a 2-D finite element model provides a way to get more information out of dummy measurements and relate those measurements to injury. However, this method has some drawbacks. A 2-D model cannot account for any displacement in the z-direction. Using only two points to load the model can also result in errors in the loading depending on how close the primary deformation occurs to the crux points. Simulating PMHS tests using a large number of loading points would be useful to quantify how much error occurs with only two loading points.

REFERENCES

[1] CAMPBELL, J.Q., TANNOUS, R.T., TAKHOUNTS, E.G., MARTIN, P., EPPINGER, R., NGUYEN, T. (2005) An Approach Towards Developing A Theoretically Based, Statistically Justified, Thoracic Injury Criterion, Proc. 19th Enhanced Safety of Vehicles, NHTSA, Washington, DC.

[2] CAVANAUGH, J. (1993) The biomechanics of thoracic trauma. In *Accidental Injury Biomechanics and Prevention*, ed. A. Nahum and J. Melvin, pp. 362-390. Springer-Verlag, New York.

[3] KROELL, C.K., SCHNEIDER, D.C., NAHUM, A.M. (1971) Impact Tolerance and Response of the Human Thorax. Proc. 15th Stapp Car Crash Conference, pp 84-134. Society of Automotive Engineers, Warrendale, PA.

[4] KROELL, C.K., SCHNEIDER, D.C., NAHUM, A.M. (1974) Impact Tolerance and Response of the Human Thorax II. Proc 18th Stapp Car Crash Conference, pp 383-412. Society of Automotive Engineers, Warrendale, PA.

[5] LS-DYNA Keyword User's Manual (2003) Vol I and II, Version 960, Livermore Software Technology Corporation, Livermore, CA.

[6] MALLIARIS, A. C., et al. (1985) Harm causation and ranking in car crashes. Paper 8500090, Society of Automotive Engineers, Warrendale, PA.

[7] RUAN, J., EL-JAWAHRI, R., CHAI, L., BARBAT, S., PRASAD, P. (2003) Prediction and Analysis of Human Thoracic Impact Responses and Injuries in Cadaver Impacts Using a Full Human Body Finite Element Model. Proc. 47th Stapp Car Crash Conference, pp. 299-321. Society of Automotive Engineers, Warrendale, PA.

[8] TROSSEILLE, X., FORET-BRUNO, J-Y., PAGE, Y., HUERE, J-F., LE COZ, J-Y., BENDJELLAL, F., DIBOINE, A., PHALEMPIN, T., VILLEFORCEIX, D., BAUDRIT, P., GUILLEMOT, H., and COLTAT, J-C. (2001) Comparison of Thoracic Injury Risk in Frontal Car Crashes for Occupant Restrained Without Belt Load Limiters and Those Restrained With 6kN and 4kN Belt Load Limiters. Proc. 45th Stapp Car Crash Conference, pp. 205-224. Society of Automotive Engineers, Warrendale, PA.

NHTSA'S THOR-NT DATABASE

Peter G. Martin

National Highway Traffic Safety Administration
U.S. Department of Transportation
Washington, D.C., USA

Lauren Shook

GESAC, Inc
Washington, D.C., USA

Paper Number 07-0289

ABSTRACT

This paper provides a comprehensive overview of the many tests involving the THOR-NT advanced frontal impact dummy that are contained within the NHTSA test database. Since its release in 2005, NHTSA has collected data from over one hundred tests involving the THOR-NT. These include sled tests, vehicle tests, and component tests at different speeds and configurations. This paper serves as a reference for describing the various test series, which include those aimed at assessing biofidelity, evaluating instrumentation, and establishing qualification and injury criteria. This paper also provides analytical examples that demonstrate the utility of the database in studying dummy-related issues. New auxiliary tools, such as data processing software and computer models, are also described. Finally, this paper summarizes some of the lessons learned from this broad test experience, and documents actions that are being taken to enhance dummy performance and acceptance by the international community.

INTRODUCTION

The origins of the THOR-NT advanced frontal impact dummy may be traced to the 7th International ESV conference, when the National Highway Traffic Safety Administration (NHTSA) announced plans to develop an advanced crash test dummy with improved biofidelity under frontal impact conditions and with expanded injury assessment capabilities (Backaitis and Haffner, 1979).

During the ensuing years, the THOR-NT has gone through several stages of development, which are summarized in Figure 1. Significant milestones in this development process are described below.

Anthropometric definition. NHTSA commissioned a study of the anthropometry of human volunteers in a

seated posture at the University of Michigan Transportation Research Institute (UMTRI). The resulting three volume report defined the coordinates of the skeletal landmarks for the seated position. Full-sized glass-epoxy reference surface shells (having since been digitally scanned) representing three occupant sizes were developed (Schneider et al, 1983; Schneider et al, 1988).

Concept definition study. Concurrent with the conclusion of the anthropometry study, NHTSA funded a concept definition study for an advanced frontal anthropomorphic test device (ATD). This study laid the foundation for the hardware development efforts to follow (Melvin et al, 1988). This effort encompassed injury assessment priority analysis, an extensive review of available biomechanical impact response and injury data relevant to the automotive environment, and preliminary development of desirable advanced ATD design characteristics and features.

Development of the TAD-50M ATD. The initial advanced ATD was developed by a NHTSA-sponsored consortium of universities and industrial partners working through the SAE Frontal Impact Dummy Enhancement Task Group (Schneider et al, 1992). This new "trauma assessment device" represented a 50th percentile male and was known as the TAD-50M. It consisted of a new torso to which stock Hybrid III arms, legs, head, neck, and a modified pelvis were attached to form a testable unit. Four TAD prototypes were produced.

Concurrent advanced neck and lower extremity development. At the same time as the TAD thorax was being developed, an advanced lower extremity (ALEX) and a new neck were under design. The ALEX eventually gave way to the THOR-Lx, which is capable of mounting to either the THOR-NT or the Hybrid III.

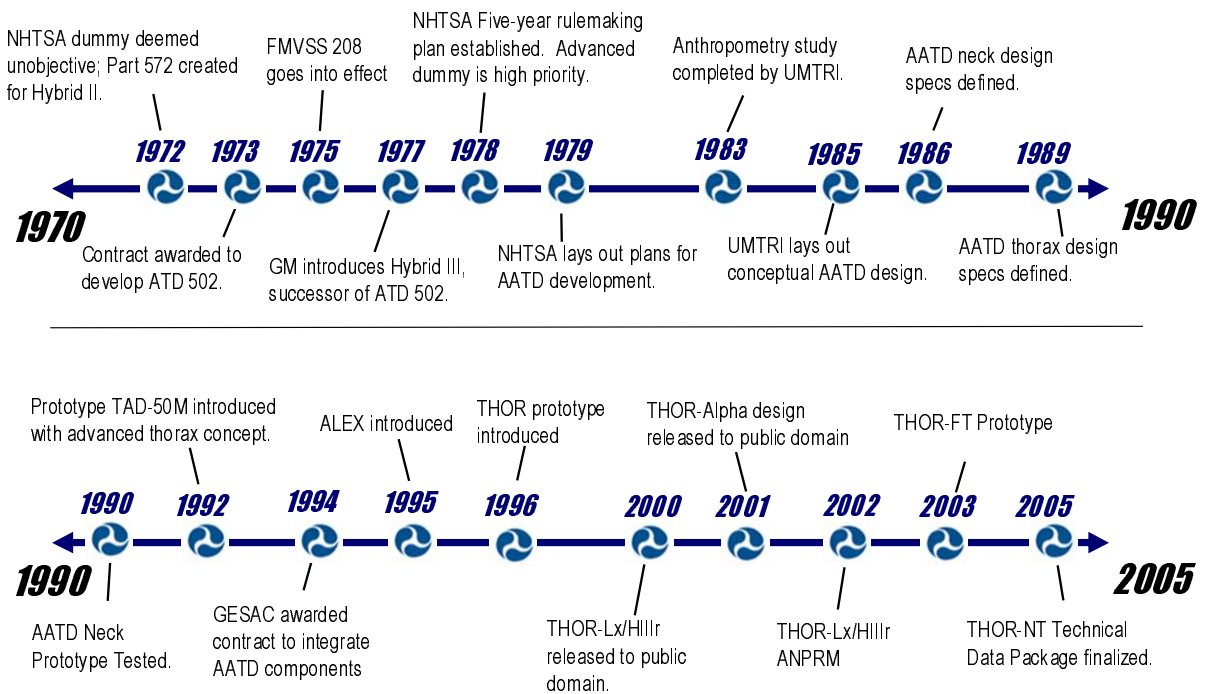


Figure 1. THOR-NT Development Chronology.

THOR prototype: Integration of design concepts. An effort to integrate the various ATD components began in 1994. Two years later, a prototype of the new dummy dubbed “THOR” was introduced. The principal features of the new crash dummy have been described by Rangarajan (1998).

THOR Alpha release. Modifications were incorporated into the design of the prototype THOR which resulted in the introduction of THOR Alpha in 2001. The modifications corrected for poor durability of flexible joints, noise in accelerometers, and problems in handling and storage. A description of the modifications is given by Haffner (2001).

THOR-NT release. An extensive set of modifications were made to the THOR Alpha during the development of the THOR-NT based on user comments and the need for improving the performance of the dummy. These updates are summarized by Shams (2005).

Since the release of the THOR-NT in 2005, NHTSA has tested the dummy in a variety of configurations. Herein is a summary of THOR-NT data that NHTSA has collected. Among the test series are those aimed at evaluating air bags, seat belt pretensioners, and rear seat restraints, one of the original purposes for the dummy.

OBJECTIVE

This paper describes a database encompassing all aspects of THOR-NT tests. The purpose of the

database is to provide a configuration management system that will be useful to a broad range of individuals and their special interests.

Biomechanics researchers. The database contains an assembly of THOR-NT data under a variety of test conditions, many of which contain matching tests with post-mortem human subjects (PMHS). This data may be used to assess the biofidelity of the THOR-NT and to suggest injury assessment response values (IARV’s).

Vehicle safety researchers. Vehicle crash tests with the THOR-NT provide insights into the measurement capabilities of the THOR-NT. For many test series, matching Hybrid III data provides a comparative benchmark that lends insights into the additional measurement capabilities of the THOR-NT. The database also contains tools such as finite element and multibody models of the dummy to assist in computational analyses of vehicle restraint systems.

Lab Technicians. The database includes information on qualification tests and procedures. The THOR-NT User’s Manual describes dummy handling and set-up procedures. Signal processing software is also offered.

ATD Manufacturers. The technical data package contains Level III engineering drawings for the manufacture of the THOR-NT. Also included are maintenance and repair reports which provide insights into future opportunities to improve the durability of the dummy.

This paper describes the elements of the THOR-NT database. Two examples are given to demonstrate its applicability to the aforementioned interest groups.

TEST DATA

The test data may be grouped into three broad categories: sled/crash test data; biofidelity and component data; and qualification data. The data itself is often accompanied by a test report and digital images in the form of still photos (JPG's) and high-speed movies (AVI's) of the test. Each test dataset is described in more detail below, with indications of whether accompanying tests were run with other dummies, volunteers, or human surrogates.

Sled Test/Crash Test Data. These tests are usually performed to evaluate a safety system or a specific

test configuration. They often include companion tests with post-mortem human subjects (PMHS) or the Hybrid III and other dummies (including the FT version of THOR developed by the European Union) in order to provide a baseline comparison responses. Table 1 lists the various series of sled/crash tests.

Component Data. Component tests include drop tests and pendulum impacts to body components of the dummy. In some instances, the test protocol requires the dummy to be partially disassembled. These tests are usually performed in order to assess the biofidelity of the dummy. Included among the component tests are abdomen tests, neck pull tests, and femur impact tests. Table 2 lists the various component test series. Multiple tests were run under each series of tests.

Table 1. THOR-NT Full-Dummy Vehicle and Sled Tests

| Test Series Focus | Test Description | THOR-NT Tests | Match Tests | Test Lab | Publications |
|---|--|---------------|----------------|---------------------|--------------|
| Air bag Evaluation: THOR-NT vs. HIII in OOP scenario | Static air bag deployments for drivers and passengers in OOP positions. | 6 | HIII | DCX | Kang, 2006 |
| Vehicle Crashworthiness: IIHS full vehicle test | 64 km/hr full vehicle IIHS-style test: SUV into an offset deformable barrier, 3-pt belt. | 2 | HIII | DCX | Ding, 2006 |
| ATD Comparison: THOR-NT and HIII | 48 km/hr sled tests; driver/passenger; frontal and frontal-oblique, 3-pt belt, no air bag. | 12 | HIII | DCX | Ding, 2006 |
| Evaluation of crushable table: study of table-to-abdomen interaction | 35 km/hr passenger train collision. | 1 | HIII | Fed. Railroad Admin | Parent, 2004 |
| ATD Response Comparison: THOR-NT and HIII | 40, 48, 56 km/hr frontal sled tests, driver/passenger, air bag, 3-pt belt and unbelted. | 18 | HIII | Ford | |
| Pretensioner configurations | 48 km/hr frontal sled tests, 3-pt belt, no air bag, various pretensioner locations. | 10 | HIII | Hyundai/UVA | Paek, 2006 |
| ATD response comparison: THOR-NT, THOR-FT, HIII | 56 km/hr Hyge frontal sled tests, belted driver w/ air bag, passenger without air bag. | 5 | HIII, THOR-FT | JARI | Onda, 2006 |
| Biofidelity of neck in extension: THOR, HIII, BioRid, Rid-2 vs. Human | 8 - 16 km/hr mini-sled, low speed Hyge rear impact tests. | 11 | HIII, THOR-FT | JARI | |
| Investigate influence of seating position on ATD response | 56 km/hr frontal sled tests, driver, 3-pt belt and air bag. | 4 | --- | JARI | |
| Air bag Evaluation: OOP behavior with fleet air bags | Static air bag deployments for five modules, OOP-1 position. | 10 | HIII | L-3/Jaycor | |
| ATD repeatability in OOP configuration | Repeatable ATS static air bag deployments, OOP-1, -2 positions. | 24 | HIII | L-3/Jaycor | Chan, 2004 |
| Seats and restraint performance in far side crashes | Far side sled tests, passenger, various seat/restraint configurations. | 6 | PMHS, WorldSID | MCW | |
| Evaluation of rear seat restraints | 48 km/hr Toyota Corolla frontal sled-mount compliance test, rear seat, 3-pt. belts. | 2 | HIII | TRC of Ohio | |
| Race car seat performance | 200 km/hr NASCAR-style car impacting a SAFER barrier at 25 degrees. | 2 | HIII | Univ. of Nebraska | |
| THOR-NT shoulder design confirmation. | 56 km/hr frontal sled testing, FL 3-pt belt, no air bag | 8 | --- | UVa | |
| Biofidelity/Injury Criteria Development | 48 km/hr frontal sled tests, passenger, FL 3-pt belt, no air bag. | 9 | PMHS, HIII | UVa | |
| Thoracic response in low speed frontal crashes | 29 km/hr frontal sled tests, passenger, 3-pt belts. | 3 | PMHS, HIII | UVa | Forman, 2006 |

Table 2. THOR-NT Body Component Tests

| Test Series Focus | Test Description | Matching Tests | Test Lab | Publications |
|---|--|-----------------|----------|--------------------|
| Neck characterization: human vs. HIII and THOR | Bending and tension, quasi-static tests | HIII | Duke | Dibb, 2006 Stapp |
| Compare THOR-NT, THOR-FT, HIII | THOR neck, thorax, and abdomen qualification tests | HIII, THOR-FT | JARI | Onda, 2006 SAE |
| ATD Comparison in neck extension with BioRid, Rid-2 | Strap pull (3 config); back impact and inertia | HIII, Volunteer | JARI | |
| THOR Design Check: Biomechanical Response Req. | Biomechanical response reqs: head, face, neck, thorax, upper and lower abdomen | --- | JARI | |
| THOR-NT lower extremity biofidelity | Pendulum impacts to the femur, lower leg ankle, and foot | --- | JARI | |
| Neck characterization: human vs. HIII and THOR | High-speed extension | PMHS, HIII | MCW | Pintar, 2005 Stapp |
| Biofidelity of the knee-thigh-hip region | Simulated knee bolster (pendulum) impact to knee. | PMHS, HIII | UMTRI | Rupp, 2003 ESV |
| ATD thorax coupling and muscle tensing effects. | Cavanaugh-style bench tests, Q-S Indenter | PHMS, HIII | UVA | Shaw, 2005 ESV |
| Head injuries sustained by football players | Impacts to head/neck - whole body tests | HIII | Va. Tech | |

Qualification Data. Prior to each series of tests, the THOR-NT undergoes a complete inspection and a series of qualification tests to assure that it is performing within specifications and meets biofidelity requirements. Qualification follows procedures described in accordance with the THOR Certification Manual. The manual describes 16 qualification tests:

Thorax certification (4 tests): Kroell test of the thorax at two speeds; MCW oblique-type tests of the right and left lower thoracic cage.

Abdomen qualification (2 tests): Upper abdomen impact test; lower abdomen impact test.

Femur qualification (2 tests): Knee impact test on both legs.

Head qualification (2 tests): Head only (head removed from body) 49CFR, Part 572.32 drop test; full dummy head impact test.

Neck qualification (4 tests): Dynamic bending tests (lateral, extension, and flexion) with pendulum; quasi-static O-C joint response.

Face qualification (2 tests): Rigid rod impact; rigid disc impact.

Together with adherence to the engineering drawings, compliance with qualification test requirements serves to assure that the dummy is performing with known, repeatable and biomechanically correct responses. Qualification data is integral in the federalization process. This topic is discussed later in more detail.

OTHER THOR-NT MATERIALS

Aside from the test data itself, the database also contains other information described below.

Journal and Conference Papers. Literature references for the tests described in Tables 1 and 2 are provided. The full-length manuscripts of select papers that are not restricted by copyright concerns are available for download.

Technical Data Package (TDP). The TDP consists of over 500 AutoCAD files of the THOR-NT engineering drawings, and includes drawing specifications and a bill of materials for the dummy. A user's manual and separate manuals for the biofidelity and qualification requirements are also included.

Design reports. These include the full-length reports referenced previously, and more recent reports generated on the development of the THOR-NT.

User Tools. These include computer modeling and data processing software and manuals.

Inspection Reports. Each time a THOR-NT unit is returned to NTHSA by a test site, it undergoes a complete inspection. The results of these periodic inspections are documented in reports. These list any maintenance problems discovered during the inspection process and detail any repair procedures found to be necessary.

APPLICATIONS

Aside from the topics discussed within the individual papers that have resulted from a particular series of tests, the database as a whole may be used to investigate many other dummy-related issues.

Two examples are provided below that demonstrate how the THOR-NT database may provide insights into: (1) thorax deflections and (2) ATD neck loads. These examples are only meant to provide a demonstration of the richness of the THOR-NT database by conducting an exploratory analysis of a few dummy-related issues. A much more exhaustive study – one that is beyond the scope of this paper – is needed to fully investigate these two examples.

Example 1. Thorax deflections. An advantage of the THOR-NT dummy is its ability to measure thorax deflections along three (x,y,z) directions at four distinct points on the ribcage: two in the upper thorax (right and left), two in the lower thorax (right and left). The database may be parsed to demonstrate how the deflections vary from location to location depending on the restraint condition and test configuration. This distinction cannot be made with the Hybrid III dummy, which measures chest deflection at a single point (mid-sternum) in the x-direction only.

As examples, four series of tests run under very different conditions were selected for consideration. The first test used for the thorax deflection comparison was from Jaycor's 24-test out-of-position (OOP) repeatability test series referenced in Table 1 and described in Chan, 2004. In this test, the THOR dummy was placed against the air bag in an ISO-1 OOP position as shown in Fig. 2. The air bag used for the test was from a 1992 Honda Accord. With the dummy's head resting on the steering wheel, compressed air was used to rapidly inflate the air bag.

The second test comes from the series of frontal sled tests run by Ford Motor Company to assess dummy behavior under compliance and NCAP test scenarios. For the test selected, the THOR dummy was positioned in the driver's seat. The only restraint was the driver's side air bag (see Fig. 3). The nominal velocity of the test was 40 km/hr.

The third test was a frontal sled test run at the University of Virginia to evaluate biofidelity. Here, the THOR dummy was placed on the passenger side. It was restrained with a three-point belt that had a 4kN force limiter (see Fig. 4). No air bag was present in this case. The sled nominal velocity was 56 km/hr.

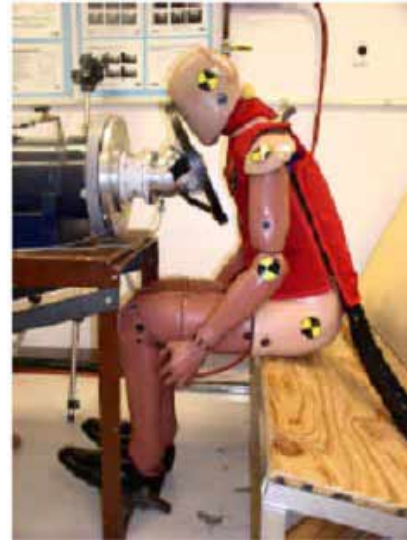


Figure 2. Jaycor OOP repeatability test configuration.



Figure 3. Ford 40 km/hr sled test configuration.



Figure 4. UVA 56 km/hr sled test configuration

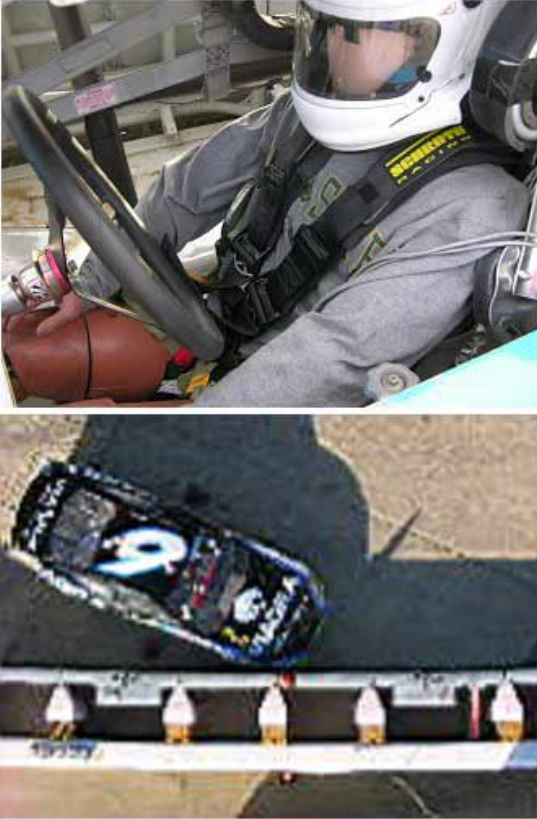


Figure 5. Top: THOR-NT positioned in a NASCAR seat with a 6-point harness. Bottom: NASCAR barrier test configuration. Nominal vehicle speed: 200 km/hr.

The fourth test was an oblique impact of a vehicle into a deformable barrier. This test was performed by the University of Nebraska for NASCAR (see Fig. 5). The THOR dummy was restrained by a six-point harness and a HANS head and neck restraint. The nominal velocity was 200 km/hr at a wall impact angle of 25 degrees.

Figure 6 shows overlays of deflections in the (x, y) directions for all four tests. (Note: significant deflections in the z-direction were also evident but are not shown herein). Thorax displacement patterns are seen to vary greatly depending on the test configuration. In the OOP tests, the dummy is placed forward, resting against the air bag. This correlates to most of the displacement (~35 mm) occurring in the -x-direction (inward) of both the upper right and upper left thorax and relatively little in the lower two quadrants.

In the Ford test, the dummy is in a typical seated position, being restrained only with the air bag. Thus, the majority of the displacement is in both the upper

right and upper left quadrants. Again, this is a compression in the -x-direction of about 30-35 mm. The difference in this case is that there is also some lateral movement of the upper chest to the right (+y-direction). There is also about ~10mm of compression of the lower right thorax and a slight shift to the right.

The UVA test configuration shows how a shoulder belt affects the deflection pattern. Here, there is moderate deflection in the -x-direction of ~15-20 mm of the upper right and upper left chest. The most deflection for this configuration is seen in the compression of the lower left quadrant (30mm) due to the seat belt. In addition, the lower right quadrant is seen to bulge outward in reaction to the compression of the lower left chest.

Lastly, the NASCAR test configuration shows how the deflection patterns change for an oblique side impact test configuration. In this case, the majority of the deflection is seen in the y-direction, with very little displacement in the x-direction. Here, the lower chest is primarily being compressed laterally, with the upper left and lower left quadrants showing deflections toward the right.

These four tests demonstrate the variation of thorax deflection patterns arising from different crash configurations. The THOR-NT – with its ability to measure (x,y,z) deflections at multiple locations – may be used to study restraint-specific thorax injury potential.

Example 2. ATD neck loads. The European Enhanced Vehicle-Safety Committee (EEVC) has issued a report on recommendations on the future of the THOR (EEVC 2006). The EEVC report includes a remark that the THOR-NT neck loads borne by the cable elements are unreliable due to improper instrumentation and friction problems. The underlying assumption of this remark is that the forces generated by the cable elements are needed to assess injury risk.

Neck tolerance depends upon the loads borne by both the ligamentous spine and the neck muscles (Chancey et al. 2003). In most dummies (including the Hybrid III) the upper head/neck load cell is installed in the head above the OC pin joint and measures all the loads which pass from the neck to the head (i.e., the “cross-sectional” neck loads). The THOR-NT incorporates a construction in which the neck column represents the load path for the osteoligamentous structures and the two cables represent load paths for external musculature. Therefore, only the loads

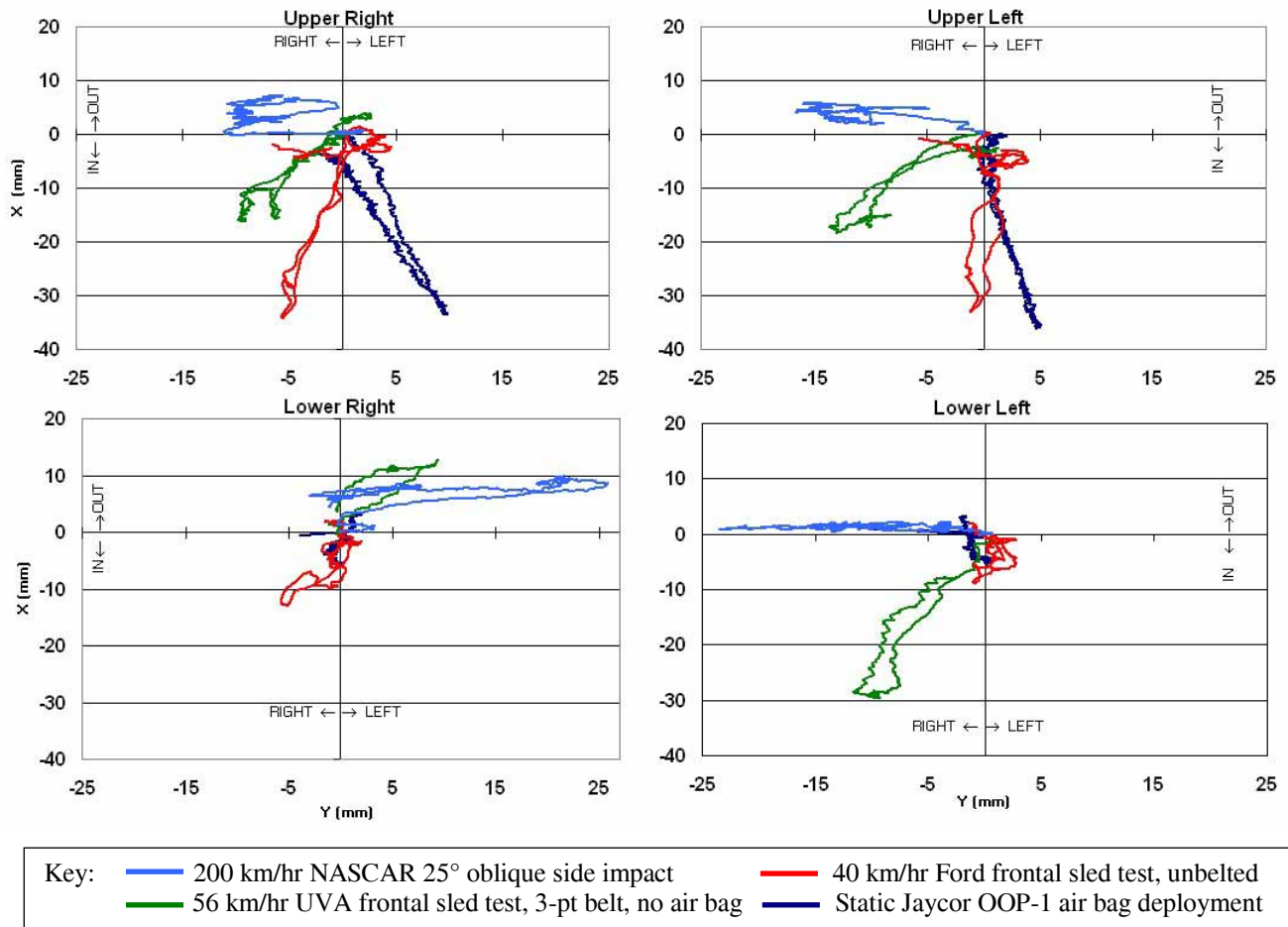


Figure 6. Comparison of (x,y) thorax deflections at the four THOR-NT thorax deflection sites.

measured in the upper neck load cell – which is placed on top of the neck column but below the head – represent injurious loads. The loads borne by the cables are not used to assess injury risk.

Nonetheless, the database may be parsed for evidence of problems related to the THOR-NT neck design. For this, the Jaycor OOP test series may again be examined for dummy neck repeatability. The test series included six repeat tests for both the Hybrid III and the THOR-NT. Figure 7 shows neck tensions measured by the upper neck load cells of both dummies. The THOR-NT shows slightly more variability but it is likely within an acceptable range (i.e., the standard deviation is within 10% of the mean). The source of the variability – whether from seating procedure, the air bag, or the dummy itself – may warrant further investigation.

In Figure 8, the THOR-NT “columnar” neck tension (representing osteoligamentous loads passing through the upper neck load cell only) and the “cross-sectional” neck tension (where the contributions of

the cable elements are included) are shown for one of the six tests. The cables are demonstrated to transfer load around the neck column in a fashion analogous to the way muscles transfer load around occipital condyles in a human neck.

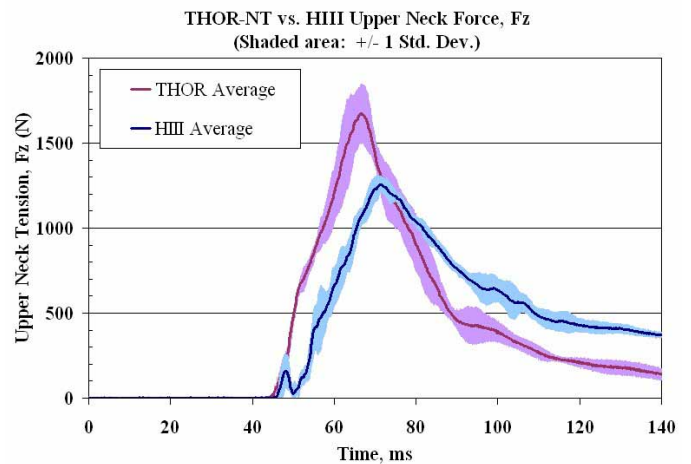


Figure 7. Neck tension repeatability in Jaycor tests

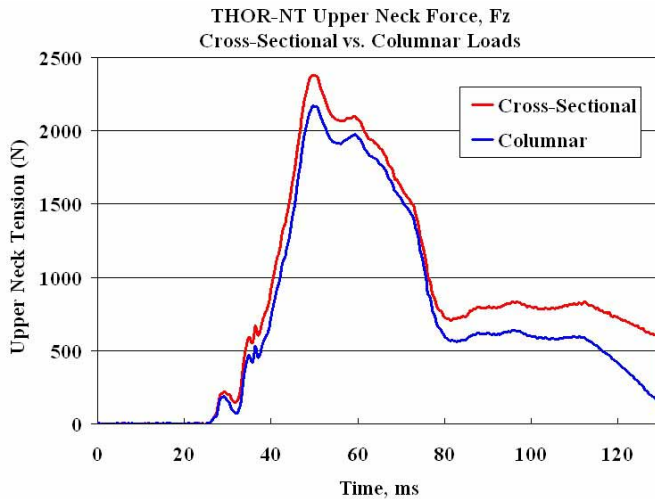


Figure 8. Neck tension: cross-sectional vs. column loads in a Jaycor OOP-1 repeatability test.

DISCUSSION

The two examples given above demonstrate how the THOR-NT database as a whole may be used to investigate safety systems and provide insights into specific dummy-related problems. For instance, the variability seen in the OOP example may lead investigators to employ a more precise THOR-NT positioning procedure than what is currently used for the Hybrid III.

Overall, the test experiences have provided NHTSA with a rich knowledge base of the capabilities and shortcomings of the THOR-NT. The benefits from these lessons learned have evoked a string of efforts to improve usability features in the form of diagnostic equipment, data processing tools, and computer models. Work on these efforts, as well as efforts to federalize the dummy, are summarized below.

Federalization. A candidate anthropometric test device (ATD), or crash test dummy, must undergo a rigorous evaluation and documentation process before it can be considered for incorporation into Part 572 of the Code of Federal Regulations. This process has been developed over many years and includes a thorough dummy and drawing inspection, establishment of dummy qualification criteria, and an evaluation of the dummy's durability, biofidelity, repeatability, and reproducibility (Rhule et al, 2005).

Engineering Drawings. The THOR-NT technical data package includes engineering drawings defining the physical dimensions of the dummy assembly, all subassemblies, and detailed drawings of all of the parts. The weight and center of gravity (CG) of the

dummy component segments are also specified in the drawing package.

NHTSA has completed the inspection of the THOR-NT manufactured by GESAC, Inc. Physical dimensions of each part of the disassembled dummy were measured and compared to the drawing package and any discrepancies were noted. Most discrepancies were simple mistakes in a drawing and easily corrected. A few modifications to the physical hardware were required, though none of these modifications significantly affected dummy response or biofidelity. Drawing revisions have been made to account for the discrepancies.

Solid Models. NHTSA has also begun efforts to acquire feature-rich solid models of all THOR-NT parts to include as part of the technical data package. This will aid tremendously in better specifying the design, manufacture, and inspection of the dummy, and could be used to more easily incorporate design modifications as well.

Dummy Qualification. For future federalization purposes, the qualification data may be used to establish upper and lower measurement targets for qualification test corridors. Peak measurements are typically used as a qualification criteria, and historically, NHTSA has used a standard deviation that is less than 10% of the mean (Rhule et al, 2005).

The THOR-NT qualification test corridors that are now used as the basis of acceptability are fairly arbitrary. In the absence of repetitive test data, they have been set to correspond with similar corridors established for the Hybrid III and with human biofidelity corridors. Most qualification tests have been run at a single laboratory (GESAC, Inc.). Over time, the body of qualification results will grow as more dummies are put into use (currently NHTSA has four THOR-NT units) as more labs acquire the capability to run THOR-specific qualification tests. This will allow a re-examination of the corridors to ascertain the proper acceptability range.

Durability. The body of data contains numerous tests from which the durability of the THOR-NT may be inferred. These tests, however, were not generally run to ascertain durability in the context of a federalization process. For example, the NASCAR tests gave NHTSA the opportunity to observe the THOR-NT in a very severe crash in which human kinematics are fairly well known. Additional high-energy component tests and full-body sled tests shall be run by NHTSA to examine the durability of the dummy.

THOR software GUI. One of the challenges associated with the THOR-NT is interpretation of the instrumentation used to determine chest deflection. These instruments, referred to as CRUX's (compact rotary units), are two-bar linkages with three degrees of freedom that measure rotation in degrees. After a test, three rotary CRUX potentiometers are combined in a post-processing routine to compute (x,y,z) deflection measurements in millimeters. In order to compute the deflections, several prescribed steps must be followed. Due to extenuating circumstances, these steps are not always straight-forward, at times making the processing of CRUX data problematic.

To facilitate the processing of CRUX angles into millimeters of deflection, NHTSA is developing a graphical user's interface (GUI) for the CRUX processing software. Aside from aiding in data processing, the more important function of the GUI is to serve as a check to assure that the user has collected the raw data properly and that the correct input information is being used.

Computer Models. NHTSA has completed two LS-Dyna finite element (FE) models of THOR-NT subcomponents: one that represents the thorax and another to represent the lower extremity. NHTSA has also developed a data set that characterizes the THOR-NT and is suitable for use with the Articulated Total Body (ATB) simulation program .

The FE work has generated a realistic geometric and material representation of the dummy with many deformable parts. The ATB work has generated a database of inertial and geometric properties

(segment mass, centers of gravity, moments of inertia), joint characteristics (location, type, stiffness) and force-deflection functions for the soft, deformable parts. This data set also serves as a building block for a future MADYMO model of the THOR-NT

CONCLUSIONS

Since the release of the THOR-NT in 2005, NHTSA has collected valuable data from over one hundred tests at various test speeds and configurations, including sled tests, vehicle tests, and THOR component tests. This paper highlights the availability of this data for use in future dummy-related assessments.

Analyses of the THOR-NT data are given that demonstrate its utility in investigating occupant safety systems and dummy-related issues. Two examples are provided herein that demonstrate the utility of the THOR-NT database in exploring dummy-related issues. The examples provide only a cursory look at these topics for the sake of demonstration, not to derive final conclusions on the issues.

Lastly, this paper summarizes lessons learned from this broad test experience, and documents actions that are being taken to enhance dummy performance and acceptance of the THOR-NT by the international community. This represents a significant step forward in demonstrating that the dummy is suitable for use in standardized tests, such as those commissioned by European Union research committees and auto racing sanctioning bodies.

REFERENCES

1. Backaitis S and Haffner M (1979), Development of the NHTSA Advanced Dummy for the Occupant Protection Standard Upgrade, 7th International Technical Conference on the Enhanced Safety of Vehicles, Paris, France.
2. Chan PC, Lu Z (2004), Laboratory Study of Hybrid-III and THOR Dummy Head/neck Responses to Airbag Load at Close Proximity, SAE Paper No. 2004-01-0320, Society of Automotive Engineers, Warrendale PA.
3. Chancey VC, Nightingale RW, Van Ee CA Knaub KE and Myers BS (2003) Improved estimation of human tensile tolerance: reducing the range of

reported tolerance using anthropometrically correct muscles and optimized physiologic initial conditions. Stapp Car Crash Journal, 47: 135-148.

4. Dibb AT, Nightingale RW, Chauncey VC, Fronheiser LE, Tran L, Ottaviano D, Myers BS (2006), Comparative structural neck responses of the THOR-NT, Hybrid III, and Human in combined tension-bending and pure bending, Stapp Car Crash Journal V50, pp 567-581.

5. Ding K, Hassan J, Nusholtz G (2006), Comparative Evaluation of the THOR-NT and Hybrid-III in Sled and Vehicle Tests, Paper no. IMECE2006-16321, 2006 ASME International Mechanical Engineering Congress and Exposition, Nov. 5-10, 2006, Chicago IL.

6. EEEV WG12–Biomechanics (2006), EEEV Recommendations on the Future of the Harmonised THOR Dummy: Report on the outcome of the Special Workshop on “Harmonisation of THOR – The Advanced Frontal Dummy”, held 4-5 May 2006 at TRL, UK, October 2006, http://eevc.org/public_docs/publicdocs.htm.
7. Forman J, Lessley D, Shaw CG, Evans J, Kent R, Rouhana SW, Prasad P (2006), Thoracic response of belted PMHS, the Hybrid III, and the THOR-NT mid-sized male surrogates in low speed frontal crashes, *Stapp Car Crash Journal V50*, pp 191-216.
8. Haffner M, Rangarajan N, Artis M, Beach D, Eppinger R, Shams T (2001). Foundations and Elements of the NHTSA THOR Alpha ATD Design, 17th International Technical Conference on the Enhanced Safety of Vehicles, Amsterdam NL.
9. Kang J, Nusholtz G, Agaram V (2006), Comparison of THOR and Hybrid-III 50th% ATDs in OOP Scenarios, SAE Paper No. 2006-06B-94, Society of Automotive Engineers, Warrendale PA.
10. Melvin, J (1988) The Engineering Design, Development, Testing and Evaluation of an Advanced Anthropometric Test Device, Phase 1: Concept Definition. DOT HS 807 224. February 1988.
11. Onda K, Matsuoka F, Ono K, Kuboto M, Martin P, Zhau Y (2006), Differences in the dynamic responses of the Thor-NT and Thor-FT dummies, SAE Paper No. 2006-01-0676, Society of Automotive Engineers, Warrendale PA.
12. Paek IC, Shaw CG, Crandall JR, Baek YO, Ko OS (2006), Responses of Hybrid-III 50th and Thor-NT 50th in Sled Tests With Different Seat Belt Pretensioner Configurations, Paper no. IMECE2006-13551, 2006 ASME International Mechanical Engineering Congress and Exposition, Nov. 5-10, 2006, Chicago IL.
13. Pintar FA, Yoganandan N, Baisden J, (2005), Characterizing occipital condyle loads under high-speed head rotation, *Stapp Car Crash Journal V49*, pp 33-47.
14. Rangarajan N, White R, Shams, T, Beach D, Fullerton J, Haffner M, Eppinger R, Pritz H, Rhule D, Dalmotas D, Fournier E (1998). Design and Performance of the THOR Advanced Frontal Crash Test Dummy Thorax and Abdomen Assemblies. Proceedings of the 16th International Technical Conference on the Enhanced Safety of Vehicles, Windsor, Ontario.
15. Rhule D, Rhule H, Donnelly B (2005), The process of evaluation and documentation of crash test dummies for Part 572 of the Code of Federal Regulations, 19th International Technical Conference on the Enhanced Safety of Vehicles, Washington DC, USA.
16. Rupp JD, Reed MP, Madura NH, Schneider LW (2003), Comparison of knee/femur force-deflection response of the THOR, Hybrid II, and human cadaver to dynamic frontal-impact knee loading, 18th International Technical Conference on the Enhanced Safety of Vehicles, Nagoya, Japan.
17. Schneider LW, Robbins DH, Pflug MA, Snyder RG (1983), Development of anthropometrically based design specifications for an advanced adult anthropomorphic dummy family, DOT HS 806 715.
18. Schneider L, King A, Beebe M (1988) Design Requirements and Specifications: Thorax-Abdomen Development Task. Interim Report: Trauma Assessment Device Development Program. DOT HS 807 511.
19. Schneider L, Ricci L, Salloum M, Beebe M, King A, Rouhana S, Neathery R. (1992) Design and Development of an Advanced ATD Thorax System for Frontal Crash Environments. Final Report, Volume 1: Primary Concept Development. Trauma Assessment Device Development Program. DOT HS 808 138. University of Michigan Transportation Research Institute. June 1992.
20. Shams T, Rangarajan N, McDonald J, Wang Y, Spade C, Pope P, Haffner M (2005), Development of THOR-NT: enhancement of THOR Alpha-the NHTSA advanced frontal dummy, 18th International Technical Conference on the Enhanced Safety of Vehicles, Washington DC, USA.
21. Shaw CG, Lessley D, Kent R, Crandall J (2005), Dummy torso response to anterior quasi-static loading, 19th International Technical Conference on the Enhanced Safety of Vehicles, Washington DC, USA.

BIOMECHANICAL DIFFERENCES BETWEEN CONTACT AND NON-CONTACT HEAD IMPACTS IN VEHICLE CRASH TESTS

Jiangyue Zhang
Narayan Yoganandan
Frank A. Pintar
Yabo Guan
Thomas A. Gennarelli
Department of Neurosurgery
Medical College of Wisconsin
United States
Paper Number 07-0352

ABSTRACT

The purpose of this research is to study brain biomechanics between contact and non-contact head impact during vehicle crash tests in head kinematics, global brain injury metrics, and region brain strain. Nine array accelerometer package data from dummy head were extracted from 13 lateral and 14 rigid pole crash tests conducted by the National Highway Traffic Safety Administration (NHTSA). Head accelerations, HIC values and their duration were computed. Cumulative strain damage measure 15% (CSDM), dilatational damage measure (DDM), and relative motion damage measure (RMDM) were studied using SIMon finite element head model (FEHM). Averaged regional brain strains were conducted by grouping brain element in SIMon FEHM into frontal, parietal, occipital, cerebellum, fronix and brain stem region. Head contact occurred in two lateral and six rigid pole tests. Head contact durations were less than one millisecond in rigid pole tests and ranged from 3-7 ms in lateral impact tests. The ratio of biomechanical measurements between contact and non-contact cases in lateral tests were: translational acceleration 4x, rotational acceleration 3.5x, HIC 12x, and CSDM 5x, regional brain 1.5x. The ratios were higher for rigid pole tests: translational acceleration 14x, rotational acceleration 25.7x, HIC 29.5x, CSDM 12x, regional brain strain 1.5-3x. Head accelerations, HIC values, DDM and RMDM increased with increasing rotational accelerations. They were the lowest in non-head contact rigid pole tests, followed by non-contact lateral impact tests, contact lateral impact tests, and the highest in head contact rigid pole tests. However, CSDM values were higher in lateral tests than rigid pole tests for head contact cases, indicating a higher chance of diffused axonal injury in head contact lateral impact tests. On the other hand, averaged brain strain in cerebellum increased 3x for contact cases, indicating high probability of injury to this region during this model of impact.

INTRODUCTION

Motor vehicle crashes are one of the major causes of traumatic brain injury in the United States [1]. High-rate head accelerations during crashes were contributed to the injury and associated with excessive strains to the brain tissue [2-10]. In particular, side crashes often result in direct head impact with the vehicle interior component or exterior object, resulting in severe head/brain injury. However, the difference in head injury biomechanics between crashes with head contact and no head contact are yet to be clearly delineated.

NHTSA conducts lateral impact and rigid pole side impact tests to obtain biomechanical data, including head accelerations. Finite element modeling is a powerful tool to study tissue level brain strain under global head acceleration [11-13]. The objective of the current study is to investigate biomechanical differences between head contact and non-head contact side impacts using vehicle crash test data and parameterized finite element modeling approach.

METHODS

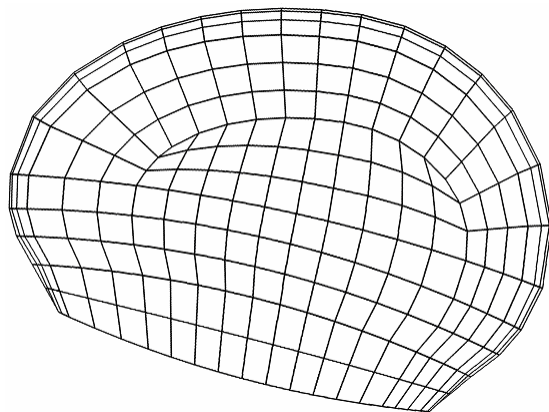
Lateral impact test and rigid pole side impact test results from the US New Car Assessment Program (NCAP) were obtained from NHTSA vehicle crash test database. Nine accelerometer package (NAP) data from the head of the test dummy in the driver seat were extracted from the results and imported into customized software to obtain head kinematics. The acceleration data were filtered with SAE Class 1000 and translational and rotational head accelerations were computed. Peak head accelerations, HIC value, and their durations were obtained.

Injury metrics from head acceleration were analyzed by using the FEHM included in the SIMon software package (Simulated Injury Monitor, developed by NHTSA). Head accelerations were applied to the model as an inertial loading, and injury measurement

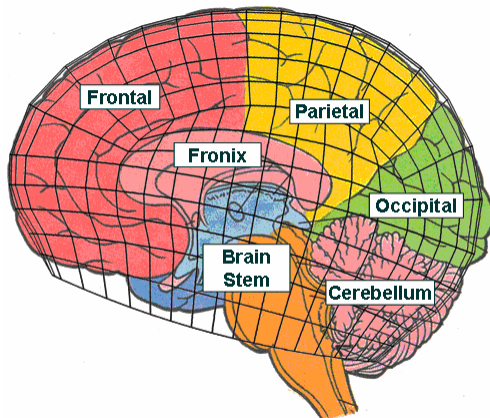
metrics: CSDM, DDM and RMDM were the major outputs from the model.

Binary output results from the SIMon FEHM were further analyzed by grouping the brain elements into six anatomical regions (frontal lobe, parietal lobe, occipital lobe, cerebellum, fronix and brain stem) by mapping the FEHM mesh to an anatomical illustration (Figure 1). Regional averaged brain strains were computed by averaging strain histories of all the elements in these regions, and peak of the regional averaged strain were obtained.

Head accelerations, HIC value, CSDM, DDM, RMDM, and regional averaged brain strains were compared between tests with head contact and tests without head contact to determine biomechanical differences.



SIMon FEHM brain mesh



Regional differentiation of SIMon FEHM

Figure 1. Region mapping of SIMon Finite Element Head Model.

RESULTS AND DISCUSSION

The study used vehicle crash test data from NHTSA database with the focus on inertial loading-induced head/brain injury. The major inclusion criteria is the dummy must have an NAP in the head so that full head kinetics, both translation and rotation, can be obtained. A query of the database resulted in 27 cases, 13 lateral impact tests and 14 rigid pole tests. Out of the selected tests, six rigid pole tests and two lateral impact tests had head contact. Vehicle in these tests were all passenger cars although there are variations in vehicle maker and model. There were 20 4Dr Sedans (10 in lateral tests and 10 in pole tests). Other vehicles include SUV, MV and 2Dr Sedan.

Three levels of biomechanical analysis were conducted: head kinematics, global brain injury metric analysis, and regional brain strain analysis.

On the head kinematics, head accelerations and HIC value were obtained from NAP data using an in-house developed software package. The software package was designed for generic head kinetic analysis using internal or external NAP data [14]. The accelerometer data from NAP and the output head accelerations were filtered with SAE Class 1000 filter.

A comparison of averaged peak head accelerations are shown in figure 2 and 3. Head accelerations in cases with head contact are considerably higher than no head contact cases. The ratio of head accelerations and HIC values between contact and non-contact cases in lateral tests were: translational acceleration 4x, rotational acceleration 3.5x, HIC 12x. The ratios were higher for rigid pole tests: translational acceleration 14x, rotational acceleration 25.7x, HIC 29.5x. Considerably higher head acceleration in contact cases indicates a high probability of severe injury in these cases.

Comparing contact cases between the two crash modes, rigid pole tests had the highest head accelerations and HIC value. Translational accelerations were 4x higher and rotational accelerations were more than 5x higher than lateral impact tests. This was due to the fact that head directly impacted the rigid pole in pole tests, whereas head impacted the vehicle interior or the incoming barrier in lateral crash tests. The higher rigidity of the pole may be attributed to the difference.

The durations of head acceleration were also obtained in addition to peak acceleration values. However, there were no significant differences between contact

and no contact cases. The duration of translational accelerations ranged from 46.8 to 60.6 ms and the duration of rotational accelerations were relatively shorter, ranging from 26.3 to 45.2 ms.

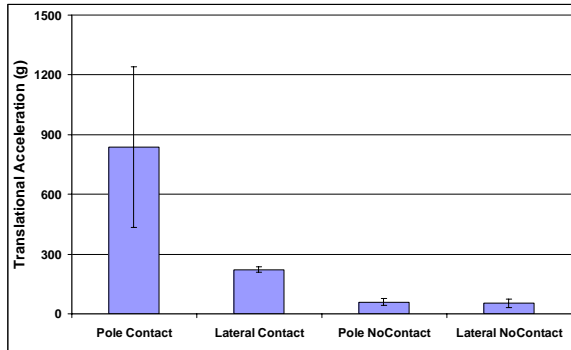


Figure 2. Comparison of average translational acceleration.

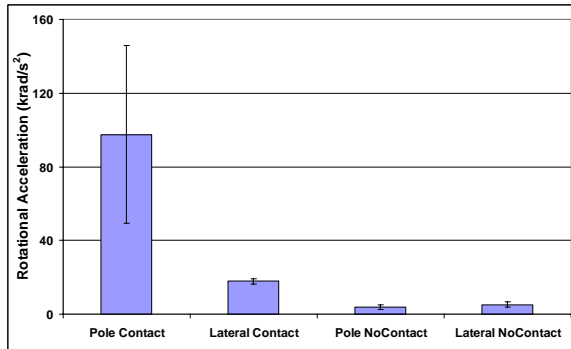


Figure 3. Comparison of average rotational acceleration.

HIC value has been widely used to evaluate head injury during vehicle crashes, although it does not include rotational accelerations. A comparison of HIC values is shown in figure 4. HIC values in all no head contact cases were well below 1000, indicating low probability of head injury. However, averaged HIC values in contact cases were approximately 10,000 for rigid pole crashes and 2,300 in lateral impact cases. The high value indicates the severity of head injury in head contact cases. HIC duration is a good indicator of the duration of major acceleration (figure 5). Average HIC duration was 3.2 ms for rigid pole tests with head contact (shortest), and 5.1 ms for lateral impact with head contact, whereas, the cases without head contact had an averaged HIC duration of approximately 22 ms, which was approximately 4x to 7x longer. This result indicates that stopping the head with a smooth continuous deceleration can significantly reduce the probability of head injury.

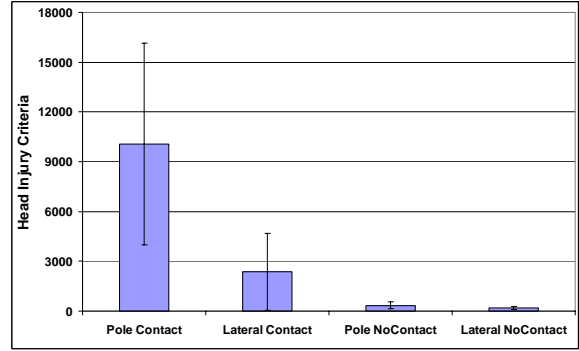


Figure 4. Comparison of Head Injury Criteria.

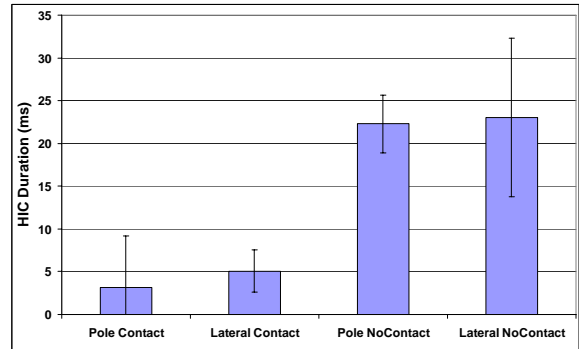


Figure 5. Comparison of HIC duration.

Head accelerations, HIC value and HIC duration give the kinematics of head motion. Specific types of brain injuries may be controlled by one or a combination of these biomechanical variables.

To study the probability of brain injury during the four modes of vehicle crash, SIMon FEHM was chosen for the global brain injury metric analysis in the current study. The model was originally developed by DiMasi et al. and enhanced by Bandak et al., and Takhounts et al. [15-18]. The model is comprised of a rigid skull, dura-CSF layer, brain, falx cerebri and bridging veins, with a total of 8,290 nodes and 5,900 elements. The model takes the head acceleration as input and computes stress-strain distribution in the brain tissue under inertial loading. The model has been validated with cadaver and animal experimental data [15, 17, 18]. It takes approximately 2 hours for the model to run a 220 ms acceleration pulse. The model was selected because of its small size, suitability for parametric studies [19], and its unique output of CSDM, DDM, and RMDM metrics for potential brain injury assessments.

CSDM in SIMon FEHM is defined as the percentage of total brain volume experiencing strains exceeding a threshold. The metric was introduced in an attempt to quantify the overall severity of injury to the whole brain, and its probability of diffuse axonal injury.

Rotational acceleration is the major contributor to this injury metric [20, 21]. It is found that a 50% probability of diffuse axonal injury is best correlated to a CSDM value of 55% at a threshold strain level of 0.15. Therefore, a CSDM value at 0.15 strain threshold was used in the current study. A comparison of CSDM value is shown in figure 6. Averaged CSDM were highest in lateral tests with head contact (CSDM 57%), although head accelerations and HIC value were highest in rigid pole tests with head contact (CSDM 47.0%), indicating higher probability of diffuse axonal injury in lateral impacts. This may be due to the fact that HIC durations were shorter in rigid pole tests. The finding also correlated well with the results in literature that higher accelerations are needed to produce equivalent injury at shorter pulse durations [22, 23].

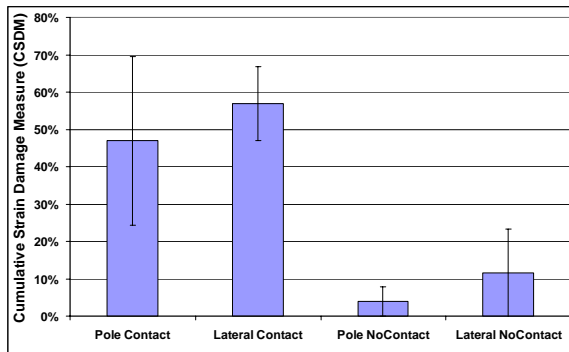


Figure 6. Comparison of CSDM.

DDM was introduced in SIMon to quantify negative pressure-induced brain contusion. It accounts for the ratio of the total volume of brain that experiences a negative pressure of 100 kPa. Physical model experiments have indicated that impacts above 150 g may cause vaporization, and impacts above 350 g can result in violent cavity collapse [24, 25]. Logistic regression based on animal and physical models have reported that 50% probability of contusion corresponds to 7.2% of brain tissue volume experiencing a pressure of -100 kPa, i.e., DDM of 7.2%. Other research indicates this injury metric to be closely associated with translation head acceleration [20, 21]. DDM value in all the non-head contact cases were well below the threshold value (Figure 7). However, rigid pole head contact cases had a DDM value of 14.8%, approximately 2x of the 7.2% threshold, indicating a high probability of brain contusion. In contrast, DDM value in lateral impact tests with head contact was only 2.2%. Brain contusion is less likely to happen in head contact lateral impacts.

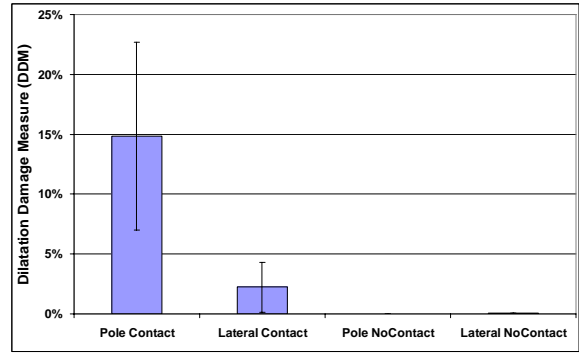


Figure 7. Comparison of DDM.

RMDM metric is introduced to evaluate the probability of acute subdural hematoma resulting from relative brain motion to the interior surface of cranium causing bridging vein rupture. RMDM is defined by calculating the ratio of a vein's current strain to the Lowenhielm threshold at the vein's current strain rate [26]. RMDM value of 1.0 is associated with 50% probability of vein failure. RMDM value in most of the cases in current study exceeded the threshold value of 1.0 (figure 8). As indicated by the authors of SIMon FEHM, there are possible sources of error in this injury metric, including its sensitivity to model geometry and selection of node pair for RMDM computation, and the justification of RMDM threshold [18]. Despite these drawbacks, RMDM value in contact cases were approximately 4x (rigid pole) and 2x (lateral impact) higher than non-head contact cases, indicating the severity of injury in head contact cases.

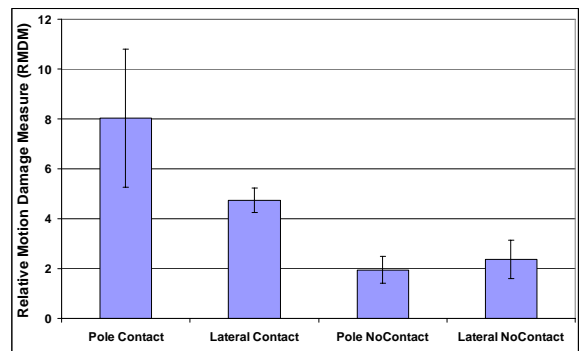


Figure 8. Comparison of RMDM.

The CSDM, DDM, and RMDM injury metrics from SIMon FEHM model treats the whole volume as one unit and does not differentiate between anatomical regions. Region-specific analysis may reveal the injury risk imposed to a local brain region and lead to a better understanding of the injury mechanism. Excessive brain strain may induce local brain tissue injury [27]. Maximum principal strain histories for all elements in an anatomical region were averaged

as an indicator of brain tissue distortion of the region. Averaged regional brain are compared between contact and non-contact cases for lateral and rigid pole crash tests in figure 9 and figure 10. Contact cases systematically had higher regional strain through all regions. For lateral impact tests without head contact, most regions had averaged brain strain less than 10%. Brain strains for contact cases were approximately 1.5x of non-contact cases, except the difference between contact and non-contact case for left occipital and partial lobe were not significant. For rigid pole crash tests, regional brain strains were around 8% for non-contact cases, and about 2x higher for head contact cases. For the right cerebellum region, averaged brain strain was 21.6%, approximately 3x higher than non-contact cases, indicating high probability of injury in this region. Because SIMon FEHM does not differential material property in different anatomical regions, the differences in regional brain strains were attributed to the geometry of the model and the crash mode.

CONCLUSIONS

Using parametric analyses and controlled motor vehicle crash test data, this study compared biomechanical head injury metrics between tests with and without head contact. Overall, all cases with head contact appear to have more severe brain injury than non-contact cases. Therefore, the ultimate goal of preventing head injury in vehicle crashes appears to be to implement safety devices that prevent/limit direct head contact.

Both head translational and rotational accelerations and HIC value indicated high potential of head injury in head contact cases, with head contact in rigid pole crash tests being the most severe. CSDM indicated highest probability of diffuse axonal injury in head contact lateral crashes. DDM indicated the highest probability of brain contusion for head contact cases in rigid pole tests. High regional strain in the right cerebellum for head contact cases in rigid pole tests indicated high probability of injury to this region. These biomechanical results may help in a better understanding of the head injury mechanism and improve therapeutic treatments.

ACKNOWLEDGMENTS

This study was supported in part by the VA Medical Research.

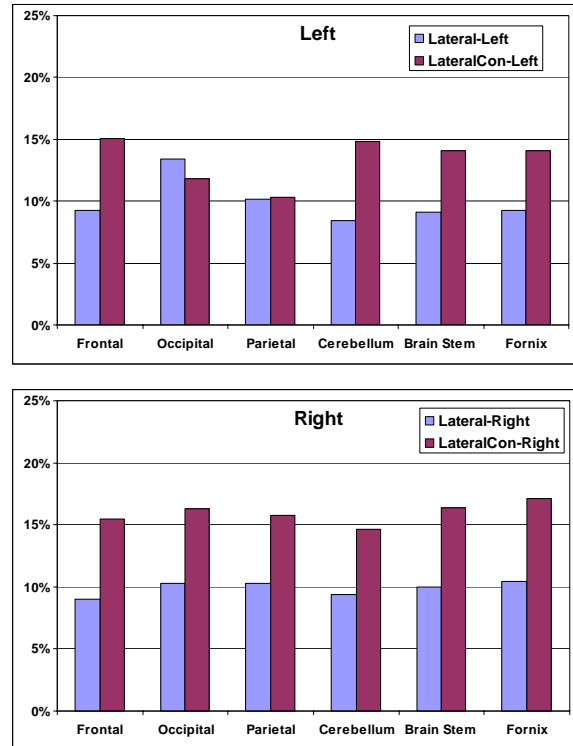


Figure 9. Comparison of regional averaged brain strain between contact and non-contact lateral crash tests

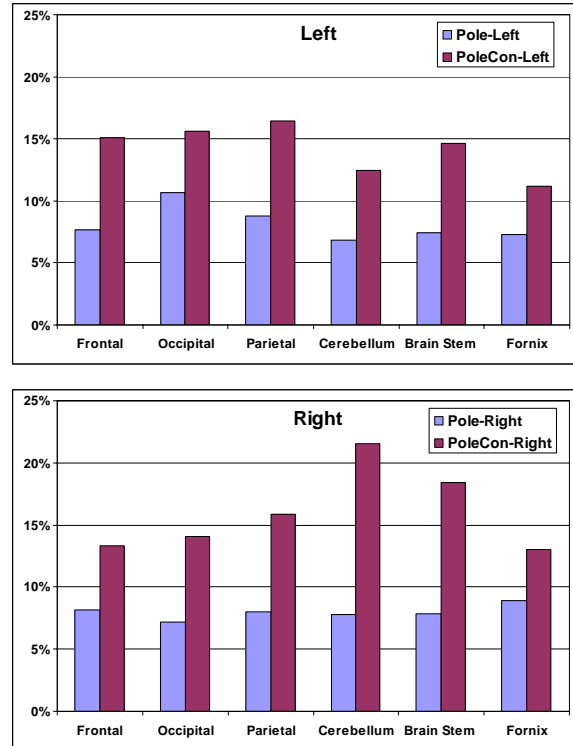


Figure 10. Comparison of regional averaged brain strain between contact and non-contact rigid pole crash tests

REFERENCES

1. Rutland-Brown, W., et al., *Incidence of traumatic brain injury in the United States, 2003*. J Head Trauma Rehabil, 2006. **21**(6): p. 544-8.
2. Versac, J. *A review of severity of index*. in *15th Stapp Car Crash Conference*. 1971. Los Angeles, CA: Society of Automotive Engineers.
3. Lissner, H.R., M. Lebow, and F.G. Evans, *Experimental studies on the relation between acceleration and intracranial pressure changes in man*. Surg Gynecol Obstet, 1960: p. 329-338.
4. Gadd, C. *Use of a weighted impulse criterion for estimating injury hazard*. in *10th Stapp Car Crash Conference*. 1996. Minneapolis, MN: Society of Automotive Engineers.
5. Gennarelli, T.A., J.H. Adams, and D.I. Graham, *Acceleration induced head injury in the monkey. I. The model, its mechanical and physiological correlates*. Acta Neuropathol Suppl (Berl), 1981. **7**: p. 23-5.
6. Gennarelli, T.A. and D.F. Meaney, *Mechanisms of primary head injury*, in *Neurosurgery*, R. Wilkins and S. Rengachary, Editors. 1996, McGraw Hill: New York. p. 2611-2621.
7. Anderson, R.W., et al., *Impact mechanics and axonal injury in a sheep model*. J Neurotrauma, 2003. **20**(10): p. 961-74.
8. Meaney, D.F., et al., *Biomechanical analysis of experimental diffuse axonal injury*. J Neurotrauma, 1995. **12**(4): p. 689-94.
9. Holburn, A.H.S., *Mechanics of head injury*. Lancet, 1943. **245**: p. 438-441.
10. Strich, J.S. and D.M. Oxon, *Shearing of nerve fibers as a cause of brain damage due to head injury: A pathological study of twenty cases*. Lancet, 1961. **2**: p. 443-448.
11. Zhang, L., K.H. Yang, and A.I. King, *A proposed injury threshold for mild traumatic brain injury*. J Biomech Eng, 2004. **126**(2): p. 226-36.
12. Ruan, J.S., T. Khalil, and A.I. King, *Dynamic response of the human head to impact by three-dimensional finite element analysis*. J Biomech Eng, 1994. **116**(1): p. 44-50.
13. Zhou, C., T.B. Khalil, and A.I. King. *A new model comparing impact response of the homogeneous and inhomogeneous human brain*. in *39th Stapp Car Crash Conference*. 1995. San Diego, CA: Society of Automotive Engineers.
14. Yoganandan, N., et al., *Lightweight low-profile nine-accelerometer package to obtain head angular accelerations in short-duration impacts*. J Biomech, 2006. **39**(7): p. 1347-54.
15. DiMasi, F., R. Eppinger, and F. Bandak. *Computational analysis of head impact response under car crash loadings*. in *39th Stapp Car Crash Conference*. 1995. San Diego, CA: Society of Automotive Engineers.
16. Bandak, F. and R. Eppinger. *A three dimensional finite element analysis of the human brain under combined rotational and translational acceleration*. in *38th Stapp Car Crash Conference*. 1995. Ft. Lauderdale, FL: Society of Automotive Engineers.
17. Bandak, F., et al. *SIMon: a simulated injury monitor: application to head injury assessment*. in *ESV 17th International Technical Conference on the Enhanced Safety of Vehicles*. 2001. Amsterdam, The Netherlands: National Highway Traffic Safety Administration.
18. Takhounts, E.G., et al. *On the Development of the SIMon Finite Element Head Model*. in *47th Stapp Car Crash Conference*. 2003. San Diego, CA: Society of Automotive Engineers.
19. Zhang, L., et al. *Recent advances in brain injury research: a new human head model development and variation*. in *45th Stapp Car Crash Conference*. 2001. San Antonio, TX: Society of Automotive Engineers.
20. Zhang, J., et al., *Role of translational and rotational accelerations on brain strain in lateral head impact*. Biomed Sci Instrum, 2006. **42**: p. 501-6.
21. Zhang, J., et al., *Brain Strains in Vehicle Impact Tests*. Annu Proc Assoc Adv Automot Med, 2006. **50**: p. 1-12.
22. Goldsmith, W., *The state of head injury biomechanics: past, present, and future: part 1*. Crit Rev Biomed Eng, 2001. **29**(5-6): p. 441-600.
23. Goldsmith, W. and K.L. Monson, *The state of head injury biomechanics: past, present, and future part 2: physical experimentation*. Crit Rev Biomed Eng, 2005. **33**(2): p. 105-207.
24. Nusholtz, G.S., B. Wylie, and L.G. Glascoe, *Cavitation/boundary effects in a simple head impact model*. Aviat Space Environ Med, 1995. **66**(7): p. 661-7.
25. Nusholtz, G.S., E.B. Wylie, and L.G. Glascoe, *Internal cavitation in simple head impact model*. J Neurotrauma, 1995. **12**(4): p. 707-14.
26. Lowenhielm, P., *Dynamic properties of the parasagittal bridging veins*. Z. Rechtsmedizin, 1974. **74**: p. 55-62.
27. Bain, A.C. and D.F. Meaney, *Tissue-Level Thresholds for Axonal Damage in an Experimental Model of Central Nervous System White Matter Injury*. J of Biomech Eng, 2000. **122**(6): p. 615-622.

A ROLLOVER HUMAN/DUMMY HEAD/NECK INJURY CRITERIA

Carl E. Nash, Ph.D.

George Washington University
United States

Donald Friedman

Xprts, LLC
United States
Paper Number 07-0357

ABSTRACT

The human neck is a remarkable device for its function, flexibility and strength. It supports the head while permitting a wide range of motion and sustains itself under some vigorous head impacts in violent sports and accidents. Nevertheless, the neck has limits both of motion and of the forces it can sustain. In rollovers, the neck is usually loaded through the top or back of the head with the torso providing an inertial reaction mass. Skull fractures, head and brain injuries generally involve higher impact velocities than are necessary to fracture the cervical spine, but which can also load and critically injure the neck.

Accident injury statistics, tests of living and post-mortem human subjects (PMHS), analysis of athletic impacts, tests of anthropometric dummies and computer simulations of human and dummy kinematics, illustrate injury mechanisms and suggest injury criteria measurements for the human neck. Using this data a simple head impact measure as a neck injury criterion was developed to address the problem of neck injury in vehicle rollovers and to help identify appropriate vehicle design considerations for rollover occupant protection.

The analysis defines a head impact speed of 3 m/sec. (7 mph) which produces a neck load of 7,000 N in a 50th percentile male Hybrid III dummy, as the onset of serious neck injury, and that a head impact speed of 4.5 m/sec (10 mph) which produces a dummy neck load of 10,000 N represents the onset of severe to fatal neck injury. NHTSA has already accepted that a head impact velocity of 7 m/sec (16 mph) is the threshold for the onset of serious head and brain injury. These criteria are shown to reasonably

represent available human injury accident and experimental statistical distributions.

DISCUSSION

The human neck is a remarkable device for its function, flexibility and strength. The cervical spine serves to transmit the brain's detailed instructions to the body that can provide the exquisite dexterity needed to play a musical instrument, the coordination for sports and dancing, and the capability of a myriad of motions used by people every day. It also transmits the feelings of touch and bodily pleasure back to the brain.

The neck is strong and flexible, supporting the head while permitting a wide range of motion and sustaining itself under some very vigorous head impacts in violent sports and accidents. Nevertheless, the neck has limits both of motion and of the forces it can sustain. Paraplegia and quadriplegia are consequences of the most severe, non-fatal injuries that the neck can sustain, and lesser injuries can result in substantial long-term disability and pain.

Critical neck injuries typically result from falling from heights, diving into a shallow pool and motor vehicle rollover accidents. In rollovers, the neck is usually loaded through the top or back of the head with the torso providing the inertial reaction mass. Skull fractures, head and brain injuries generally involve higher impact velocities or more concentrated loading. Neck injuries are generally a consequence of lower velocity, longer stroke forces on the head.

Despite the importance of head/neck injuries and fatalities in rollovers, there are no generally recognized injury criteria. NHTSA established head/neck injury criteria as part of its air bag

standard, but these were set at very conservative levels that can easily be met under the particular test conditions defined by the agency.

In a rollover the position and orientation of the human head (whether the occupant is belted or not) can only be specified as being in the vicinity of the seat, longitudinally between the A and B pillars and laterally between the outside of the roof rail and the middle of the seat. Roof impacts with the ground can result in very non-linear distortion and buckling of the roof panel and supporting structure. Therefore to choose a position and orientation for a dummy (or to presume that a restrained dummy will stay in the FMVSS 208 designated seat position) prejudices the ability of the test to evaluate the injury potential and risk of the roof design.

To circumvent these problems and facilitate dynamic rollover test evaluations, a simple head/neck injury criteria based on the best available data is necessary.

There is a substantial amount of data available based on tests of cadavers (post-mortem human subjects, or PMHS) and on experiments using anthropometric test devices (principally the 50th percentile male Hybrid III dummy). A recent, unpublished paper by Viano summarized and analyzed this data[1]. That paper summarized research conducted by a variety of biomechanics researchers and presented statistical summaries of the available data. In his paper, Viano estimated that a neck fracture was probable with a head impact speed in excess of 3 m/sec and an impact force of 4,000 N. In comparisons between cadavers and Hybrid III dummies that a 3 m/sec head impact will produce a reaction force of just under 4,000 N on the cadaver, but approximately 7,000 N on the dummy (see Figure 1). Viano's. His statistical conclusions were strongly challenged as having methodological flaws by a knowledgeable and experienced statistical academic analyst [2]. However, other studies including a review of dummy and specimen head/neck speeds and forces by Sances [3] the data from 16 Malibu rollover tests [4], volunteer human drop tests [5] and studies of NFL football impacts [6] all suggest that Viano's conclusion is reasonable, and suggest a 4.5 m/sec head impact (which would produce a 10,000 N neck force in a Hybrid III dummy) would be the limit for producing severe to fatal neck fractures.

Viano claimed that in general human head impact speed, neck force, and neck injury (classified only as serious or fractures) are poorly correlated. Nevertheless, he showed that the cadaver data demonstrated a low probability of a serious neck fracture for head impacts below 2 m/sec (4.5 mph) and high probability in head impacts above 4 m/sec (9 mph) as shown in his Figure 13 (our Figure 1).

In deriving the probability function Viano assumed all injuries were serious and did not differentiate among serious to fatal injuries. As can be seen, all of the cadavers that sustained a "serious" neck injury in the available data had a head impact at a speed greater than 4 m/sec, but there was a dearth of data from head impacts below this level.

The available PMHS (cadaver) data comes from a wide range of impact circumstances and a variety of head impact modes and mostly from the bodies of people who were older or diseased.

It is well known that the probability of serious injury increases dramatically with age. Thus, this data establishes a lower limit for the probability of serious injury as a function of resultant head impact speed. Viano describes his figure as follows:

"Figure 1 shows the 68 tests plotted with serious injury = 1 and no injury = 0. A Logistic regression model was fit to the data. This gives a sigmoidal injury risk function that is typically used in biomechanics research to determine human tolerances. The Logistic functions are plotted in Figure 1. For the upper curve, there is a weak relationship with a 32% probability for neck fracture at 2,000 N impact force, 50% at 3,472 N, 57% at 4,000 N and 85% probability of fracture at 7,000 N." Viano found no detailed relationship between head impact speed and neck force while classifying all the cadaver tests as either serious or non injuries.

Contrary to this general statistical analysis, single mode cadaver drop tests (most closely related to rollovers) of Sances, Yogananda and Nuscholz analyzed by Sances[3] found that severe to fatal (clinical fracture) injuries occurred at drop heights of 1 meter (4.4 m/s or 10 mph) and in tests of 1.2 to 1.5 meters (4.8 to 5.4 m/s or 11 to 12 mph) as shown in Viano's Figure 5 below, Figure 2.

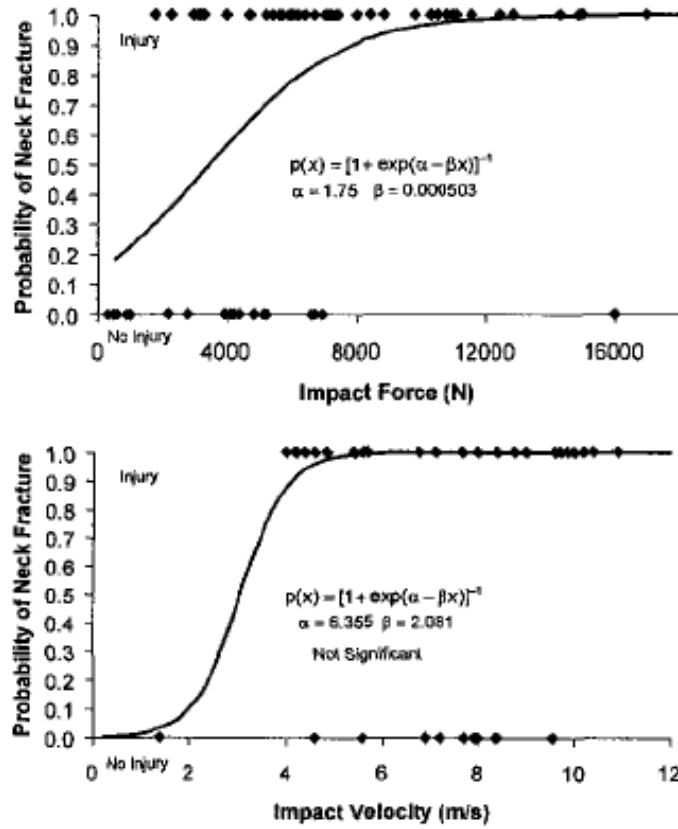


Figure 1 – PMHS data from Viano.

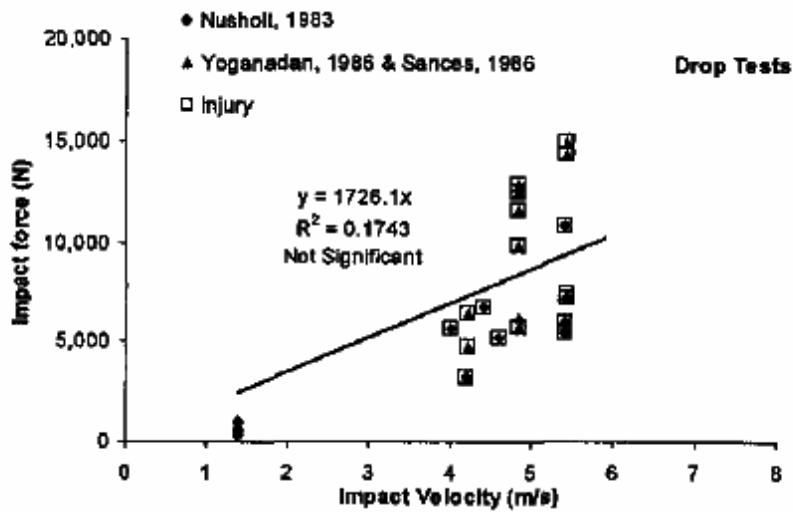


Figure 2. Figure 5 from Reference [1].

Viano also conducted research into football player injuries from head impacts.[4] For this work, videos of such impacts in actual football games were analyzed for impact speed, angle, point of contact, and other variables. Then, the impacts were emulated using fully instrumented Hybrid III dummies to determine the head acceleration and neck responses. Most important about this work is the insight it provides on the healthy human head impact velocity in which *no* head or neck injury occurs.

Although 22 of the 27 struck players whose impacts were studied suffered concussions (at 16.1 ± 4 mph) none sustained a neck fracture. Struck players were uninjured at impact speeds of 11.2 ± 2.5 mph. None of the striking players suffered significant head or neck injury at 9 ± 2.7 mph. As the study points out, “There are many reasons why the striking player is not injured, including the collision mechanics, strength and ability of the players and strength training of the neck musculature to maintain alignment during impact.” These players were all young men.

We can conclude that these athletes define the opposite end of the spectrum of injury susceptibility from the cadavers discussed above. The impact velocities of the striking players involved ranged to above 11 m/sec and the change in velocity of their heads in most cases ranged from about 3 to over 6 m/sec (there were 4 with change in head velocity under 3 m/sec and one with a change in head velocity of 7.3 m/sec).

Another source of human non-injury data comes from tests conducted with volunteers in 1996⁵ and 1998⁶ in rigidized roof fixtures. In these spit and drop tests, belted occupants whose heads when inverted were at the rigidized roof, fell or were dropped at distances of 7.6 cm (3” producing an impact speed of 2.7 mph), 23 cm (9”, 4.7 mph), 30.5 cm (12”, 5.4 mph), 50 cm (20”, 7 mph) and 91 cm (36”, 9.5 mph). None was injured in these tests.

It is important that a neck injury criterion not be set at unrealistically low levels. To do so would unnecessarily constrain the design of products in which neck injuries might occur. In a motor vehicle rollover, for example, occupant head contact with the roof is likely, and the occupants of the vehicle may actually be falling toward the ground at a small velocity (rarely more than 1.5

m/sec) at the time of roof impact with the ground. Thus, the injury criteria should recognize that a human can survive such an impact without serious injury.

Because Hybrid III dummies are generally used in motor vehicle crash research and testing, it is important to understand the relationship between dummy measurements and the probability of human injury.

Viano’s tests varied according to the impact surface, orientation and the use of helmets. Viano’s Figure 22 (below) provides a summary of these previously reported test results.

Again Viano didn’t differentiate between top/back impacts and more general orientations. Although these general results show substantial scatter, the data points obtained from tests with the same focused test conditions (top and back of the head impacts) are highly regular.

This suggests that for given test conditions, such as in a rollover, there is a linear relationship between dummy top/back of the head impact speed and neck force.

Sances[5], in 2002 addressed this problem. He compared his cadaver drop tests with Hybrid III dummy drop tests as well as various tests conducted to determine the neck compression force measured on the dummy as a function of head impact speed. He also considered recent evaluations under the similar rollover conditions of the Malibu dolly rollover tests, which measured and plotted the neck forces versus both neck compression velocity and roof intrusion velocity on the Hybrid III dummies. These results were also linear and of somewhat lower slope than the lower neck forces he originally measured.

He concluded that: “The data indicated that the hybrid III system transmits about 70 to 75% of the applied force from the head or upper neck to the lower neck area. In contrast, the cadaver studies showed for drops from 0.9 to 1.5 meters, about 20 to 30% of the applied force was transmitted from the head to the lower neck.” In effect the human neck is at least twice as good an absorber of forces from the head as the dummy neck.

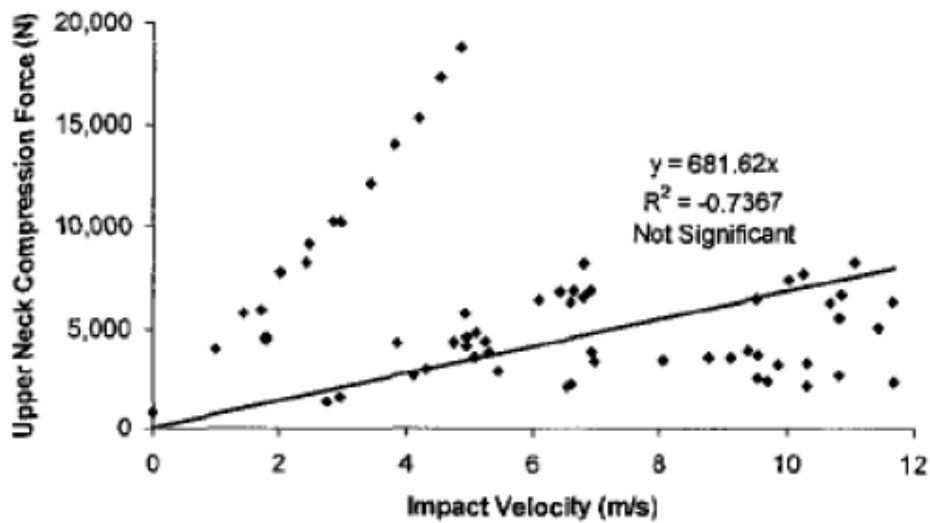


Figure 3. Figure 22 Dummy Tests: Neck Compression Force as a Function of Head Impact Velocity, from unpublished study [1].

To compensate when using the hybrid III dummy in rollover testing, the dummy force criteria at the upper neck sensor would be twice as high as the human criteria. Applying Sances cadaver to dummy conversion, an impact to a human at 3 m/sec would produce a force of around 3,500 N at the human neck while a dummy would measure a neck force of 7,000 N under the same head impact conditions.

Both of Sances' human and dummy comparisons were in drop tests to a solid surface, while the Malibu neck compression and intrusion velocity data was taken during vehicle rollovers. For rollover test purposes then, choosing the lower Malibu Hybrid III neck force versus velocity would err on the side of caution as shown below.

The data analyzed in the Viano paper strongly suggest that a simple, general mode, biomedical neck injury criterion, based on the probability of serious (AIS = 3) neck injury, is that the occupant's head not sustain an impact at a resultant speed greater than around 3 m/sec (7mph) and a force of 7,000 N. This is the level at which the probability of a *serious* neck injury or fracture (but not necessarily a spinal cord injury) to the most vulnerable members of society is around 50 percent. The probability of injury to a younger, healthier individual would be substantially lower than 50 percent.

Similarly, the single mode (rollover related) drop tests of Nuscholz, Yogananda and Sances as analyzed by Sances, establish the biomedical likelihood of *severe to fatal* neck injury or clinical fractures (involving spinal cord injury) occurring at 4.5 m/sec (10 mph) or more to more vulnerable members of society. The likelihood of such injury to a young, healthy individual would be lower.

A reality check on these criteria come from NHTSA accident data [2002 NASS] and the Malibu series of experimental rollovers. The accident data indicates that 91.4% or about 427,000 people are not seriously injured in rollovers, while about 18,000 (3.9%) are seriously injured, an estimated 12,000 (2.6%) are severely or critically injured and ten thousand are killed (2.1%). As shown in figure 5 and 6 there were 94 potentially injurious impacts among the two dummies in the 16 Malibu rollovers. In those tests, there were 87 (93%) impacts at less than 7,000 N (from a 7 mph impact), there were 3 (3%) impacts at over 7,000 N (7 mph) and 3 (3%) at over 10,000 N (10 mph), and 1 that was greater than the 16 mph head injury criteria. All of the impacts greater than 7,000 N (7 mph) were in production vehicles and their distribution is consistent with the accident data.

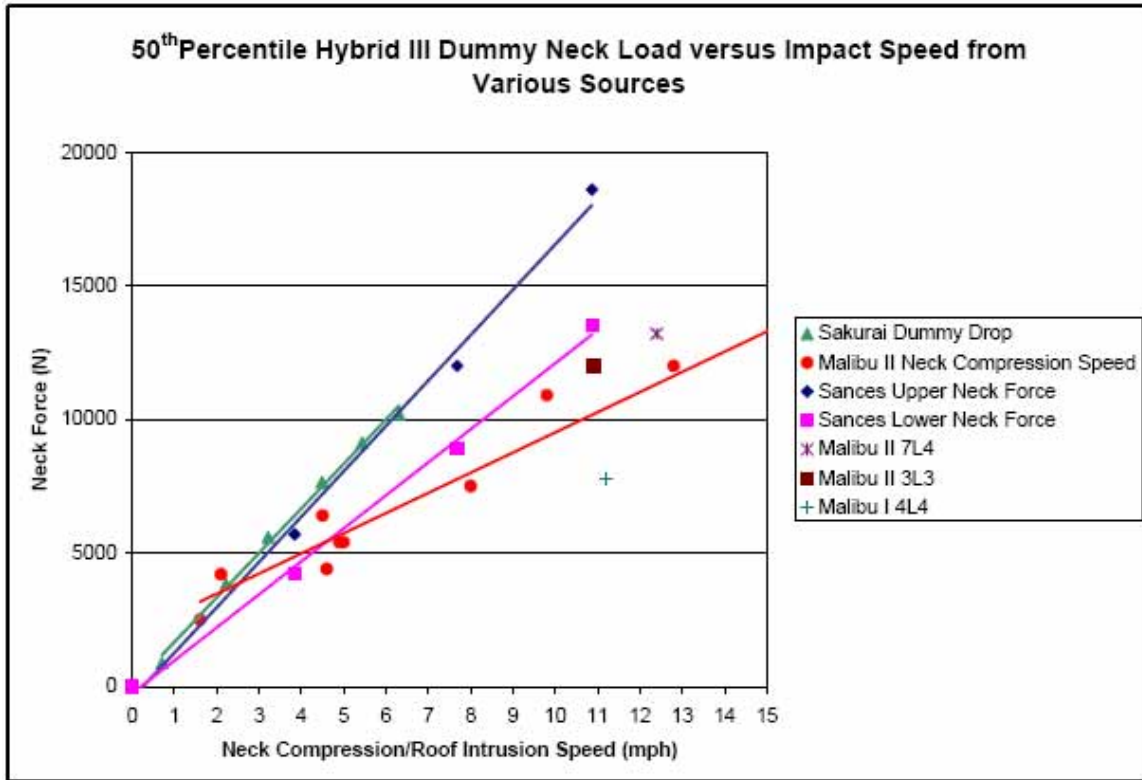


Figure 4. Various Hybrid III neck force vs. impact speed sources.

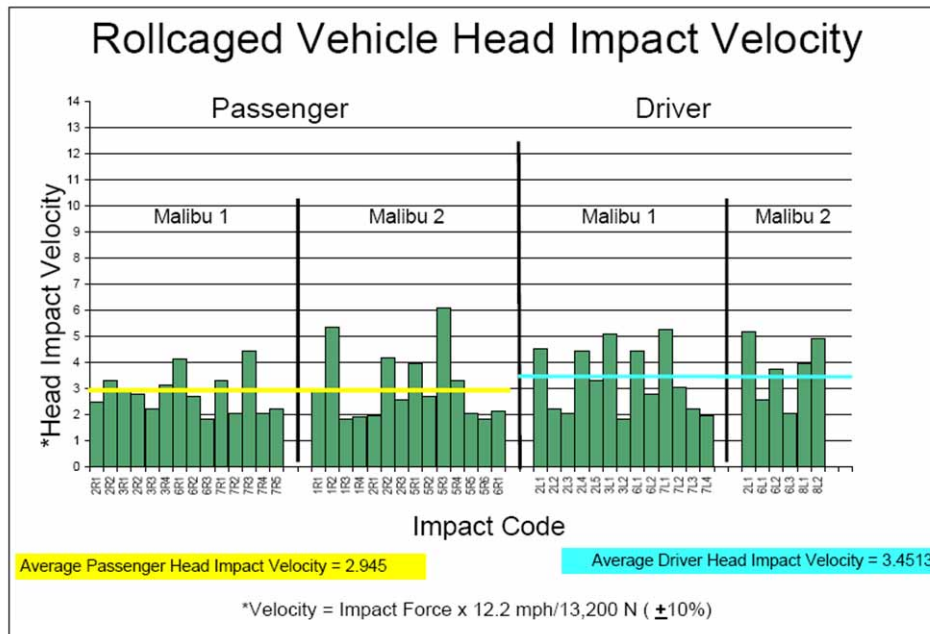
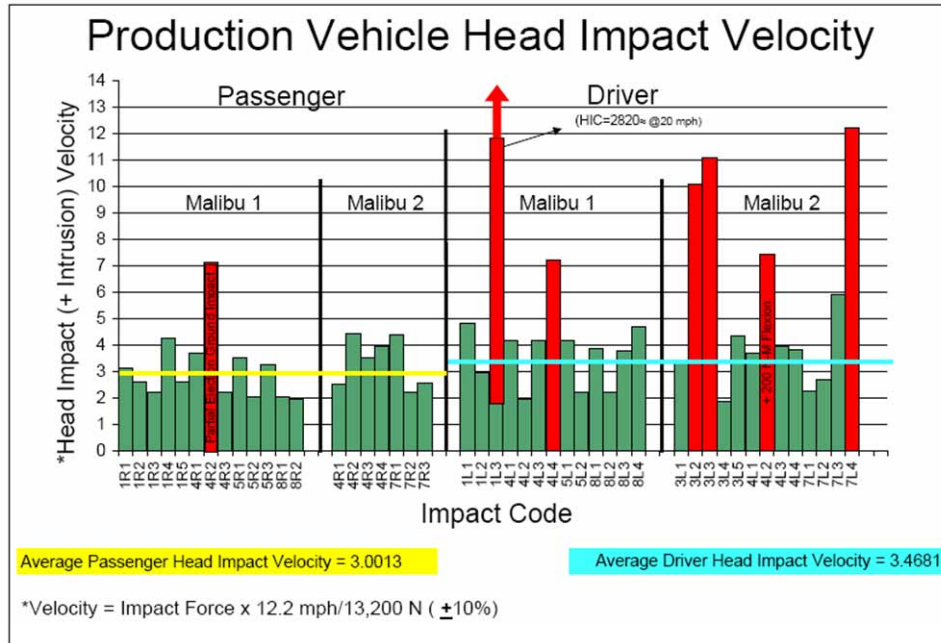


Figure 5. Malibu roll caged vehicle head impact speeds.



Red Bars are Head Impacts that Exceed 7 mph

Figure 6. Malibu production vehicle head impact speeds.

APPLICATION

Rollover crashes, according to NHTSA, account for about 10% of towaway accidents, but are 6 times more lethal and 3 times more serious than frontal and other accidents. There are about a quarter million rollover crashes involving cars, pickups, vans and SUVs with nearly a half million occupants, more than ninety percent of whom are not seriously injured. About 3% are seriously injured and recover, 3% are severely or critically injured and are permanently debilitated and 2% die.

Within each of those categories a significant number of occupants are partially or totally ejected. Cumulatively, eighty percent of all rollovers and 65% of the serious to fatal injuries occur in a one-roll event, and 95% of such injuries occur within 2 roll events.

In 2001, the non-profit Center For Injury Research and Xprts, LLC developed the Jordan Rollover System or JRS, a machine for conducting repeatable dynamic rollover roof impact tests. More than forty tests have been conducted on the JRS that have explored the effect of varying the test parameters and protocols.

The JRS holds the vehicle on an axis that goes through its center of gravity. It is rotated and dropped in coordination with the movement of a road segment under it. After impacts with the initially leading (near) side and the initially trailing (far) side, the vehicle is caught so that it sustains no further damage. In Figure 7, the vehicle rotates toward the left as the road surface moves along the rails below from left to right.

To quantify the roof crush during the roll there are thin cables that run from 6 points on the driver’s side, the far side of the roof, to the center of rotation of the vehicle. Those cables measure the change in inches and the speed of the roof towards the vehicle center.

The JRS can facilitate the development and evaluation of occupant protection alternatives under a wide, but range of dynamic rollover conditions. With the proposed injury criteria, it can also provide comparisons and objective rankings of the injury potential of different vehicles and alternative designs.

The severity of the JRS test increases with the vehicle’s pitch. We have conducted tests at both 5° and 10° of pitch. Increasing the roll rate of the vehicle increases the severity of the initially leading side (near) impact (which is less important because head and neck injuries rarely occur to occupants

seated on this side) but decreases the severity of the initially trailing (far) side.

The roll angle at initial impact strongly affects the far side impact. A greater roll angle will impose a greater force on the far side and is therefore a more severe impact. A lower roll angle will impose a greater force on the near side, but if the roof is strong, it will lift the vehicle and reduce the force on the far side.

We have tested vehicles that have minimal strength roofs (i.e. those that just meet the requirements of FMVSS 216) and vehicles with strong roofs on the JRS. A vehicle with a minimal strength roof, such as the 2000 Ford Explorer, show structural buckling and collapse even when tested at 5° of pitch and other lower severity conditions. The maximum intrusion speed was over 5 m/sec. Many other vehicles that we have tested show similarly poor performance in this test.

We have also tested vehicles with relatively strong roofs. The strongest production roof vehicle, the Volvo XC90, did well in a series of three runs. In the first two runs, at 5° pitch, there was no roof collapse or buckling and roof intrusion was only a couple of

inches with an intrusion speed of only 1.4 m/sec. (3 mph), see Figure 8.



Figure 7. JRS Test Setup

Since the injury criteria is that serious injury is probable at head impact speeds of 3.6 to 5.4 m/sec (7 to 10 mph) and severe to fatal injury is probable at more than 5.4 m/sec (10 mph), it is easy to see which vehicle is safer.

| 2000 Ford Explorer 4dr Roll 1 | Crush (in) | | Peak Crush Speed (mph) |
|----------------------------------|------------|-------------|------------------------|
| | Peak | End of Test | |
| A-Pillar | -8.7 | -5.9 | -6.3 |
| Mid Point Between A and B Pillar | -9.1 | -5.9 | -6.7 |
| B-Pillar | -6.7 | -3.9 | -5.5 |
| Inboard of A-Pillar | -7.0 | -4.9 | -5.8 |
| Inboard of Roof Rail Midpoint | -11.5 | -8.5 | -12.1 |
| Inboard of B-Pillar | -8.7 | -6.2 | -9.1 |
| Center of Roof | -8.2 | -6.3 | -7.6 |
| Near Side A-Pillar | -4.2 | -2.0 | -3.8 |

2000 Ford Explorer 2 Roll JRS Test Series

Peak Dynamic Crush – 11.5 inches
 Peak Cumulative Crush – 14.5 inches
 Peak Crush Speed – 12.1 mph

| 2004 Volvo XC90 Roll 1 | Crush (in) | | Peak Crush Speed (mph) |
|----------------------------------|------------|-------------|------------------------|
| | Peak | End of Test | |
| A-Pillar | -1.0 | -0.1 | -1.5 |
| Mid Point Between A and B Pillar | -1.5 | -0.3 | -2.2 |
| B Pillar | -1.2 | -0.1 | -1.9 |
| Header Inboard of A-Pillar | -0.6 | 0.0 | -1.2 |
| Front of Sunroof | -1.1 | -0.4 | -1.8 |
| Side of Sunroof | -1.5 | -0.3 | -2.3 |
| Near Side A-Pillar | -2.1 | -0.9 | -3.3 |
| Near Side B-Pillar | -3.2 | -1.1 | -3.7 |

2004 Volvo XC90 2 Roll JRS Test Series

Peak Dynamic Crush* – 2.6 inches
 Peak Cumulative Crush* – 1.1 inches
 Peak Crush Speed* – 3.0 mph

* Far side only

| 2000 Ford Explorer 4dr Roll 2 | Crush (in) | | | Peak Crush Speed (mph) |
|----------------------------------|------------|-------------|------------|------------------------|
| | Peak | End of Test | Cumulative | |
| A-Pillar | -9.2 | -6.4 | -12.3 | -9.6 |
| Mid Point Between A and B Pillar | -9.9 | -7.0 | -12.9 | -9.3 |
| B-Pillar | -9.9 | -6.7 | -10.6 | -8.8 |
| Inboard of A-Pillar | -6.3 | -4.2 | -9.1 | -7.0 |
| Inboard of Roof Rail Midpoint | -9.5 | -6.0 | -14.5 | -9.9 |
| Inboard of B-Pillar | -8.9 | -5.6 | -11.8 | -8.1 |
| Center of Roof | -5.7 | -3.1 | -9.3 | -8.5 |
| Near Side A-Pillar | -2.4 | 1.0 | -1.0 | -4.1 |

| 2004 Volvo XC90 Roll 2 | Crush (in) | | | Peak Crush Speed (mph) |
|----------------------------------|------------|-------------|------------|------------------------|
| | Peak | End of Test | Cumulative | |
| A-Pillar | -1.9 | -0.5 | -0.6 | -2.0 |
| Mid Point Between A and B Pillar | -2.6 | -0.7 | -1.0 | -2.9 |
| B Pillar | -2.6 | -0.7 | -0.9 | -3.0 |
| Header Inboard of A-Pillar | -1.2 | -0.3 | -0.3 | -1.4 |
| Front of Sunroof | -1.6 | -0.5 | -0.8 | -2.1 |
| Side of Sunroof | -2.5 | -0.7 | -1.1 | -2.9 |
| Near Side A-Pillar | -0.3 | 0.2 | -0.7 | -1.1 |
| Near Side B-Pillar | -0.9 | 0.3 | -0.8 | -1.8 |

Figure 8. JRS Test Results.

CFIR and XPRTS have also conducted two roll, 15 mph JRS tests at 5° of 8 other production vehicles, see Figure 9. These equal severity tests provide the basis for an injury potential

ranking system shown here. Note that a one mph allowance for the occupants falling speed has been made, higher rankings are not directly related to increased roof strength to weight ratio

(SWR), and that the best ranking is awarded only to those vehicles that meet the crush speed criteria and do not create ejection portals.

and ejection potential of vehicles in rollovers and can definitively identify vehicle safety component defects and their causal relationship to death and injury in accidents.

In conjunction with the proposed test injury criteria, the JRS can rank and compare the injury

JRS 15 mph Low Severity Dynamic Rolls Ordered by Max. Roof Crush Speed at any Point for Injury Potential Evaluation

| Model Years | Make/Models | 216 SWR | Max Crush (Inches) | Maximum Speed (MPH) | Injury Probability | Case Injury |
|-------------|-------------------------|---------|--------------------|---------------------|--------------------|--------------|
| 2002-2006 | Volvo XC90 SUV | 3.6 | 3.2 | 3.7 | Best | NA |
| 1999-2005 | Hyundai Sonata Sedan | 1.8 | 6.4 | 8.0 | Fair | Quadriplegia |
| 2003-2006 | Kia Sorrento SUV | 1.9 | 6.9 | 9.0 | Poor | Quadriplegia |
| 1995-1999 | Nissan Sentra Sedan | 3.2 | 9.1 | 9.6 | Poor | Quadriplegia |
| 1995-2001 | GMC Jimmy SUV | 2.4 | 6.7 | 9.8 | Poor | Quadriplegia |
| 1995-2005 | Chevy Blazer SUV | 2.4 | 9.6 | 10.1 | Not Acceptable | Quadriplegia |
| 1999-2001 | Isuzu VehiCross SUV | NA | 6.8 | 11.1 | Not Acceptable | Brain Injury |
| 2001-2006 | C2500 HD Reg Cab Pickup | 2.2 | 9.9 | 11.2 | Not Acceptable | Fatal |
| 1995-2001 | Ford Explorer SUV | 1.6 | 11.5 | 12.1 | Not Acceptable | Quadriplegia |
| 1994-1999 | Mitsubishi Eclipse | 2.5 | 7.6 | 12.1 | Not Acceptable | Fatal |

(Criteria: Best = < 6mph and no ejection portals; Good = < 6 mph; Fair = < 8 mph; Poor = < 10 mph; Not Acceptable = > 10mph)

Figure 9. JRS Test Results.

The proposed injury criteria is validated by being consistent with the actual injury suffered by the victim for whom the test was conducted.

CONCLUSIONS

These injury criteria are appropriate and valid for use in research, design and testing of a vehicle’s injury potential in rollover accidents. Specifically, a 3.6 m/sec (7 mph, 7,000 N head impact as measured by a Hybrid III dummy) resultant head impact speed represents the onset of serious neck injury and a resultant 5.4 m/sec (10 mph, 10,000 N) represents the onset of severe to fatal neck injury. NHTSA specifies that a head impact velocity in excess of 15 mph must not produce a HIC that represents the onset of serious head and brain injury. On the other hand the head and torso may be tilted and the serious injuries are not just in Fz.

REFERENCES

[1] Viano, David, “Analysis of Reports and Literature on Head Impacts Causing Neck Compression Injury,” Bloomfield, MI: July 12, 2006, prepared at the request of Keith D. Heinhold.

[2] Richie et. al. Personal Communications.

[3] Sances, Anthony and Kumararesan, Srirangam, “Comparison of Biomechanical Head-Neck Responses of Hybrid III Dummy and Whole Body Cadaver During Inverted Drops ---

[4] Viano, David C. and Elliot J. Pellman, “Concussion in Professional Football: Biomechanics of the Striking Player – Reconstruction Neurosurgery, Vol. 56, No. 2, February 2005, p 266-280.

[5] Sances, 2002.

COMPARISON OF TETRAHEDRAL AND HEXAHEDRAL MESHES FOR ORGAN FINITE ELEMENT MODELING: AN APPLICATION TO KIDNEY IMPACT

Xavier BOURDIN

INRETS - LBMC (UMR_T9406 INRETS/UCBL1), Bron, France

Xavier TROSSEILLE, Philippe PETIT

LAB PSA Peugeot-Citroen, Nanterre, France

Philippe BEILLAS

INRETS - LBMC (UMR_T9406 INRETS/UCBL1), Bron, France

Paper Number 07-0424

ABSTRACT

Hexahedral elements with a single integration point have been the solid elements of choice to represent organs in human finite element models for impact. While those elements have been known to be efficient in terms of stability and computational cost, they are difficult to generate and meshing represents a significant part of a model development time. The ever increasing level of details of biomechanical models further increases these meshing difficulties. In recent years, computing power has become affordable and new formulations of tetrahedral elements – that can be generated automatically even for complex shapes – have been introduced in the explicit finite element codes. The aim of this study was to evaluate the performance of two meshing approaches – semi-automatic hexahedron meshing vs. automatic tetrahedron meshing – for a simple biomechanical application. In this study, a kidney model was build based on the geometry from Visible Human Project dataset. Five types of 3D solid elements (8 node bricks with a single and 8 integration points, 20 node bricks, 4 and 10 node tetrahedrons) and two material laws (linear visco-elastic, hyperelastic viscous) were used to simulate a kidney blunt impact described in Schmitt and Snedeker [1].

While the drawbacks of tetrahedral elements were observed in particular in terms of computing cost, the difference in model response was found to be acceptable in a biomechanical characterized by large specimen to specimen variability. Furthermore, the tetrahedral element stability was found to be excellent.

For more complex shapes, the increased computing cost may be largely outweighed by the advantages of an automatic meshing approach.

INTRODUCTION

Hexahedral elements with a single integration point and hourglass control have been the elements of choice for human explicit finite element modeling.

Tetrahedral elements have rarely been used despite the fact that they are easy to create automatically while the generation of high quality hexahedral elements is very difficult for complex shapes such as those seen in the human body. One reason maybe that the hexahedral elements had important computing cost, stability and mechanical response advantages over the tetrahedral elements available in the past.

Human finite element models have become essential tools in automotive safety research. Besides numerous models of anatomical regions, several whole body human models are currently available (HUMOS2 from the HUMOS European consortium, THUMS from Toyota RD and the H-Model from ESI). However those models still need to be improved before they are able to reliably predict the risk of injury resulting from an impact. Future improvements may include:

- a more detailed description of the anatomical structures in order to better localize the injury prediction;
- better numerical stability and robustness;
- the consideration of specimen to specimen variations, both from geometrical and material properties standpoints.

Such developments are likely to make even more difficult the meshing, which is critical and very time consuming in human finite element modeling. For example in the case of the abdomen, if we compare the mesh of the HUMOS2 [2] model with a more detailed description of the abdominal anatomy derived from the Visible Human Project, it becomes apparent that further refinement will make the meshing task very difficult if the organs such as the intestines and their mesenteric attachment are simulated individually (Figure 1). The mesh quality - in terms of quality metrics such as the Jacobian, internal angles etc - resulting from such a complex mesh would likely be relatively poor, affecting in turn the stability of the model.

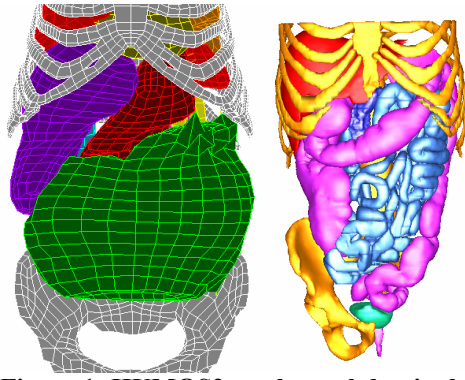


Figure 1: HUMOS2 mesh vs. abdominal geometry contoured at the L BMC (half of the pelvis only is displayed). Currently, the level of detail of HUMOS2 and of other finite element models of the abdomen does not allow simulating all organs individually.

Finally, the generation of different sets of meshes to take into account specimen to specimen variations would be time consuming even using scaling methods such as those used for the HUMOS2 model, as such methods are known to degrade the mesh quality, requiring manual corrections.

Those expected difficulties, associated with the availability of improved tetrahedral elements in the explicit codes and the development of low cost-high performance computing capability may make the drawbacks of tetrahedral elements acceptable, at least for research models. This can be evaluated by comparing simulation results using both approaches - tetrahedral and hexahedral meshing – while keeping all other modeling parameters identical (material properties, geometry etc).

This comparison was already made in the past for quasi-static simulations of the femur: Ramos and Simões [3] compared the results of 4-node and 10-node tetrahedral elements to 8-node and 20-node hexahedral elements and found the difference on the Von Mises stress predicted when loading the femoral head to be acceptable. While this is encouraging, these results obtained for hard tissues in an implicit code and quasi-static conditions are not necessarily applicable to soft tissues subjected to impact.

In this paper the use of tetrahedral element for soft tissues simulation during an impact were evaluated using a simple kidney model.

MATERIALS AND METHODS

Choice of loading condition

Schmitt and Snedeker [1] studied the biomechanical response of isolated kidneys

subjected to blunt impact. In their experiments, a pendulum was used to impact human (N=3) and porcine (N=65) kidneys. For the current study, the porcine dataset was selected because of its large number of specimen and because it provides tests results for various impact energies – from 1J to 6.08J – which are useful for the finite element model calibration. When comparing the human to the porcine kidneys results, the respective force versus displacement curves were of similar shape but slightly different amplitude. Based on their study, porcine and human kidneys are of similar geometrical shape and size.

Model generation: geometry and meshes

For the current study, a finite element model of the human kidney has been created based on the Visible Human Project dataset from the National Library of Medicine (Bethesda, MD). The image segmentation was performed manually using the IMOD (Univ. of Colorado, Boulder) software package in order to reconstruct a triangular surface representation of the organ. This surface was then scaled according to the geometrical average properties provided by Schmitt and Snedeker [1].

In order to simplify the problem and avoid a large number of numerical parameters, the kidney was assumed to be homogeneous and covered by a layer of shells representing the capsule covering the parenchyma. Two sets of meshes with similar number of elements were created using the ANSA software package (Beta-CAE, Thessaloniki, Greece): one hexahedral mesh with 1888 elements and one tetrahedral mesh with 1912 elements. The tetrahedral mesh was build automatically while the hexahedral mesh was build using surface to surface mapping. Those meshes were declined in five formulations of solid elements (Table 1) defined in the Radioss finite element code that was used for all simulations (Altair Engineering, Troy, MI). They were covered by 4-node shell or 3-node shell with coincident nodes on the outside surface.

Material properties

Two different types of material properties – hyper-elastic viscous (law 62 in Radioss) and linear visco-elastic (Bolzman law 34 in Radioss) – were used for the kidney.

Table 1. Elements used in the current study.

| Simulation name | Element type |
|-----------------|---|
| Brick8-1P | 8 nodes brick, single integration point and hourglass control |
| Brick8-8P | 8 node brick, 8 integration points |
| Brick20 | 20 nodes brick |
| Tetra4 | 4 nodes tetrahedron |
| Tetra10 | 10 nodes hexahedron |

The law 62 is an hyper-elastic law where the strain energy function is given by:

$$W = \sum_{i=1}^n \frac{2\mu_i}{\alpha_i^2} \left(\lambda_1^{\alpha_i} + \lambda_2^{\alpha_i} + \lambda_3^{\alpha_i} - 3 + \frac{1}{\beta} (J^{-\alpha, \beta} - 1) \right),$$

where the λ_i are the principal stretches, J the volume variation and μ_i , α_i and β the material parameters. β can be defined using the Poisson ratio. The viscosity is modeled by a Prony series applied to all shear parameters.

The material parameters of the first order Mooney-Rivlin viscous material law (law17 in Pamcrash) used by Snedeker et al. [4] for the parenchyma in their model could not directly be used in this study because the respective formulations of the laws (62 in Radioss and 17 in Pamcrash) differ in the way the bulk response and the viscosity are handled. Furthermore, the current study makes the assumption that the kidney is homogenous while the study of Snedeker et al. [4] identified the properties of the parenchyma while a (softer) fluid component was simulated inside the kidney.

The material parameters used in the current study were therefore derived from the study of Snedeker et al. [4] properties as follows:

- an order $n=2$ was selected for the strain energy function, with $\alpha_1=2$ and $\alpha_2=-2$. This would be equivalent to a 1st order Mooney-Rivlin model in the case of incompressibility (see Appendix). In that case, if the Mooney Rivlin model used by Snedeker et al. [4] was transposed to this study, the constants μ_1 and μ_2 would be the double of their C_{01} , C_{10} constants (see Appendix): $\mu_1=410$ kPa and $\mu_2=363$ kPa respectively.
- a second order Prony series was used for the relaxation, keeping the same time constants as Snedeker et al. [4] (10 ms and 0.5 ms) and keeping similar ratio between the instantaneous and infinite moduli ($\gamma=G_\infty/G_0=0.6$ for the first time constant and $\gamma=G_\infty/G_0=0.35$ for the second time constant).
- A Poisson ratio of 0.47 was assumed in order to simulate the quasi-incompressibility of the solid
- The values of μ_1 and μ_2 were decreased by the same factor until a reasonable agreement was reached in terms of maximum displacement and maximum force in the 4.9J impact condition.

A similar approach was used for the linear visco-elastic law 34, keeping only one time constant (0.5 ms), and the same Poisson ratio (0.47). The

properties finally selected are summarized in the Tables 2 and 3.

It must be noted here that this approach does not aim to identify precisely material properties to use for the kidney subjected to blunt impact but only to be able to approximate the overall kidney response in order to compare the numerical performance of element types and laws.

For the capsule, the material properties were based on quasi-static experimental results by Snedeker et al. [5]. The capsule was assigned a thickness of 43 μ m and an elastic modulus of 15MPa as in their study. It was also assigned the same Poisson's ratio as the parenchyma (0.47) in the current study.

Other simulation parameters

The impactor and the wall were simulated with rigid bodies. The wall was fixed while the impactor was free to translate in the direction normal to the wall and was assigned an initial velocity. The contact between the kidney, wall and impactor were simulated using a bi-lateral surface to surface contact (type 7) in parallel with an edge to edge contact (type 11). A 0.05 friction coefficient was used for all contacts as used by Schmitt and Snedeker [1]. For the brick20 elements, all nodes – including the nodes located on the middle of the edges – were used in the contact interface with the impactor. In order to attach the shells of the kidney capsule to those nodes, a tied interface (type 2) was also defined. An overview of the simulation setup is provided Figure 2.

Simulation matrix

First, a parametric study with impact energies used by Schmitt and Snedeker [1] was performed in order to verify the ability of the selected material parameters to approximate the kidney impact response. The selected simulation matrix is available Table 4. This study was only performed using the brick8-1P elements.

Then, the 4.9J simulation was selected as the baseline condition and all types of elements were compared.

Finally, the impact velocity was increased until the model became unstable in order to test the tetra4 and brick8-1P elements ability to handle extreme conditions.

Table 2. Selection of material parameters for the law 62 used in the current study

| Strain energy function parameters | Viscosity parameters (Prony series) |
|---|---|
| $\alpha_1=2$, $\mu_1=205$ kPa $\alpha_2=-2$, $\mu_2=181$ kPa $\nu=0.47$ | $\tau_1=10$ ms, $\gamma_1=0.60$ $\tau_2=0.5$ ms, $\gamma_2=0.35$ |

Table 3. Selection of material parameters for the law 34 used in the current study.

| | |
|---|--|
| $G_0 = 205 \text{ kPa}$ $\nu = 0.47$ | $G_\infty = 82 \text{ kPa}$ $\tau = 0.5 \text{ ms}$ |
|---|--|

Table 4. Summary of impact conditions for the test of the material parameters

| | | | | | | |
|--------------------|-------|------|------|------|------|------|
| Velocity (m/s) | 0.652 | 1.38 | 1.48 | 1.30 | 1.44 | 2.35 |
| Impactor mass (kg) | 4.7 | 2.2 | 2.2 | 4.7 | 4.7 | 2.2 |
| Energy (J) | 1 | 2.1 | 2.4 | 4.0 | 4.9 | 6.08 |

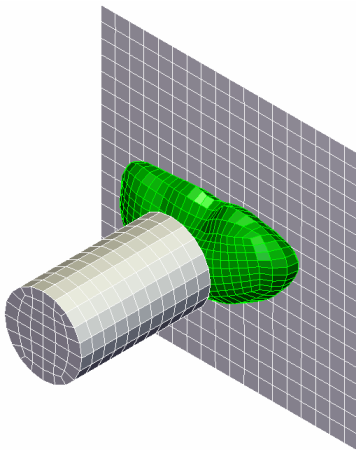


Figure 2. Overview of the simulation.

Comparison metrics

The model response was analyzed in terms of impactor force vs. impactor displacement curves, peak force and peak displacement, and energy dissipation. The force and displacement time histories were not available from the experimental studies and therefore could not be used to evaluate the models. The numerical behaviour was analyzed in terms of conservation of the energy balance, hourglass energy (when applicable), and time step conservation.

Regarding the computational cost, all simulations were run on the same machine (a dual Xeon EM64T at 3.06GHz) on two processors using the version 5.1d SMP Linux version. The machine was not running other jobs, and the user time, total time (sum of user and system time) were always within 1% of the wall clock time. The user time, number of time steps needed to finish the simulation and the cost per thousand cycles were used for the cost evaluation.

RESULTS

Comparison with the experimental data from Schmitt and Snedeker [1] at different energy levels (brick8-1P element only)

All the simulations performed with the brick8-1P element at energy levels between 1J and 6J ended with a normal termination, even for the highest energy case. Also, the hourglass remained within 10% of the energy of the simulation but there was a tendency for the hourglass to increase with impact energy, resulting in higher energy loss (from 3.2% at 1J, law 34 to 9.2% at 6J, law 62). Figure 3 shows a section of the mid-plane of the kidney at the peak impactor displacement for the 4.9J simulation. The force versus displacement response of the model was compared with the corresponding experimental results published by Schmitt and Snedeker [1] (Figure 4). Overall, the model response was similar to the experimental results, both in terms of peak force and peak displacement for all the energy levels with the exception of the 4J case. It must be noted that in the 4J test, the experimental peak force was between 650N and 850N, which is higher than the forces observed in the 4.9J test (between 600 and 735N). If comparing the responses of the laws 34 and 62, the two material models give very similar loading paths, peak force and peak displacement. However they differ significantly in unloading path and energy dissipation in the impact (area under the curve). The energy dissipation for the law 62 was 4.4J against 3.95 to 4.7J in the experiment. The energy dissipation for the law 34 was only 2.5J.

Comparison of the results for the different elements types at 4.9J

When testing the various element types, all simulations but two terminated normally. The law62 models using the brick8-8P and brick20 elements terminated with a negative volume after 19 ms and 32.4 ms respectively. All other simulations had energy balance errors lower than 6% at the end of the simulation (see Table 5, summary of the runs)

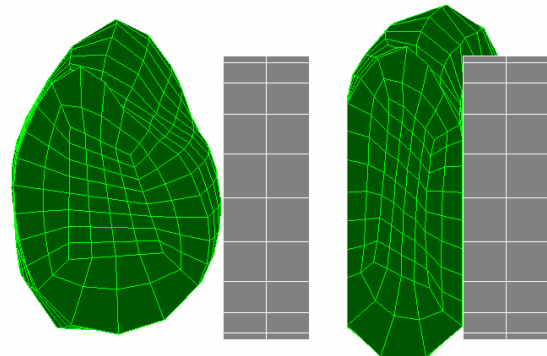


Figure 3. Mid section of the kidney at initial impactor position and peak impactor displacement for the 4.9J simulation.

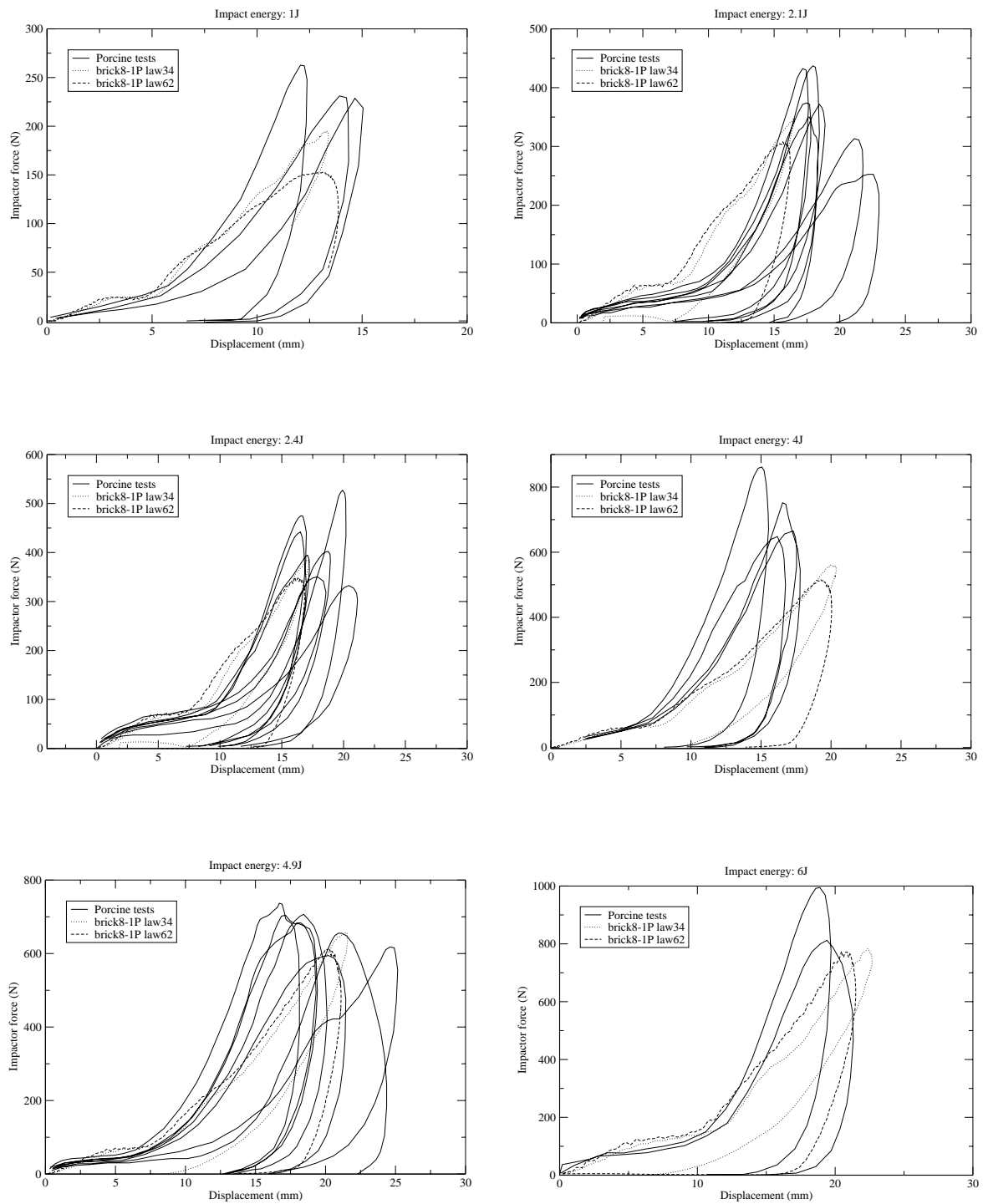


Figure 4. Comparison of the model response and the porcine test results for six impact energies from 1J to 6.08J. The solid lines represent typical tests results for each energy level.

Table 5. Summary of the runs

| Elem. | Law | Term. Time(ms) | Error (%) | Total kCycles | Total User (s) | Time / kCycle | Av Tstep (μs) |
|-----------|-------|----------------|-----------|---------------|----------------|---------------|---------------|
| brick8-1P | law62 | 40 | -5.7 | 58 | 816 | 14 | 0.69 |
| brick8-1P | law34 | 40 | -6.7 | 59 | 367 | 6 | 0.68 |
| tetra4 | law62 | 40 | -0.1 | 121 | 1427 | 12 | 0.33 |
| tetra4 | law34 | 40 | -0.4 | 153 | 599 | 4 | 0.26 |
| brick8-8P | law62 | 19.2 | 99.9 | 51 | 3848 | 75 | 0.39 |
| brick8-8P | law34 | 40 | -0.7 | 247 | 3125 | 13 | 0.16 |
| tetra10 | law62 | 40 | -0.1 | 121 | 5025 | 41 | 0.33 |
| tetra10 | law34 | 40 | -0.5 | 157 | 1606 | 10 | 0.26 |
| brick20 | law62 | 32.4 | 99.9 | 70 | 6563 | 93 | 0.46 |
| brick20 | law34 | 40 | -0.4 | 283 | 8137 | 29 | 0.20 |

Where:

Termination time: number of ms simulated (40 for a normal termination)

Error (%): percentage of error in the energy balance at the end of the simulation

Total kCycle: total number of cycles run to reach the termination time divided by 1000

Total User (s): the computing time spent at the end of the simulation

Time / kcycle: the average computing time needed to run 1000 cycles

Av Tstep: average time step over the simulation

The force vs. displacement curves for all elements types and the law 62 are presented on Figure 5. After an initial non linear section (up to 7mm approximately) where the response of all elements is very similar, the force vs. displacement curves become more linear and differences between the element types appear. However, the difference between all element types is small when compared with the specimen to specimen variations. Also, for the given element density, the responses of the tetra4 vs tetra10 elements were almost identical. Similarly, the responses of the brick8-1P, brick20 and brick8-8P elements were very close until the computation terminated with an error for the brick8-8P. Overall; the tetra elements appeared stiffer than the brick8 elements with a 7% higher peak force and a 8% smaller peak displacement. The average stiffness was also calculated for each of the models in the region where the loading curves are almost linear (Figure 6). The tetra elements (48.5 N/mm) were approximately 14% stiffer than the brick8-1P elements (42.7 N/mm). Similar results were obtained for the law 34 (Figure 7). A summary of all stiffness results is provided Table 6. The stiffening for the tetra elements was lower than 10% (approx. 47 N/mm vs. 43 N/mm). The difference in peak force between tetra and brick was less than 6%, while the difference in peak displacement was less than 5%.

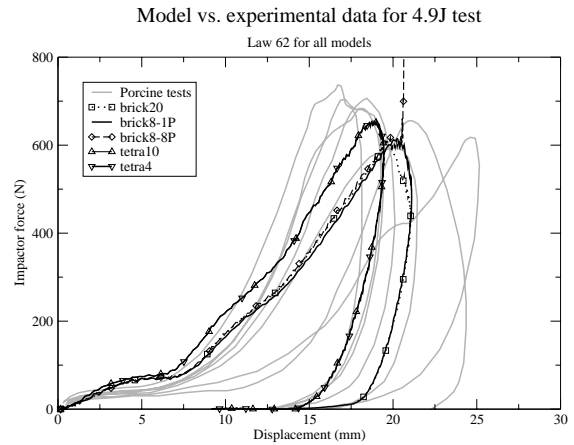


Figure 5. Force vs. displacement response for all elements types and the law 62 at 4.9J. The response of the 4 nodes and 10 nodes tetrahedron appears to be superimposed.

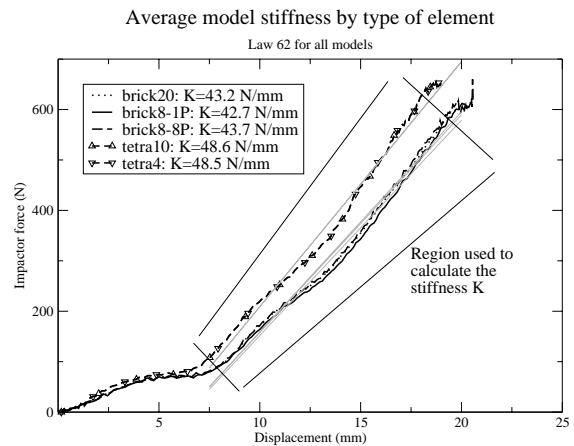


Figure 6. Stiffness calculation per element type. The stiffness was obtained by linear regression in the region plotted on the graph. The regression line obtained are plotted in light gray.

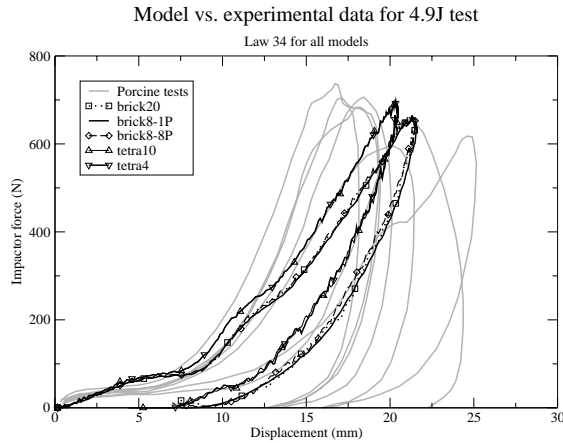


Figure 7. Force vs. displacement response for all elements types and the law 34 at 4.9J. The response of the 4 nodes and 10 nodes tetrahedron appears to be superimposed.

Table 6: Summary of stiffness depending on the element and the material law. All stiffness data are in N/mm

| | brick20 | brick8 1P | brick8 8P | tetra10 | tetra4 |
|-------|---------|--------------|--------------|---------|--------|
| Law34 | 43.1 | 42.9 | 43.4 | 47.0 | 47.0 |
| Law62 | 47.6 | 42.7 | 43.7 | 48.6 | 48.5 |

Computing cost

There were large differences in computing time since they varied from approximately 5min (brick8-1P law34) to 2h26mn (brick20 law62) as described in Table 5. Multiple factors are responsible for those large variations, including:

- the material law, with the law 62 being 2 to 6 times more time consuming per cycle than the law 34;
- the type of element, with variations of up to 1 to over 6 on the cost per cycle (brick20 vs. tetra4) at identical material law;
- the average time step for the simulation, with variations of 1 to 4 approximately (that factor being also linked to the element type).

For a given material law, the tetra4 elements were faster than the brick8-1P if only the cost per cycle is considered, but the tetra4 models had a longer computational time since their average time step was lower.

Numerical Stability in extreme conditions (brick8-1P and tetra4 only)

When increasing incrementally the impact energy to 21.5J, the response of the brick8-1P and tetra4 elements was very different (Figure 8).

For the brick element, the hourglass energy increased rapidly with the impact velocity, resulting in a large loss in the energy balance: at 21.5J (4.7kg at 3m/s) with a law34, the simulation terminated

normally but the energy loss reached 48% (Figure 9). The deformation of the solid elements inside the mesh showed very large distortion in hourglass modes (Figure 10). The model with the law 62 terminated with error (Negative Volume) during the unloading phase at 21.05 ms of simulation time. The model terminated with error (Negative Volume) for higher impact energies.

For the tetra element, much higher energy levels could be reached (Figure 11) with a better energy balance without apparent abnormal element distortion (Figure 9). At 37.6J (4.7kg at 4m/s), the simulation terminated normally with an error of 2.6% on the energy balance for the law 62, and a 14.6% error for the law 34. When further increasing the impact energy to 58.7J (4.7kg at 5m/s), the model with the law 34 terminated with error (Negative Volume) at 11 ms at simulation time but the model with the law 62 terminated normally with only a 5.2% error on the energy balance (Figure 12).

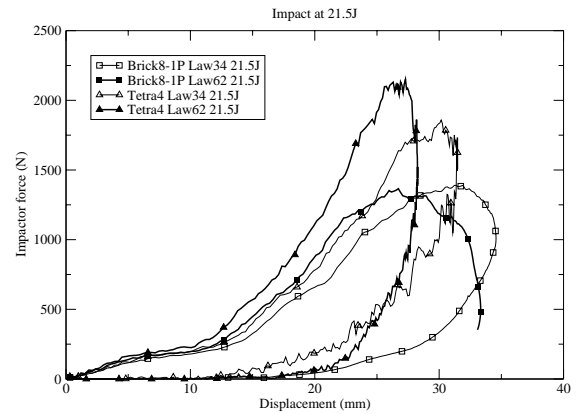


Figure 8. Force vs. displacement response for brick8-1P and tetra4 for laws 34 and 62 at 21.5J. The brick8-1P in law 62 terminated the simulation with an error during the unloading phase.

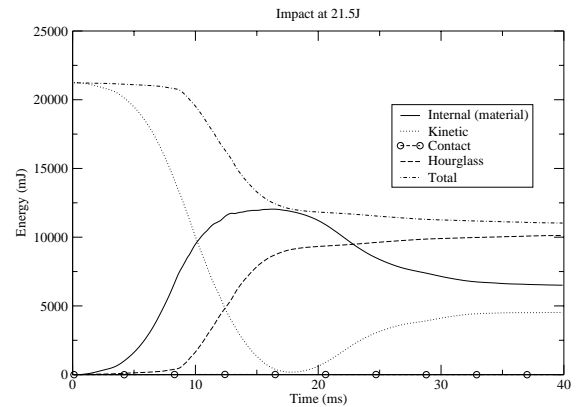


Figure 9. Energy vs. time response for hexahedron elements types and law34 at 21.5J.

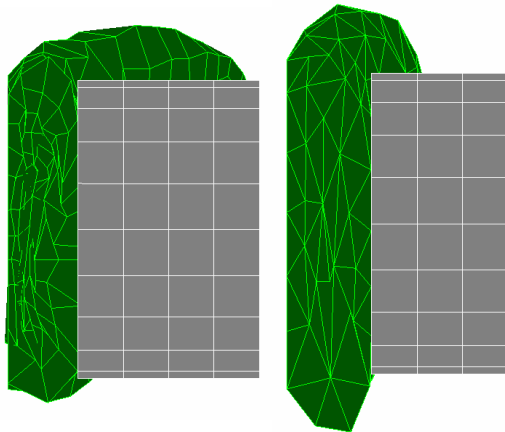


Figure 10. Examples of effect of extreme loading conditions on the model response: hexahedron elements for 21.5J at 16ms (left) and tetrahedron for 58.7J at 6ms (right)

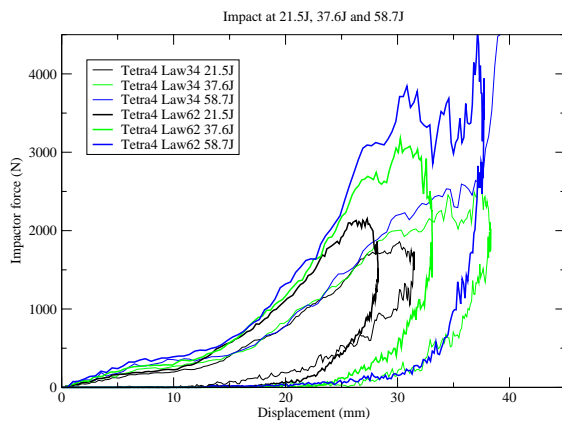


Figure 11. Force vs. displacement response for tetra4 elements and for laws 34 and 62 at 21.5J, 37.6J and 58.7J. The simulation terminated normally at 58.7J for the tetra4

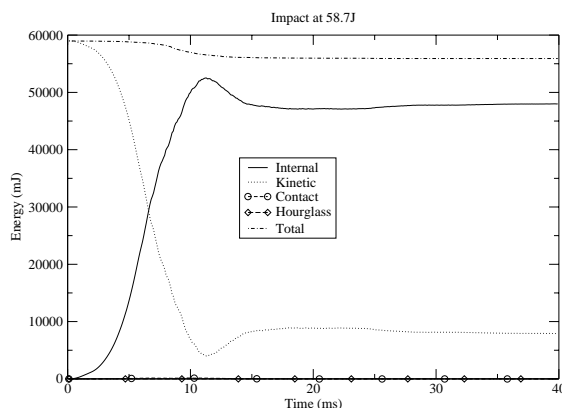


Figure 12. Energy vs. time response for tetrahedron elements types and law62 at 58.7J.

DISCUSSION

The material parameters used in the current study were identified by adapting properties proposed by Snedeker *et al.* [4] to approximate the overall response observed in the 4.9J experiments by Schmitt and Snedeker [1]. The laws selected were sufficient to approximate the overall response at other energy levels. There were larger discrepancies for some of the levels (4J in particular) but the comparison of the experimental results between different energy levels (4J vs. 4.9J) suggests that it may not be possible to match all the experimental responses with a single set of material properties or that other parameters that were not simulated have affected the testing results (positioning for example). While the material properties selected in this study may be inappropriate for other loading conditions, they are most likely sufficient for the current study which is only focusing on numerical aspects.

Both material models showed a fairly linear response after the initial loading where the non linear response may be due to contact non linearity and inertial loading. This phase of the response may be too linear when comparing it with the experimental data. A higher non linearity of the loading curve could be obtained by increasing the value of the α exponents in the hyperelastic viscous law but this is beyond the scope of this study. The main difference between the two laws is that the energy dissipation was lower for the law 34, which can be explained by the lack of the second time constant used in the law 62.

The effect of the number of integration points on the response was very limited: the brick20 and brick8-8P (fully integrated) were only marginally different from the brick8-1P element (with hourglass control) and the responses of tetra4 and tetra10 elements were virtually indistinguishable (Figures 5 and 7).

This result is of course very likely to change if the number of elements is decreased or if the loading mode is changed to include larger strain and stress gradients. A study on the effects of the mesh density would be useful. In the current application, a 1900 element model only represents a refinement lower than 3 of the HUMOS2 model which has approximately 100 elements as dividing the element size by 2 multiply their number by 8. In the current study, the mesh average element size was 5mm, and such a size may be needed to represent the complex anatomical structure of the abdomen.

When comparing the mechanical response of the various elements, the tetra (4 and 10 nodes) elements used in Radioss appeared to be 14% stiffer

(in the 4.9J case) than the brick8 elements. These differences are small when compared with the specimen to specimen variations and the uncertainties associated with the determination of material parameters.

In terms of stability, the brick8-8P and the brick20 were the only elements that did not terminate successfully the baseline level runs (4.9J). The detailed reason for the failure – and the possibility to stabilize the simulation – was not investigated as the interest of those elements with the current mesh density is very limited: they were at least 6 times as costly per cycle as the brick8-1P element but gave almost identical results. Similarly, the interest of the tetra10 is limited with the current mesh density as it did also provide virtually identical results as the tetra4 at a cost per cycle almost 4 times higher. Overall, this makes the brick8-1P and the tetra4 the two most interesting elements for the current mesh density.

When comparing the cost of the tetra4 and the brick8-1P, the lower time step of the tetra elements prevailed over its lower cost per cycle, resulting in a higher computing time (1.75 times higher in the case of the law 62).

Overall, this lower time step for the same average volume is the main drawback of the tetra4 element when compared with the 8 node brick element with a single integration point. In a larger model, this may be mitigated by the fact that the time step may not be determined by the soft tissues but by harder tissues like bone.

Regarding the stability of the brick8-1P elements, it must be noted that no effort was made to stabilize the simulations and it may be possible to further increase the brick stability in particular by changing numerical parameters such as the hourglass control formulation. Despite this and while using default options, both brick8-1P and tetra4 elements were stable for energies that were higher than the injurious energies proposed by Schmitt and Snedeker [6] (AIS = 5 for energies over 8J). This is a very encouraging result. For the conditions tested, the tetra element was much more stable than the brick, which had important hourglass problems. It was possible to reach very high compressions of the tetrahedral mesh, as the 58.7J simulation resulted in a compression of approximately 37.7mm while the initial thickness of kidney was 44mm. It is unclear if results obtained for such extreme deformations are realistic but the ability to terminate normally a simulation while respecting the energy balance is important when the complexity of a model increase and that the error termination of any of its components results in the failure of the simulation.

CONCLUSIONS

Simulations of the kidney subjected to blunt impact were conducted using an approximately 2000 element finite element model. Five element formulations and two material laws were tested. The model was able to approximate the kidney response to impacts of various energies ranging from 1 to 6J. For the element density selected, the number of integration points in the elements had little effect on the response. The tetrahedral elements appeared to be slightly stiffer than the hexahedral elements but the stiffness difference was limited to less than 14%. The tetrahedral elements were also more stable than the bricks when subjected to very high impact energies.

Overall for the current element size, the use of tetrahedral elements over 8 nodes bricks with a single integration point seems very promising. In the present study, their main drawback was their lower time step (at equivalent volume size) that led to higher computing cost (up to almost double). This would not be a significant drawback for research models considering the rapid evolutions of computing capability and the difficulty to generate hexahedral meshes for complex geometrical shapes.

Possible extensions of this evaluation could include the study of the effects of mesh density and complex in-situ loading on the model response.

REFERENCES

- [1] K.U. Schmitt and J.G. Snedeker. 2006. "Analysis of the biomechanical response of the kidney under blunt impact". *Traffic Injury Prevention*, 7:171–181.
- [2] P. Vezin and J.P. Verriest. 2005. "Development of a set of numerical human models for safety". *Proc. of the 19th Int. Tech. Conf. on the Enhanced Safety of Vehicles*. Paper 05-0163.
- [3] A. Ramos and J.A. Simões. 2006. "Tetrahedral versus hexahedral finite elements in numerical modelling of the proximal femur". *Technical note in Medical Engineering & Physics*, 28:916–924.
- [4] J.G. Snedeker et al. 2005. "Strain energy density as a rupture criterion for the kidney: impact tests on porcine organs, finite element simulation, and a baseline comparison between human and porcine tissues". *Journal of Biomechanics*, 38:993–1001
- [5] J.G. Snedeker et al. 2005. "Strain-rate dependent material properties of the porcine and human kidney capsule". *Journal of Biomechanics*, 38:1011–1021.

[6] K.U. Schmitt and J.G. Snedeker. 2006. "Kidney injury: an experimental investigation of blunt renal trauma". Journal of Trauma, 60:880–884.

APPENDIX: Mooney Rivlin vs. Ogden formulations for the strain energy function in the case of incompressibility.

The Mooney Rivlin strain function is:

$$W = C_{01}(I_1 - 3) + C_{10}(I_2 - 3)$$

where: C_{01} , C_{10} are material constants. The invariants are:

$$I_1 = \lambda_1^2 + \lambda_2^2 + \lambda_3^2$$

$$I_2 = \lambda_1^2 \lambda_2^2 + \lambda_2^2 \lambda_3^2 + \lambda_1^2 \lambda_3^2$$

$$I_3 = \lambda_1^2 \lambda_2^2 \lambda_3^2 = 1$$

In the Ogden strain energy function:

$$W = \sum_{i=1}^n \frac{2\mu_i}{\alpha_i^2} (\lambda_1^{\alpha_i} + \lambda_2^{\alpha_i} + \lambda_3^{\alpha_i} - 3)$$

where the μ_i and α_i are the material constants and λ_i are the principal stretches. If using $n=2$, $\alpha_1=2$ and $\alpha_2=-2$, we obtain:

$$W = \frac{2\mu_1}{4}(I_1 - 3) + \frac{2\mu_2}{4}(I_2 - 3)$$

Finally: $\mu_1 = 2C_{01}$ and $\mu_2 = 2C_{10}$

HUMAN/DUMMY ROLLOVER FALLING (EXCURSION) SPEEDS

Donald Friedman

Justin Caplinger

Xprts, LLC

United States

Jack Bish, Ph.D.

Consultant

United States

Paper Number 07-0503

ABSTRACT

Measurements of human and dummy falling (often referred to as diving) speeds were made from four series of experiments. The first series consisted of a 5th and 50th percentile human and a 50th percentile dummy in a production vehicle with production belts, in a spit test at roll rates to 200 degrees per second. The second series was conducted with surrogates in dynamic repeatable rollover test roof impacts in the Jordan Rollover System (JRS) fixture. The third series photo analyzed dummy motion in the interior of dolly rollover tests with belted and unbelted hybrid III dummies to determine independently, the excursion and intrusion speeds of the dummy and roof. The fourth series analyzed Malibu rollcaged and production vehicle occupant belt loop load vs neck impact force similar to a previous analysis of Autoliv rollover tests.

The first series measured the near and far side lateral and vertical excursion, excursion speed, roll rate, and belt loads, as well as, documenting occupant kinematics by lateral and frontal view video cameras. The second series measured the near and far side excursion and excursion velocity of a belted surrogate in 15 mph, 350 degree per second JRS roof impact tests. The third series photo analyzed high resolution video of dolly rollover tests with 50% hybrid III dummies in addition to the parameters collected in the tests associated with roll rate, dummy head impact speed and belt loads. The fourth series analyzed Malibu roll caged and production belt loop load vs. neck impact force at roll rates up to 500 degrees per second.

The measurements are presented in a graphical format with discussion in the context of rollover injury potential. The conclusions are that belted humans and dummies with 3 to 5 inches of excursion, have excursion speeds of little more than 0.5 mph.

The unbelted dummies with a similar amount of initial headroom have only slightly greater falling speed because of the short duration of the roof contact acceleration. Photo analysis of dolly rollover head impact speeds as measured by dummy neck loads, separated the excursion and roof intrusion speeds and indicated similar falling speeds. An inch or more of intrusion from a roll caged roof in combination with the close proximity of the head of a dummy result in composite head impact speeds of 3 mph or more.

INTRODUCTION

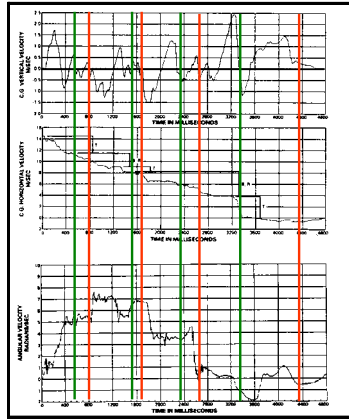
Rollover accidents in the US result in 30,000 serious to fatal injuries and 10,000 fatalities annually. Occupant motion in rollover accidents is an important parameter in determining injury causation and crashworthiness improvements.

One theory of rollover head and neck injury propounded in 1975[1] is that the occupant dives into the roof which is stopped on the ground and that the injury occurs before the roof crushes. This might be correct if the diving height (or equivalent falling speed) of the vehicle and occupant were sufficient to produce a severe to fatal injury.

The Malibu experiments, were 16 rollovers with 8 production vehicles and 8 with roll cages, each with restrained and unrestrained occupants[2,3]. The production roofs typically struck the ground at 1 mph and rollcaged vehicles struck at 3 mph as shown in Figures 1 and 2. Roll caged roofs are not rigid: they typically intruded two inches at speeds of up to 5 mph. The roll caged vehicle and occupant falling speed in combination with the intrusion speed are insufficient to produce serious to fatal injury[4].

We analyzed the same Malibu and other experimental data to demonstrate that injuries are caused by a

production vehicle's compartment crushing and impacting an occupant's head at increased speed. Measuring the crush speed of the roof and the excursion speed of the dummy during a rollover with different strength roofs determines how head and neck injuries are actually caused.



**GM Malibu I
Test 5**

(All data from GM)

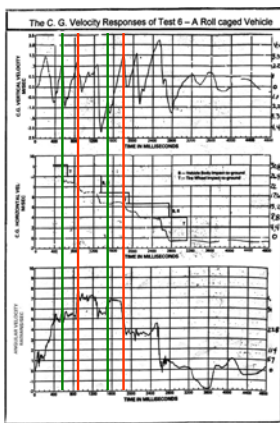
Near Side Contacts:
(Green Lines)

- 550 ms = 0.6 mph
- 1500 ms = 0.3 mph
- 2350 ms = 1.2 mph
- 3350 ms = 1.2 mph

Far Side Contacts:
(Red Lines)

- 790 ms = 0.6 mph
- 1677 ms = 0.4 mph
- 2662 ms = 1.2 mph
- 4330 ms = 0.7 mph

Figure 1. Malibu production vehicle roof contact speed with the ground.



**GM Malibu I
Test 6**

(All data from GM)

Near Side Contacts:
(Green Lines)

- 575 ms = 2.2 mph
- 1500 ms = 2.5 mph

Far Side Contacts:
(Red Lines)

- 836 ms = 2.7 mph
- 1802 ms = 3.1 mph

Note: Similar data between vehicle types. The main difference is the rollcaged vehicle does not crush.

Figure 2. Malibu rollcaged vehicle roof contact speed with the ground.

Previous work on this topic has focused mostly on quasi-static testing with low rotation rates. Initial dynamic studies were conducted by Herbst, et al. (1996)[5], Friedman, et al. (1996)[6], Friedman, et al. (1998)[7] and Meyer et al. (2000)[8]. These studies found that safety belts in production vehicles from the 1990s allowed substantial excursion toward rigid roofs without injury, that cinching latch plate belts arrested human occupant falling velocity, and that people were not seriously injured with roof intrusion of less than about four inches and were serious to fatally injured with roof intrusion of more than 6 inches as shown in Figure 3.

| Restrained Occupant Injuries | Average Roof Crush | |
|-------------------------------|--------------------|-------|
| | cm | in |
| None | 4.67 | 1.84 |
| No Head, Face, or Neck | 6.12 | 2.41 |
| Head, Face and Neck @ AIS 1-2 | 9.80 | 3.86 |
| Neck @ AIS 2-6 | 18.38 | 7.24 |
| Head and Face @ AIS 3-6 | 26.69 | 10.51 |

Figure 3. Table 4 from [7]. Injury Severity vs. Roof Intrusion.

Dynamic rollover occupant kinematics were investigated further by Friedman et al. (2000)[9] in a roll fixture composed of a vehicle buck suspended between two large hoops. The system had an eccentricity of nine inches allowing the structure to be rotated subjecting the occupant to dynamic rollover motion with falling but without impacts.

A dynamic rollover occupant study was conducted by Moffatt et al. (2003)[10] using both humans and dummies. This study determined that there were minimal differences between the motion of anthropomorphic dummies and human volunteers. The excursion exhibited in this study did not increase with an increase in roll rate from 220 to 360 degrees per second as expected. This study determined by photo analysis that far side occupants had a larger excursion than near side occupants. This study did not investigate occupant motion due to the impact phase of a rollover accident and did not examine the occupants' falling velocities during the tests.

In the current study, we examined occupant motion in dynamic spit tests and utilized a Hybrid III dummy in a dynamic rollover experiment. Further analyses of existing dolly rollover test results enabled us to verify our results.

DYNAMIC SPIT TESTING

Spit testing is important to determine how an occupant can move during a rollover. It can be determined whether an occupant can strike the roof or pass through a window opening under specific rollover conditions. Dynamic testing is the most realistic method of examining these issues without actually conducting a rollover test. In this study, instrumented vehicles were rotated about the longitudinal axis of rotation. Both human and dummy surrogates were placed into the vehicles to determine their excursion and excursion velocities through the use of string potentiometers. The rotation was accomplished by spinning the vehicle by hand. This allowed for quick start up and stopping of

the vehicle after the test phase of three to four rotations was completed. In general, the vehicles were up to speed within one rotation and could be stopped within one rotation while achieving peak rotation rates of 208 to 237°/second.

We used the Jordan Rollover System (JRS) fixture for this study. The vehicle was suspended between the two drop towers which allowed the vehicle to be freely rotated about its longitudinal roll axis as shown in Figure 4.

All the vehicles used in this study are production models. The majority are late model mid-sized SUV's, but the study also incorporates one sedan.

The occupants for this study were volunteers and ranged in size from a 5'2", 109 lb female to a 5'11", 165 lbs male. In addition a Hybrid II dummy with seated pelvis was also used to determine how this compared to the human surrogates.

The first part of this analysis examined the motion of a restrained occupant relative to the interior of a vehicle in a dynamic spit test. In this test, the occupant was in a vehicle that is free to rotate about its longitudinal axis.

The occupants were all volunteers. Prior to each test the occupant witnessed the rotation of the vehicle and was rotated slowly in the vehicle at least once to become accustomed to the motion of the vehicle and their motion in the interior of the vehicle.

The occupant was instrumented with various devices including a string potentiometer positioned underneath the seat and attached to the occupant. This device allowed the direct measurement of the motion of the occupant during the test and calculation of the excursion velocity. In addition, the vehicle was instrumented to allow monitoring of the roll rate throughout the test sequence. Other instrumentation varied, but typically included a string potentiometer to measure lateral motion, a set of belt load cells, a string potentiometer to monitor retractor motion and video cameras. Occupant data was collected by an onboard data acquisition system and transmitted to a stationary system.

In the first test series, three occupants were used; a 5'2", 109 lbs female, a 5'11", 155 lbs male and a 50th percentile Hybrid II male dummy. The occupants were placed in the driver's seat of a midsized SUV, which was then rotated both passenger and driver side leading monitoring the motion of the occupant and the vehicle. In general, the vehicle was rotated

four or more times in each direction. The peak roll rates are shown in Table 1. The occupant positioned the seat in a comfortable location prior to the test and donned the seat belt in a comfortable position. This resulted in unlocked restraints on properly seated occupants. This study did not look at out-of-position occupants.



Figure 4. Spit Test Setup.

**Table 1.
Peak Roll Rates**

| Subject | Peak Roll Rate |
|-----------------|-----------------------|
| Human Female | 237 deg/sec |
| Human Male | 223 deg/sec |
| Hybrid II Dummy | 208 deg/sec |

The production, mid-sized SUV used in this study was mounted in the test fixture as a buck with the front of the vehicle and running gear removed. It was ballasted at the rear and front to rebalance the vehicle around its longitudinal roll axis. The nature of this test did not require the vehicle to have mass properties equivalent to the production condition except for the location of the roll axis.

This vehicle had ample headroom, see Table 2. During these tests, none of the occupants struck the upper roof panel. There was light contact in one of the tests with the grab handle at the driver's seating location on the roof rail. This contact did not affect additional excursion. In addition, none of the occupants' heads went outside of the vehicle through the side window opening.

Data from two of the tests with the same occupant on both the near and far side of the vehicle are shown in Figures 5 and 6. The near side excursion was lower than the far side excursion. In addition, the near side excursion is fairly consistent from roll to roll, while

the far side excursion increases modestly with increasing numbers of rolls.

Table 2.
Normally Seated Occupant Headroom

| Subject | Headroom |
|-----------------|----------|
| Human Female | 9.25" |
| Human Male | 5.25" |
| Hybrid II Dummy | 7.5" |

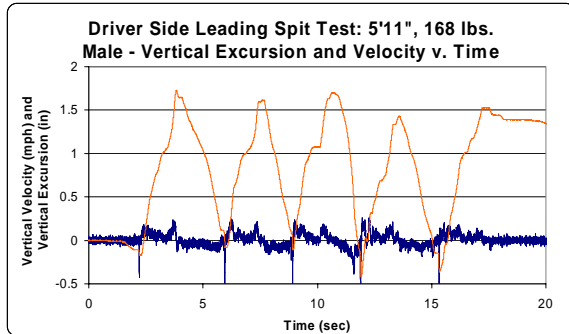


Figure 5. Spit Test Results – Near Side Occupant. Excursion (inches) in orange and velocity (mph) in blue.

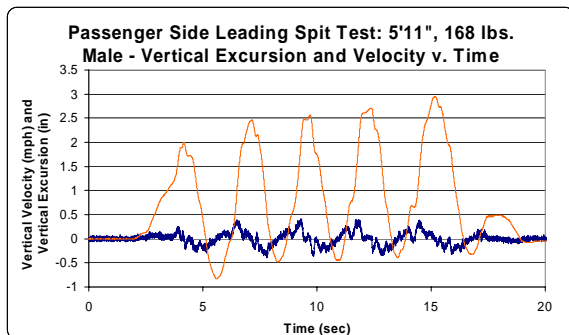


Figure 6. Spit Test Results – Far Side Occupant. Excursion (inches) in orange and velocity (mph) in blue.

Table 3 lists the peak excursion and excursion velocities for the various occupants. The data traces for these tests are similar to Figure 5 and 6. In general, the far side excursion was higher than the near side excursion. The excursion velocities were low with a peak velocity of ~.52 mph.

The prior study focused on a range of occupants in one vehicle moving as both near and far side occupants. Additional testing was conducted in other production vehicles with a range of occupant sizes. This testing was both near and far side leading, with and without pretensioners. The instrumentation was

similar and this study focuses on the vertical excursion and vertical excursion velocity measured during the tests.

Table 3.
Test Results

| Subject | Near Side Excursion | | Far Side Excursion | |
|-----------------|---------------------|---------------|--------------------|---------------|
| | Peak | Peak Velocity | Peak | Peak Velocity |
| Human Female | 3.8" | .32 mph | 5.2" | .36 mph |
| Human Male | 1.7" | .26 mph | 2.9" | .41 mph |
| Hybrid II Dummy | 2.5" | .47 mph | 3.3" | .51 mph |

The results of these tests are similar to those of the prior study. Dynamic excursion ranged from 1.35 inches (with a pretensioner) to 2.6 inches at peak excursion velocities of 0.69 mph with a range of occupant sizes.

The tests were conducted in the same way as the prior study. Table 4 illustrates the results of these additional tests. The results of these tests were very similar to the first test series.

Table 4.
Results from Additional Tests.

| Subject | Near Side | | Far Side | |
|-----------------------------|----------------------|-------------------------|-----------------|-------------------------|
| | Peak Excur-sion | Peak Excursion Velocity | Peak Excur-sion | Peak Excursion Velocity |
| 5'8", 165 lbs Male | 2.2" | .36 mph | 2.6" | .33 mph |
| 5'5", 144 lbs. Female | | | 2.2" | .69 mph |
| 5'7", 145 lbs. Female | Without pretensioner | | 2.6" | .68 mph |
| 5'7", 145 lbs. Female | With Pretensioner | | 1.4" | .33 mph |

In order to further examine the question of occupant motion and roof crush in rollover accidents, experimental data must be examined in which there are impacts to the roof allowing impact effects and roof crush as mentioned in Moffat (2003)[10].

DYNAMIC ROLLOVER TESTING

While spit testing can be used to examine occupant motion during a rollover, it is limited in that it does not examine the effects of roof impacts and crush on the occupant. This is important in both determining the occupant excursion velocity, the roof intrusion rate, the motion of the vehicle and how this relates to occupant injury.

The spit testing in this study was conducted in the Jordan Rollover System (JRS). This system can be used to conduct repeatable, rollover testing. This testing allows for the positioning of anthropomorphic dummies in the vehicle and a direct examination of the excursion velocity, roof crush and neck load due to a rollover impact to the roof.

In the first phase of the study, it was seen that the Hybrid II dummy is an effective surrogate for human occupants in vertical occupant motion with fairly similar excursion and excursion velocity. This is also noted in other studies [10] with a Hybrid III (HIII) dummy. This allows an examination of excursion and excursion velocity under impact conditions.

This test is similar to the spit testing portion of the study where an instrumented HIII dummy was placed in the near side of a midsize SUV, which underwent a dynamic impact, see Figure 7. The test vehicle, which had a strong roof, had previously undergone two dynamic rollover tests with only slight damage to the near side. The impact was from a drop height of 4 inches, at 214 degrees per second of roll and a roadway velocity of 15.7 mph. The vehicle struck the ground at a roll angle of 153 degrees, a yaw angle of 10 degrees and a pitch angle of 10 degrees.

The impact resulted in roadway loads of approximately 8,500 lbs. After this impact, the vehicle continued to rotate striking the ground on the far side of the roof before the test was completed. The only significant neck load to the HIII dummy was measured in the impact directly at the dummy's seating location.

The Hybrid III dummy was instrumented with a head accelerometer, neck load cells and string potentiometers measuring the lateral and vertical motion of the dummy. The vertical string potentiometer was positioned underneath the dummy through a hole in the seat. The lateral string

potentiometer was placed on the center console adjacent to the dummy.



Figure 7. JRS Test Setup.

In addition to the dummy instrumentation, the roof of the vehicle was instrumented with string potentiometers placed approximately at the roll axis of the vehicle. The near side string potentiometer was attached to the top of the A-pillar. This allowed for monitoring the motion of the roof towards the roll axis of the vehicle. This data gives timing information on the roof crush and the relative motion of the roof structure. The head contact point of the dummy is rearward of this position, but the roof crush timing should be equivalent.

The data traces of interest in this study are presented as a function of time in Figure 8. The vehicle roll angle is 158 degrees at the 1.725 seconds and 163.4 degrees at 1.75 seconds.

Figure 8 illustrates the motion of the roof at the A-pillar, the hybrid III dummy and the resulting neck load during the near side impact. In this case with a near side occupant, a peak neck load of 2,670 N was recorded at which time the A-pillar was intruding into the occupant compartment at ~ 0.5 ft/sec while the dummy was moving towards the roof at less than 1 ft/sec due to the impact and excursion. At the time of this impact, the dummy had moved outward and upward and was positioned under the roof rail near the intersection with the door window frame. At this point, the excursion of the dummy was limited by the roof. The neck load was due to a combination of the motion of the dummy and the roof.

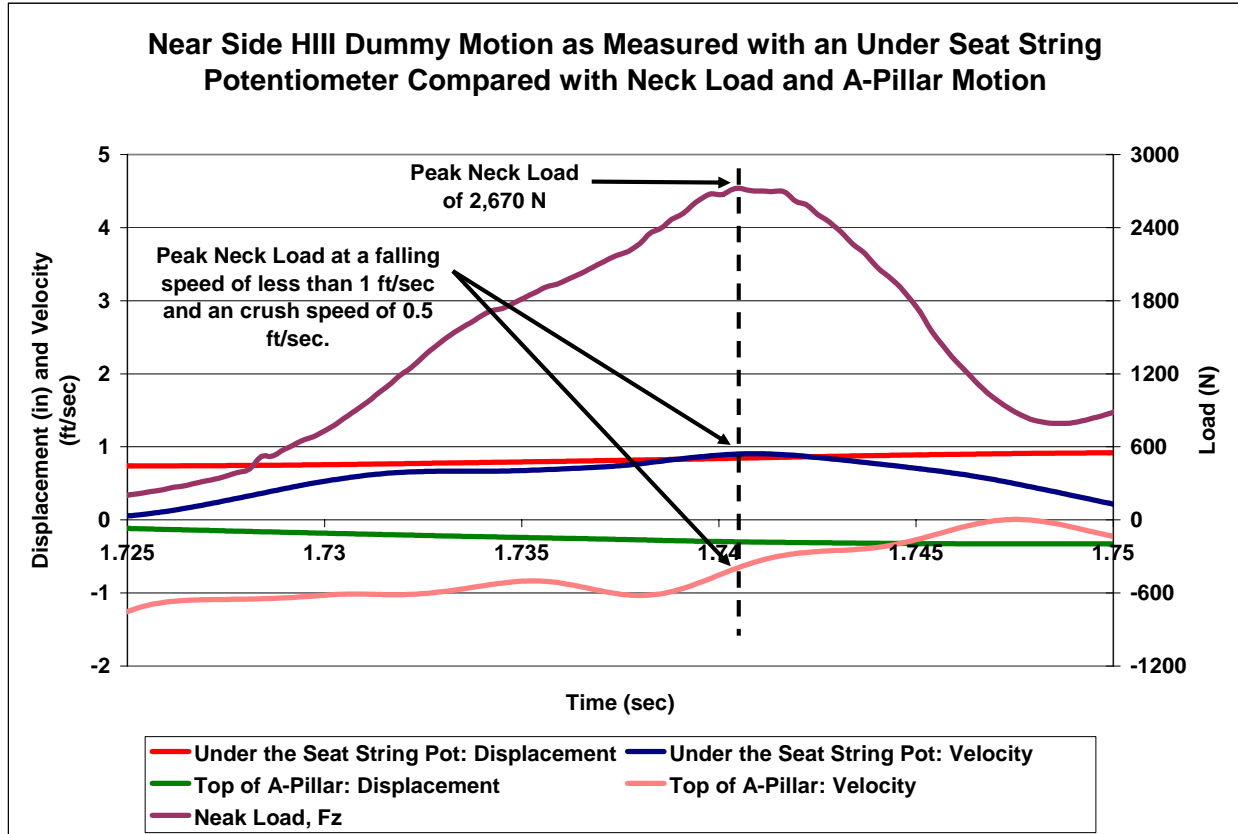


Figure 8. JRS test results focusing on the near side impact.

Figure 9 illustrates the same test sequence over a longer time period illustrating the effects of the far side impact. Figure 9 represents the vehicle traveling from 142 degrees of roll to 230 degrees. In the far side impact, the roof was moved upward and outward away from the near side occupant. This allowed the dummy to move further upward at higher velocities with the deforming roof. This resulted in the highest recorded excursion velocity of ~3 feet per second. However, due to the motion of the roof/vehicle and the dummy there is only a small increase in neck load at this time.

This test clearly illustrates the motion of the dummy, roof and resultant neck load during a near side impact. The excursion velocity is only above 1 ft/sec when the matchboxing roof allows a higher velocity. The peak neck load is due to a combination of roof intrusion and dummy excursion.

The near side impact during this test was significant with a vertical load of 8,500 lbs measured by the instrumented roadbed. This device allows for direct measurement of the load applied to the structure. This load was approximately 1.8 times the weight of

the vehicle and is illustrated in Figure 10. After the near side impact, the vehicle continued to roll striking the far side of the roof prior to the end of the test. In this case, the load was much higher on the far side of the roof with a peak load of ~19,300 lbs (or 4 times the weight of the vehicle). It should be noted that the near and far side loads do not always follow this pattern. Larger near side than far side loads have been seen in several tests.

In this dynamic rollover test, the circumstances around a near side impact are investigated examining the excursion velocity of the near side occupant and the timing of the peak neck load as compared to the roof and dummy motion. The peak neck load occurs due to motion of both the dummy and the roof structure. This light, non-injurious impact occurred at a head impact speed of approximately 1.5 ft/sec. At this point, the roof has crushed only a minor amount, ~0.3 inches, with the peak crush speed, ~2.0 ft/sec, prior to the peak neck load. The occupant has moved upward ~0.8 inches and the peak neck load does correspond to a local peak excursion velocity at ~0.9 ft/sec. A clearer picture of occupant injury will

be seen in a far side impact where larger neck loads are typically seen

This test was done at rotation rates of less than 240 deg/sec, although the dynamic rollover test achieved higher rotation rates after the near side contact.

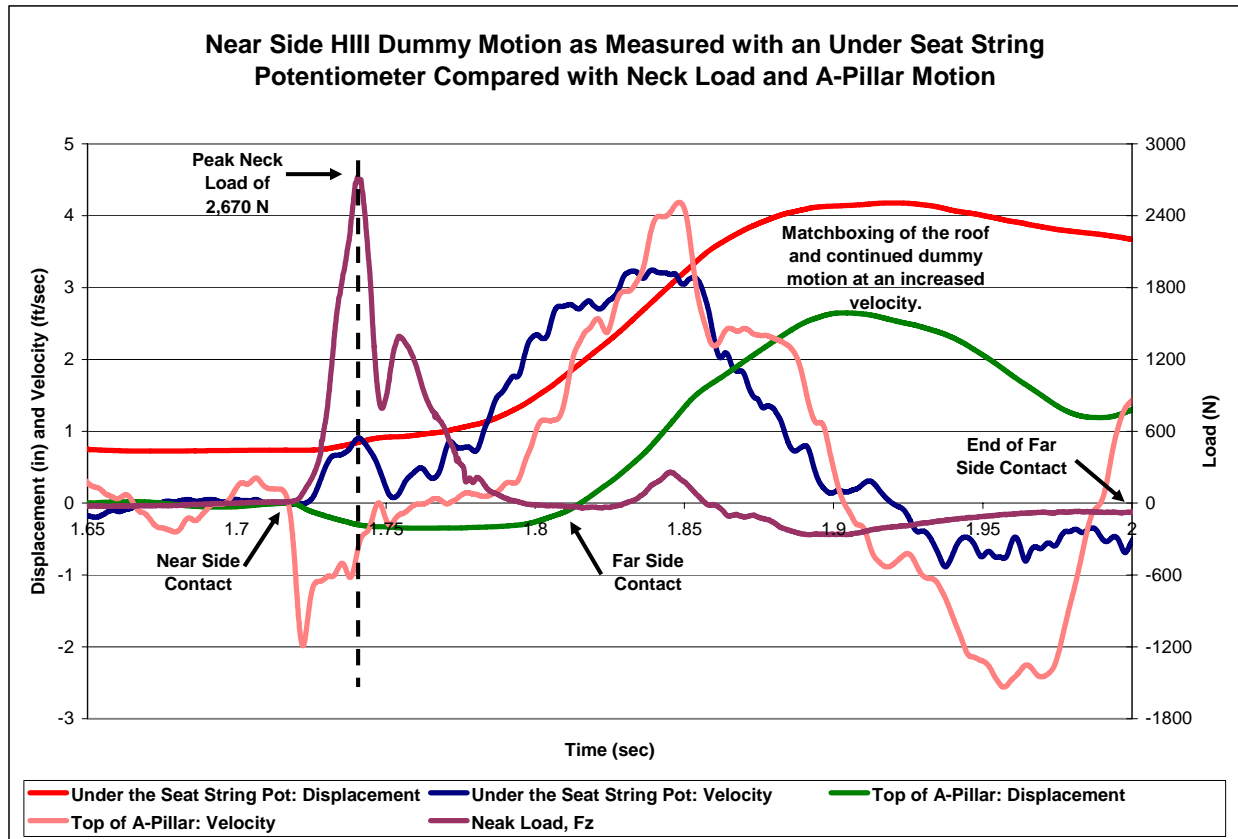


Figure 9. JRS test results focusing on the near side impact.

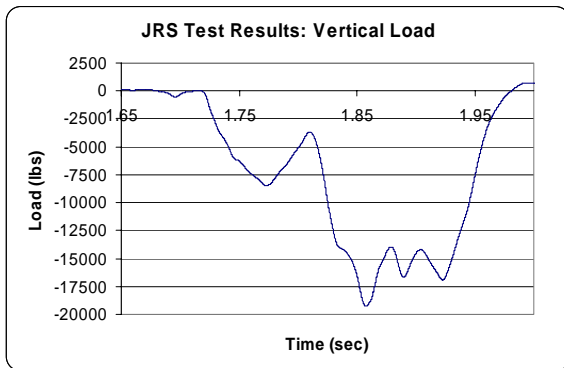


Figure 10. Vertical load during impact.

OTHER EXPERIMENTAL PROOFS

At higher rotation rates, the occupant becomes pinned to the vehicle at the upper corner. In those cases, the only component of occupant “diving” velocity has to come from the bulk motion of the

vehicle. This can be examined from dolly rollover tests in which data is publicly available. The Malibu II study [3] can be used for this purpose.

The Malibu II study is an examination of eight dolly rollover tests with two restrained front seat occupants. Half of the vehicles were reinforced while the remaining were in the production state. The vehicles and occupants were instrumented and filmed both internally and externally.

For this study, it is also of interest to look at the Malibu II neck loads, belt loads and vehicle roll rates. This allows an examination of the occupant motion through the belt loads, impact with the roof through neck load and vehicle dynamics through the roll rate. If the occupant was undergoing a “diving” type loading the belt load would need to increase with increasing neck load. A graphical examination of this data is illustrated in the following figures.

These figures from Malibu II were created by digitizing the graphical data provided with the study. The electronic data has never been released to the public for independent analysis. They provide another method for examining the cause of the high neck loads seen during several of the tests in this series. Figure 11 is a graph of Malibu II Test 2, a

reinforced vehicle. A peak neck load is at the end of the sequence where the roll rate has decreased to less than 200 degrees per second from an earlier peak of more than 500 degrees per second. In effect this relieves the lap belt loop load as the dummy reacts to lower centrifugal force.

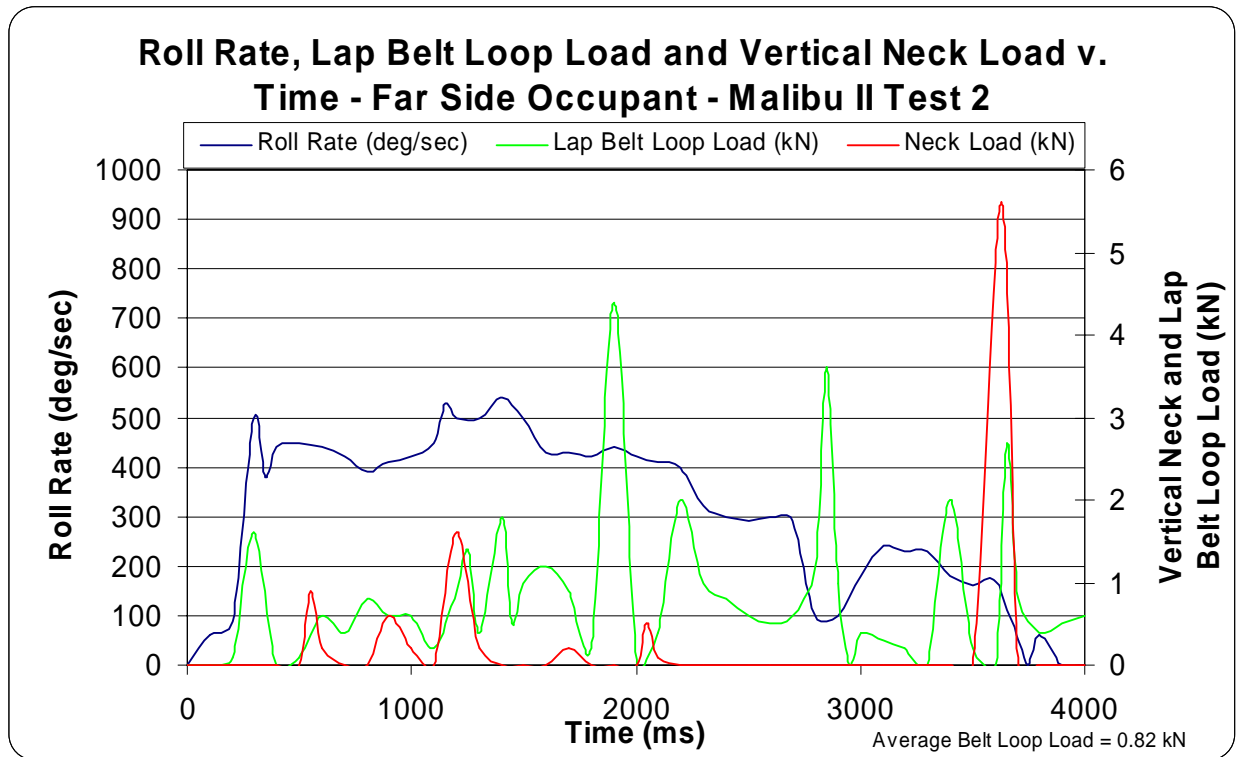


Figure 11. Malibu II Test 2 – Rollcaged Vehicle Data.

The occupant excursion and excursion velocity during this impact can be analyzed by examining the high speed video of the test and utilizing the timing data determined during the original analysis of the tests. In this impact, dubbed Potentially Injurious Impact (Pii) 2L1 (Test 2, left dummy, first impact over 2000 N) the interior photoanalysis of 2L1 roof and occupant motion is shown in Figure 12 just as roof/head contact starts. The intrusion velocity of the rollcaged roof after 0.97 inches of intrusion is 4.7 mph while the occupant is moving towards the roof at 0.9 mph as identified by the by the dummy buttocks motion.



Figure 12. Split screen of Malibu II 2L1 roof and dummy motion.

Figure 13 examines Malibu II Test 3 of a production vehicle. In this test, there are two spikes in the neck load early in the test at approximately 700 and 1300 ms. An examination of these neck load spikes illustrates a corresponding decrease in the lap belt load. The decrease in belt load is caused by the roof deformation pushing the dummy towards the seat and

unloading the belt. Any lessening of belt load due to moving of belt anchor points, typically the D-ring on the B-pillar, would occur with the roof crush after the diving theory would predict an injury – prior to roof crush.

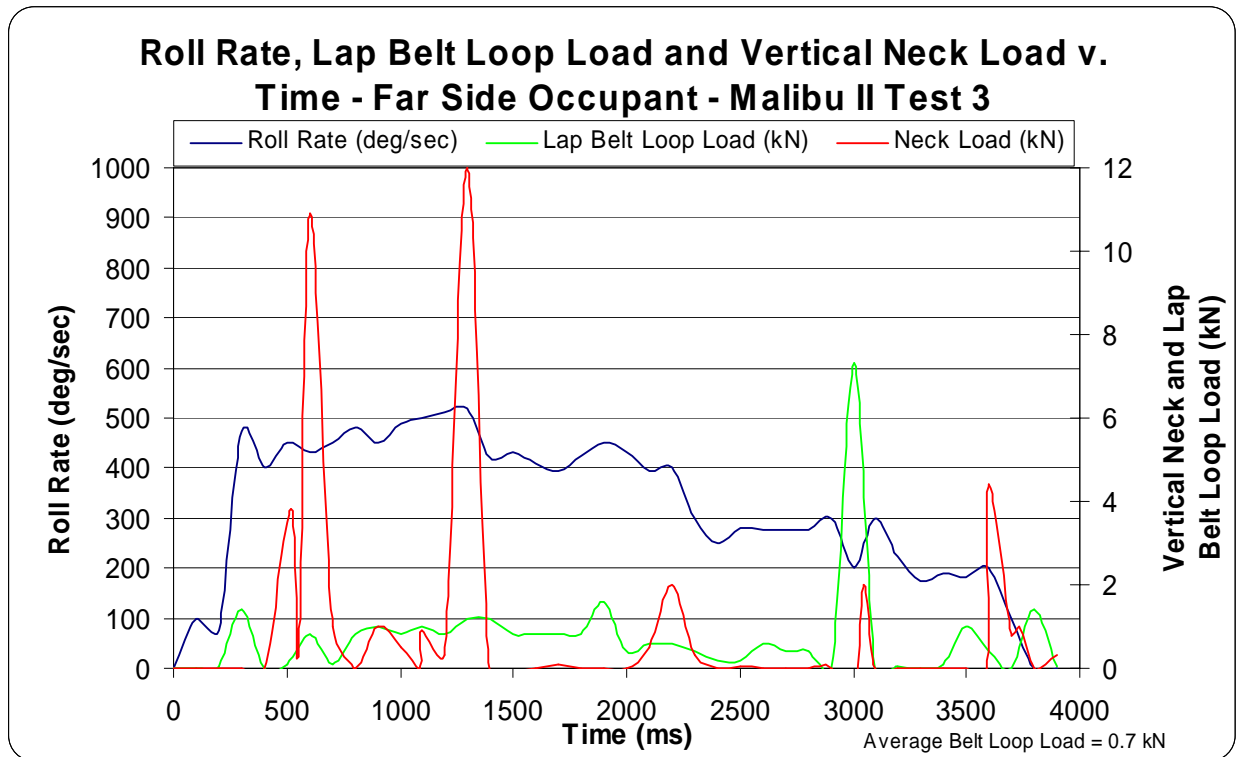


Figure 13. Malibu II Test 3 – Production Vehicle Data.

Figure 14 examines Malibu II Test 7 of a production vehicle. This is similar to the graphs from Test 3. In this case, the peak neck load is near the end of the sequence where the roll rate has decreased to approximately 200 degrees per second. The belt load is relatively low as compared to the peak belt load in the test at which point there was no neck load of note. If a diving type mechanism was the prime force in this event, then you would need to see an increase in belt load, but this is not present. The data clearly indicates something else is driving the neck load. Examination of the test video illustrates a moving buckle, as described in Malibu I [2], striking the dummy’s head and reported in a 2005 ESV paper [11].

This study also looked at a comparison between neck and belt loads realizing that diving could only occur with an increase in belt load as the torso loads the neck of an occupant. In a similar fashion to this study, the article concluded that diving type injuries can occur at low impact speeds in the absence of roof crush with the neck load increasing with increasing neck load. However, in the presence of roof crush and higher neck loads, the belt load decreased with increasing neck loads illustrating the crushing roof forcing the dummy towards the seat and possibly the loosening of the belt due to the deforming roof and moving seat belt anchor locations. Either of these motions preclude the diving theory as both necessitate the presence of roof crush and the diving theory states that the injury occurs prior to roof crush.

A similar study was conducted on a series of Ford Explorer rollover tests and presented to NHTSA [12].

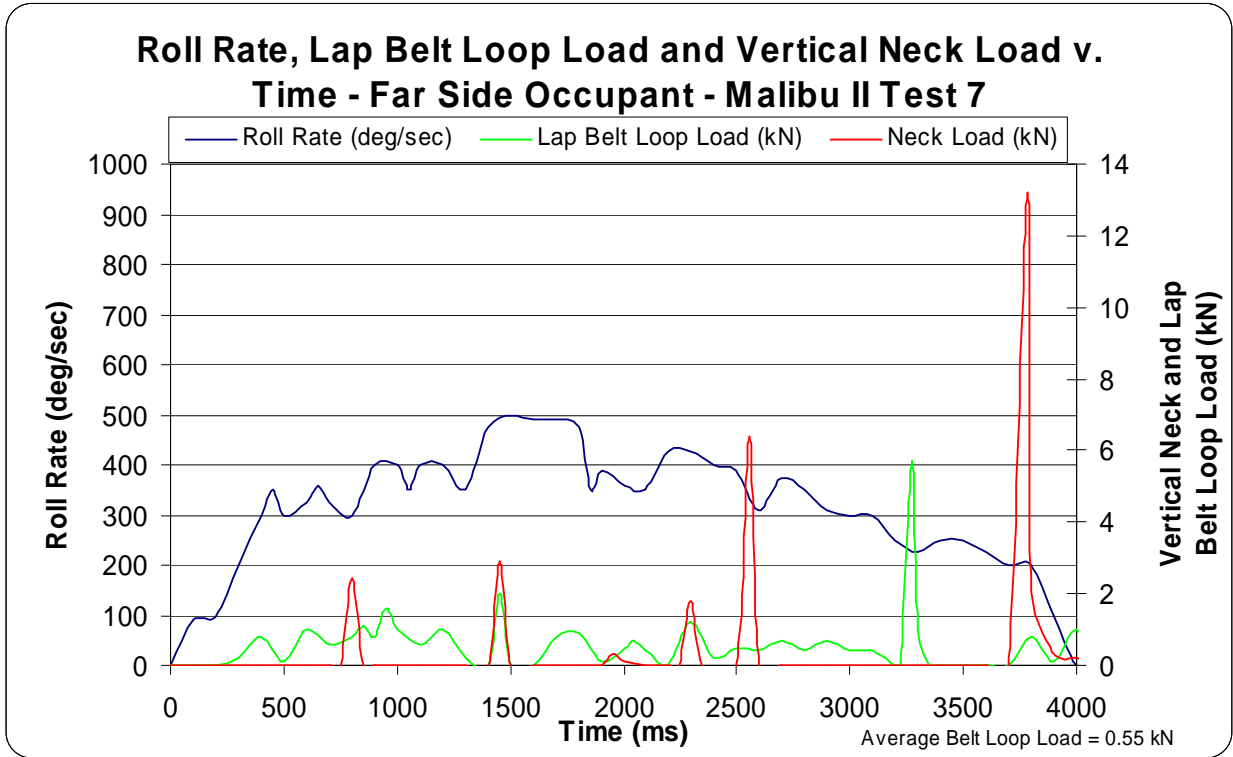


Figure 14. Malibu II – Production Vehicle Test 7 Data.

A comparison of neck load, belt load and roof crush was also made experimentally in a dynamic rollover test utilizing the JRS. In this test, a mid-sized SUV was tested with a restrained, instrumented Hybrid III 5th percentile occupant in the far side rear seat. The vehicle was instrumented with string potentiometers on the near and far side with an interior high speed camera. The test was an examination of small occupant motion in rollover accidents as no roof contact was expected during the test. However, a large buckle was formed due to the design of the roof and the occupant was contacted. This impact can clearly be seen on the high speed interior camera, see Figure 15.

The data from this test clearly demonstrates the peak neck load occurring as the belt load is decreasing with little or no motion of the restraint system anchor points, see Figure 16.

While there were no string potentiometers immediately above the rear seat dummy, a string potentiometer was located above the driver’s seat and recorded the motion of the buckle that struck the occupant. The timing and motion of this buckling structure is very similar to the effects above the dummy. Figure 17 illustrates the motion of the roof and comparison to the neck load in the dummy.

While this test did not include a under the seat string potentiometer to examine excursion velocity, it clearly illustrates the non-injurious motion of the occupant in the absence of roof crush. With this small occupant, the roof crush is the reason the dummy was struck and had a peak neck load of 2,622 N.

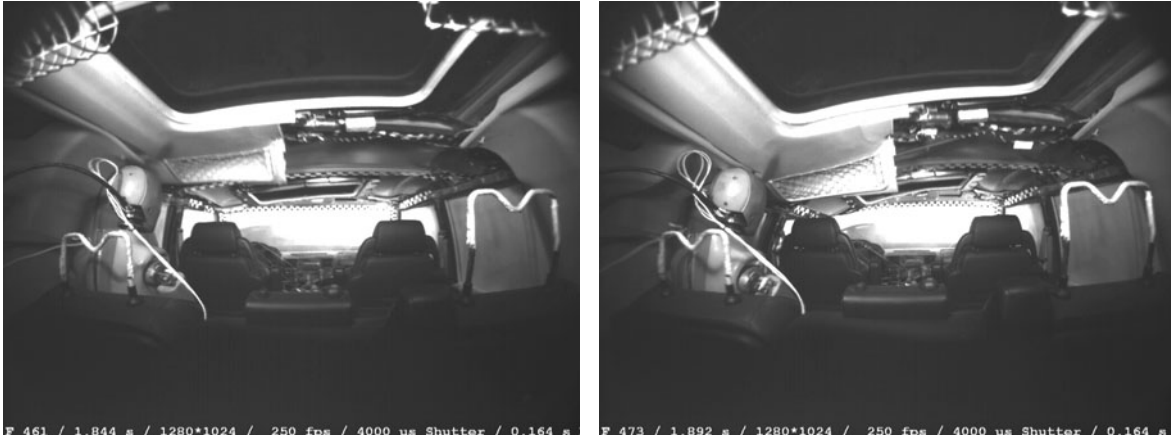


Figure 15 A and B. Video excerpts from test. In the first picture, the dummy has moved upwards toward the roof and the roof is beginning to crush. In the second picture, the roof is loading the dummy.

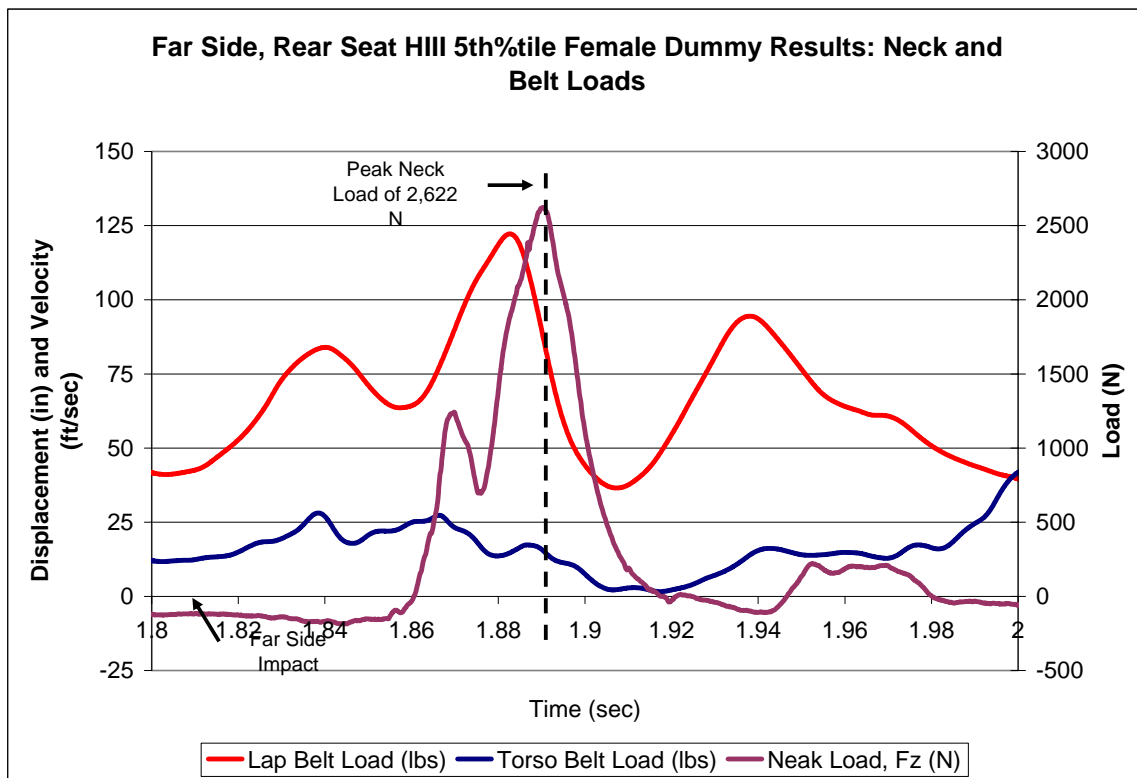


Figure 16. JRS test results focusing on belt and neck loads during a far side impact.

DISCUSSION

This study is an initial look at occupant motion in rolling vehicles with a focus on excursion velocity and effects on occupant injury. It was found that occupant excursion inside the vehicle is not at injurious speeds. Further examination of additional studies illustrate that the diving mechanism is not the

main factor in rollover injuries. While torso augmentation may contribute to neck loading, it is not enough to cause injury in the absence of roof crush and additional occupant loading due to intrusion into the occupant survival space as is found in all other accident modes – front, side and rear.

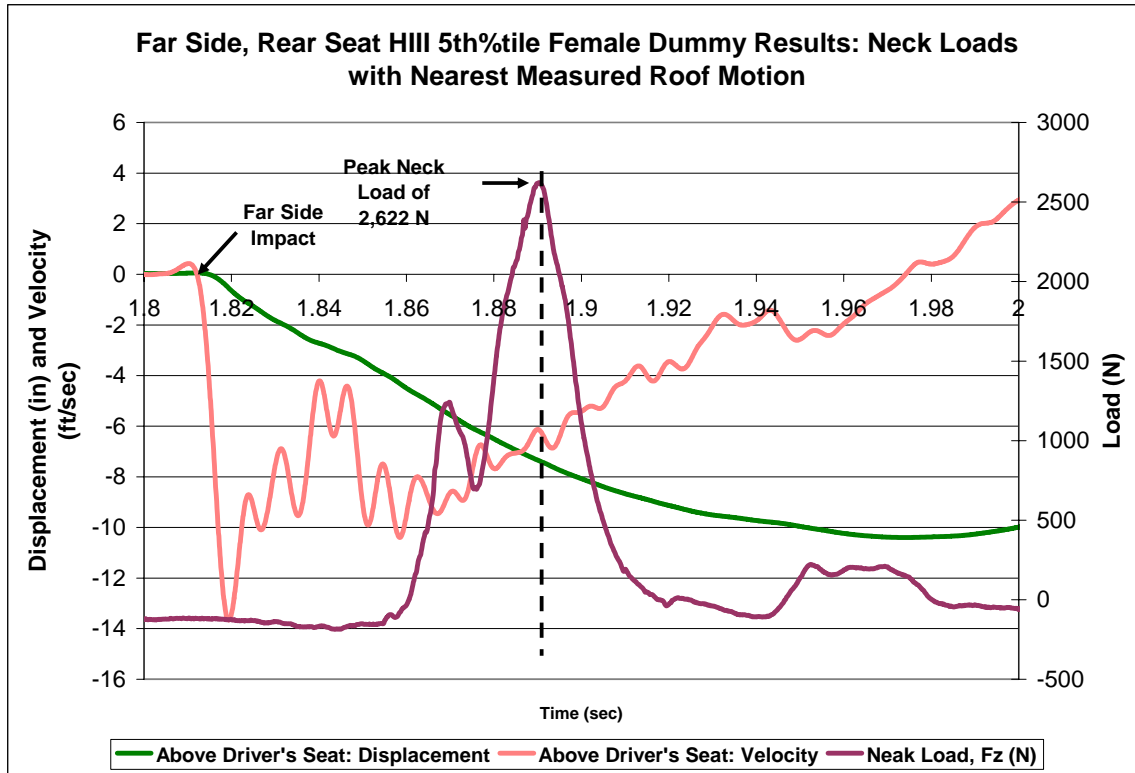


Figure 17. JRS test results focusing on roof motion and neck loads during a far side impact.

CONCLUSIONS

The Jordan Rollover System allows for dynamic spit testing and dynamic repeatable rollover testing.

In dynamic spit testing, it was seen that:

- Occupants do not necessarily contact the roof structure when rotated at rates up to above 200 degrees per second.
- Occupant excursion velocities are in the range of 0.5 mph. The occupant does not move faster than this relative to the seat in a non-deforming structure.
- Human and Dummy surrogates are both effective in this type of testing. However, the human occupants move differently in the motion of their arms, legs and especially the flexing of the neck.

In the dynamic rollover testing, it was seen that:

- Peak neck loads are caused by a combination of roof crush and occupant motion.
- Even with an impact, peak excursion velocities are limited to less than 1 mph. However, a higher speed was observed when the roof moved away from the occupant at a higher rate.

- In the test of the near side occupant, the dummy occupant moved upward a small amount and then was retained by the roof.
- In the test of a far side, rear seat occupant, the dummy moved upward without contacting the roof. Roof contact and neck loads were made when the crushing roof structure contacted the dummy due to a large buckle formed by the design of the roof and roof rack assembly.

REFERENCES

- 1 Moffatt, E., "Occupant Motion in Rollover Collisions", 19th Proceedings of the American Association of Automotive Medicine, November 20-22, 1975.
- 2 Orłowski, K., Bundorf, R.T., Moffatt, E., "Rollover Crash Tests- The Influence of Roof Strength on Injury Mechanics", SAE 851734, 1985.
- 3 Bahling, G., et al., "Rollover and Drop Tests - The influence of roof strength on Injury Mechanics Using Belted Dummies," SAE 902314, 1990.

4 Nash, C.E., and Friedman, D., "A Rollover Human/Dummy Head/Neck Injury Criteria," 2007 ESV Conference.

5 Herbst, B., et. al., "The Ability of Three Point Safety Belts to Restrain Occupants in Rollover Crashes", 15th ITC on ESV, 1996.

6 Friedman, K., et al., "Restraint Effectiveness During Rollover Motion", 1996 IRCOBI Conference, 1996.

7 Friedman, D. and Friedman, K., "Roof Crush Versus Occupant injury From 1988 to 1992 NASS", SAE 980210, 1998.

8 Meyer, S.E., et al., "Three Point Restraint System Design Considerations for Reducing Vertical Occupant Excursion in Rollover Environments," SAE 2000-01-0605, 2000

9 Friedman, D., et al. "Human Response to Dynamic Rollover Conditions," 2003 ASME International Mechanical Engineering Congress & Exposition, November 16 – 21, 2003, Washington, D.C.

10 Moffatt, E., "Head Excursion of Restrained Human Volunteers and Hybrid III Dummies in Steady State Rollover Tests", 47th Annual Proceedings of the AAAM, September 22-24, 2003.

11 Friedman, D., Nash, C.E., "Reducing Rollover Occupant Injuries: How and How Soon"; ESV 05-417-W; 19th ESV Conference, Washington D.C., June 6-9 2005

12 Bidez, et. al., Submission to NHTSA Docket, NHTSA-2005-22143-242, 10/27/2007, dms.dot.gov.

APPLICATION OF ACN DATA TO IMPROVE VEHICLE SAFETY AND OCCUPANT CARE

**Jeffery Augenstein, Kennerly Digges,
Elana Perdeck and James Stratton**
William Lehman Injury Research Center
University of Miami
United States

George Bahouth
Pacific Institute for Research and Evaluation
United States

Peter Baur and George Messner
BMW
Germany

Paper Number 07-0512

ABSTRACT

In MY 2007 nearly all of the BMW's sold in the US will be equipped with an Automatic Crash Notification System (ACN) called "BMW Assist". The service is provided to the customer for a period of 4 years free of charge. This fleet of BMW's will notify the Telematics Service Provider (TSP) when they have been in moderate or severe crashes. This service will continue to be provided for a period of 4 years. The resulting body of information will be of unprecedented value for research purposes. For example, researchers will be able to determine the time between the initiation of the emergency call and the arrival of rescue. For cases with long rescue times research can focus on ways to shorten the time and improve the service. In addition, cases with injuries can be identified as candidates for in-depth investigation. This capability will resolve one of the greatest impediments to crash investigation research – how to find crashes of interest. Finally, by having a complete census of all crashes involving ACN equipped vehicles less than four years old, the crash exposure can be determined and crash involvement risks can be accurately calculated. When combined with sales exposure data, the crash involvement rates will permit the benefits of accident avoidance countermeasures to be assessed. There is no other data system that will provide the resolution or accuracy of this system – particularly for the assessment of crash avoidance countermeasures.

INTRODUCTION

The introduction of Automatic Crash Notification (ACN) technology offers new opportunities for conducting research to improve the safety of vehicles

as well as the care and treatment of injured occupants. For the past five years the William Lehman Injury Research Center (WLIRC) and BMW have been conducting a pilot project to find ways to improve the service offered by the ACN system. This research also produces unique safety research opportunities. In past papers, we have reported on the benefits of using data from the crashed vehicle sensors to assess the risk of injury to occupants and the need for urgent rescue response. This paper also deals with the added benefit of using the data from ACN calls for pioneering safety research.

Existing ACN systems send a signal to emergency responders if a crash exceeding a pre-determined severity threshold occurs. This severity is roughly equivalent to that required to deploy the belt pretensioners or the airbags. The rapid notification of rescue services in the event of a crash increases the chances that an occupant who needs medical attention will receive potentially life saving care as quickly as possible. It is well established that ACN systems offer life saving benefits due to the immediate notification that a crash has occurred and the accurate description of crash location (Augenstein 2006, Donnelly 2000, Champion 2003, Evanco 1999). However, ACN data currently collected also offers a unique opportunity to analyze other aspects of pre-crash and post crash safety of drivers.

The ACN system currently offered in all BMW's are known as the BMW Assist System. This technology was optional in the past. However, in MY 2007 nearly all of the BMW's sold in the US will be equipped with an ACN system. BMW Assist currently transmits geographic coordinates of the vehicle and the vehicle identification number to a Telematics Service Providers or TSP's within seconds of a crash. As systems become more advanced in the future, additional data elements may be transmitted which characterize crash severity. The addition of crash severity data will help rescue providers to select and deploy the most appropriate type of rescue care. The transmitted data can also be used as a basis for identifying crashes of interest for in depth investigation. Such investigation would be undertaken only after gaining permission from the owner of the vehicles involved.

Since 2005, BMW and the William Lehman Injury Research Center (WLIRC), at the University of Miami School of Medicine, have conducted pilot research using ACN data. This paper presents the

methodology used to improve post-crash safety to analyze the benefits of accident avoidance countermeasures.

IMPROVEMENTS IN ACN SYSTEMS AND POST-CRASH SAFETY

The automatic crash notification system offers the possibility of providing three types of data to aid in the rescue. First the geographic coordinates of the crash are provided. Second, the voice communication with the crashed vehicle occupants provides valuable information. Third, useful data from the vehicle could be provided.

The first generation of ACN systems only transmitted the geographic coordinates and voice communication. The vast majority of crashes with restraint system deployment do not result in significant injury to the vehicle occupants. Voice communications with the occupants can further verify the need for rescue. However, in a fraction of the cases there may be no voice response. In some of these cases the reason for the lack of response could be due to injuries caused by the crash. The added data from the vehicle would be particularly valuable in these cases.

The ability to identify injured occupants has become more difficult as vehicle safety systems have improved (Augenstein, 2003, Champion, 2003). As restraint systems have improved, the residual injuries have become more subtle and difficult to identify at a crash scene. Occupants may not display the physiological cues to assist first care providers in recognizing injuries, and injured occupants may “feel fine”. Improved technology from the ACN system might help in identifying these injuries.

BMW and WLIRC have pioneered the development of methods to identify crashes in which there is a high probability of injury and a need for rapid post-crash response. This research has included the development and continued improvement of an algorithm called URGENCY. The URGENCY algorithm uses the restraint deployment data from the crashed vehicle to predict the risk of injury to the occupants involved in the crash.

Previous papers have discussed the difficulty in identifying crashes with injuries and the application of URGENCY to improve the injury recognition (Augenstein 2003, 2006). The single most valuable data element is the change of velocity of the crash (deltaV). However, the injury risk is also highly

dependent on the direction of the crash. This dependence is shown in Figure 1. The Figure shows the injury risk vs crash severity for different crash modes, based on data from NASS/CDS 1997-2003 (Augenstein, 2006). It is evident from Figure 1 that for a given deltaV (30 mph for example), the probability of injury varies with crash direction. Consequently, crash direction is an important variable for accurately determining injury risk.

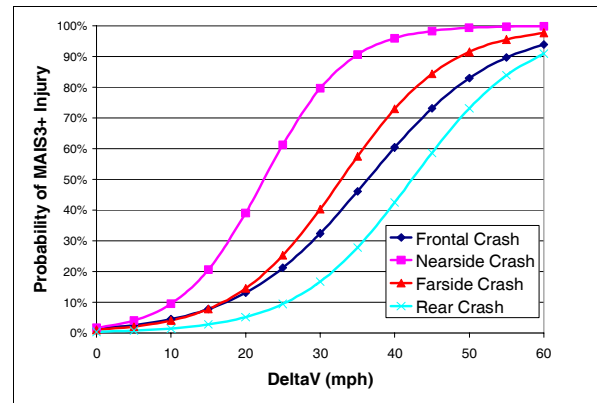


Figure 1. MAIS3+ Injury Probability by Delta-V and Crash Direction

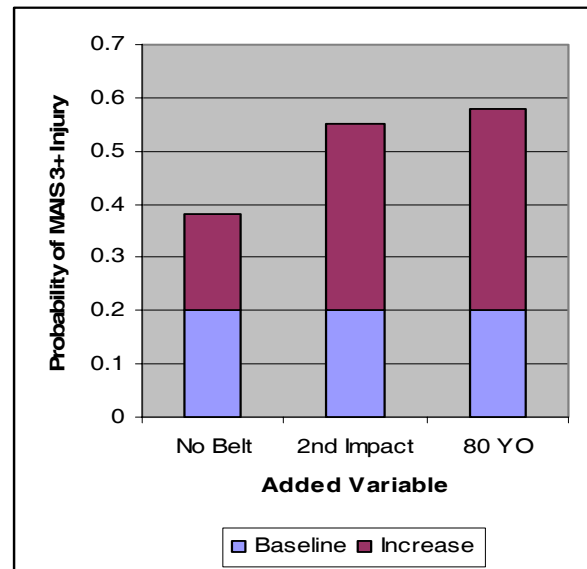


Figure 2. MAIS3+ Injury Probability Increase for Added Variables in Frontal Crashes

There are other important variables that are measured before or during the crash that are also useful. In addition, the ages of the occupants would be useful, when available. The benefits of these added variables are illustrated in Figure 2. This figure shows how different variables influence the injury probability for a 25 mph frontal crash with a baseline

injury risk of 20%. For example, the absence of safety belts increases the risk from 20% to 38% (Augenstein 2003).

The influence of the variables shown in Figure 2 varies with crash direction. In addition, other variables become important in non-frontal crashes. To simplify the presentation of the complex relationships, the URGENCY algorithm can be used. A typical presentation from the algorithm is shown in Figure 3.

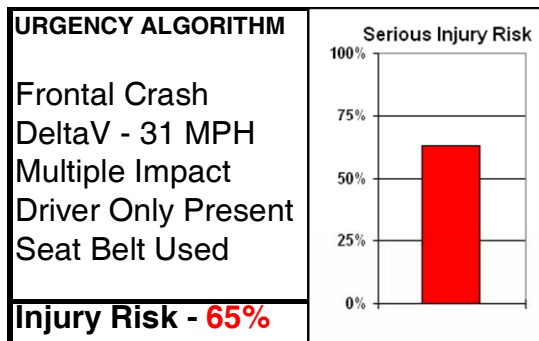


Figure 3. Typical Presentation of the URGENCY Algorithm

The presentation shown in Figure 3 permits the rapid identification of the combination of crash events that could increase injury risk. It could assist in rapidly identifying crashes that may need rapid response from rescue.

There are several types of crashes that URGENCY could be particularly helpful to the occupants of the crash. The first type is the severe crash with no response from the occupants. Heightened concern over the need for rapid response could be transmitted to the emergency responders. Reducing the rescue time for these rare cases could have life-saving benefits. Another potential benefit is for people with injuries that are not immediately recognized. The algorithm could raise the suspicion of an injury so that immediate care could be sought. In some cases, unrecognized and untreated injuries can lead to subsequent disabilities and even death.

BMW and WLIRC are continuing to evaluate ways to improve the post-crash safety environment. One of the impediments is the novelty of using crash data from the vehicle to assist in recognizing crashes with high probability of injuries. Continuing efforts are underway to develop publications and training materials to advise emergency responders and care

givers of the technology available that could assist in post-crash safety.

ASSESSMENT OF THE BENEFITS OF CRASH AVOIDANCE COUNTERMEASURES

ACN data can provide a wealth of information to analyze the pre-crash safety of vehicles. Unlike other available datasets, ACN data includes a census of crashes involving a know population of vehicles where the criteria for inclusion within the dataset are consistent and well defined. Only those that exceed the deployment threshold of the ACN system are automatically included. Manual transmissions are also possible if a driver or other occupant manually activates the system. Figure 4 below shows the population of BMWs equipped with ACN technology in use on US roadways. Using this data in combination with crash counts, crashes per vehicle in service can be accurately calculated for any population of interest.

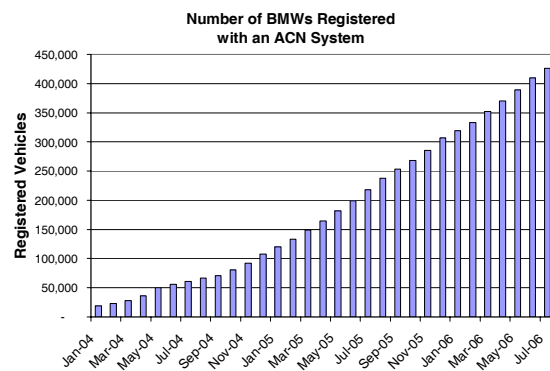


Figure 4. Registration Count by Month for BMWs with Active ACN Systems

For vehicles equipped with an ACN system, a notification that a crash has occurred is transmitted to the telematics service provider for all crashes exceeding the deployment threshold. For this reason, a wealth of data is available to analyze crash involvement rates for the population of vehicles deployed. Sales data exists which defines the exact size of the exposed population. The impact of crash avoidance technologies can be assessed by comparing crash involvement rate before and after the introduction of a safety feature or through direct comparison of crash rates for populations with and without an optional feature.

Using ACN data, exact vehicle specifications, including the presence of optional features, can be

determined using the available vehicle identification number (VIN). In the future, this data will allow for the evaluation of the safety improvement of emerging active safety systems. Some examples include Adaptive Cruise Control, Heads-Up Displays, Lane Departure Warning Systems, Active Steering Systems and Blind Spot Warning Systems. In addition, it is possible to compare user interfaces and communication strategies for crash warning systems and for driver assistance systems like in-dash Navigation devices.

Compared to currently available crash data collected by NHTSA and US states, ACN data provides a significantly larger number of observations from which conclusions can be drawn. Some publicly available US crash data systems provide only a small sample of crash cases including all makes upon which general safety conclusions can be drawn. The National Automotive Sampling System, Crashworthiness Data System (NASS CDS) is an example of a database that contains very detailed information for a very small sample of crashes. Since the data is only a sample of 4,500 crashes per year, few conclusions regarding specific vehicle platforms and the impact of newly introduced technologies can be drawn unless the technology is deployed nearly fleet wide. Further, since NASS CDS collects crashes involving both new and older vehicle models such that it may be necessary to compile multiple years of observations before any meaningful changes can be detected. Alternatively, US state crash data systems include a census of police reported crashes occurring in a particular state. Each state data file contains a large number of records however; the quality of data collect by police is questionable. Further, state files are compiled by state and made available for analysis long after a safety device first enters the vehicle fleet. As not all states report crash counts, national level analysis of data is not possible.

In the past, several researchers have analyzed the effectiveness of safety devices including Anti-lock Brake Systems (ABS) and Electronic Stability Control (ESC) technology using US state crash data (Evans 2000, Farmer 2004, Bahouth 2005, Green 2006). State data files were the only available crash data source with a sufficient number of observations required to draw statistically significant conclusions.

Such evaluations have lead to important and noteworthy findings, however the use of police reported crash data from multiple states is problematic and could be biased in some cases. With regard to the evaluation of ESC, the first such evaluation was possible only 2004 even though the technology emerged in some vehicles in 1999. It was necessary to pool data from as many as 10 US state files in order to estimate statistically significant effects. Similarly, it is difficult to pool data from multiple files due to inconsistencies in case inclusion criteria from state to state. As the ACN data is collected in real time across the entire US and collected using consistent inclusion criteria, it offers a significantly better alternative to the use of state crash files.

The ACN dataset available for analysis contains a large sample of crashes and is expected to grow significantly based on expected sales of new ACN equipped vehicles. Figure 5 shows the projected number of crashes expected for the coming 4 year period. This plot was created using current ACN equipped vehicle crash rate (approximately 0.008 crashes per month per registered vehicle in service) times the projected number of vehicle registrations based on 2005 and 2006 new vehicle sales estimates. The sales estimates assume equivalent sales for 2007-2010 where 100% of the vehicles sold are equipped with an ACN system. By June, 2010, these estimates indicate that more than 1,000 vehicles will be involved in crashes per month exceeding the deployment threshold of the ACN systems. Currently, the ACN dataset includes over 8,000 crash events and is expected to exceed 44,000 crashes by December 2010.

The ACN dataset provides a unique resource to study newly emerging active safety technologies. If we were to conduct an analysis of a technology with 25% penetration into the vehicle fleet, with the current crash population as shown in Figure 5, we have 71.1% power to detect a presumed effect size of 5% or greater. As the population grows over the next 4 years as shown in the figure, this power to detect 5% difference in crash involvement will increase to over 99%.

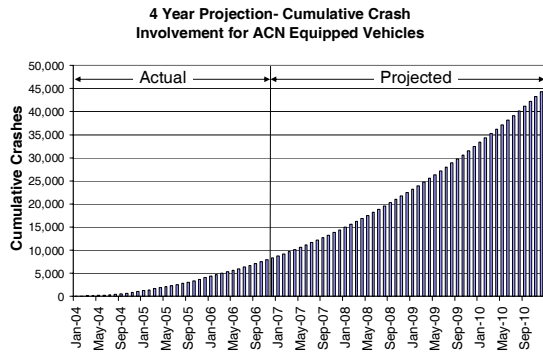


Figure 5. Projected Number of Vehicle Crashes Involving BMWs with and ACN System (sales rates and crash rates based on 2005 and 2006 data).

CONCLUSIONS

The ACN system on BMW vehicles provides unique opportunities for studying pre-crash and post-crash safety. Our studies of factors that influence injury risks in vehicles is providing guidance in how to best use the information from the vehicle to improve post-crash safety.

The decision by BMW to offer ‘BMW Assist’ free of charge for four years will create a unique database for evaluation accident avoidance countermeasures. It will be possible to develop a database of all BMW’s that crash in the US and the crash avoidance features on each of those each of those vehicles. Such a database, in conjunction with the vehicle sales database will permit an unprecedented capability to evaluate accident avoidance countermeasures such as active cruise control, lane departure warning, blind spot warning, heads-up displays and many other features associated with communicating information to the driver. BMW and the William Lehman Injury Research Center are working together to continue to improve the safety of motor vehicle occupants, focusing on new technology.

ACKNOWLEDGMENTS

The authors would like to acknowledge BMW for their support for this research.

REFERENCES

Augenstein, J, Digges, K., Bahouth, G. and others,

“Characteristics of crashes that increase the risk of injury”, 47th Annual Proceedings of the Association for the Advancement of Automotive Medicine, p. 561-576, September, 2003

Augenstein, J., Digges, K., Bahouth, G. T., Dalmotas, D., & Perdeck, E. A more effective post-crash safety feature to improve the medical outcome of injured occupants, Society of Automotive Engineers World Congress (SAE Paper 2006-01-0457): Detroit, MI, 2006.

Bahouth, G. T.,” Real world crash evaluation of vehicle stability control technology”, Annual Proceedings of the Association for the Advancement of Automotive Medicine (Vol. 49, pp. 19–34): Association for the Advancement of Automotive Medicine, 2005.

Champion H.R., Augenstein J.S., Blatt A.J., Cushing B., Digges K.H., Hunt R.C., Lombardo L.V., Siegel J.H., Reducing highway deaths and disabilities with automatic wireless transmission of serious injury probability ratings from vehicles in crashes to EMS, Proceedings of the 18th International Technical Conference on the Enhanced Safety of Vehicles, 2003.

Clark D.E., Cushing B.M., “Predicted effect of automatic crash notification on traffic mortality,” *Accident Analysis and Prevention*, 34 (2002) 507-513.

Donnelly B., Funke D., Bellis E., Blatt A., McClellan R., Wilson G., Automated Collision Notification (ACN) Field Operational Test Final Report, National Highway Traffic Safety Administration, U.S. DOT HS 809 303, October 31, 2000.

Evanco W. M., The Potential impact of rural mayday systems on vehicular crash fatalities, *Accident Analysis & Prevention*, 1999, 31:455-462

Evans, L. Antilock Brake Systems and Risk of Different Types of Crashes in Traffic, Enhanced Safety of Vehicles Conference, Paper #98-S2-O-12, Windsor, Canada; 1998.

Farmer, C.M., Effect of electronic stability control on automobile crash risk, *Traffic Injury Prevention*, 5:317–325, 2004.

Green, P.E., Woodrooffe J., The effectiveness of electronic stability control on motor vehicle crash prevention. Report Number UMTRI 2006-12, Ann Arbor, MI, University of Michigan Transportation Research Institute 2006.